UNIVERSIDADE D
COIMBRA

Ana Catarina Baptista de Sousa

Sex-dependent changes in brain microstructures organization and neurochemical profile in TSC2 mouse model

VOLUME 1

Thesis submitted to the Faculty of Science and Technology of the University of Coimbra for the degree of Master in Biomedical Engineering with specialization in Neuroscience, supervised by Dr. Joana Teresa Ferreira Gonçalves and co-supervised by Dr. João Filipe Martins.

October of 2021

FACULDADE DE CIÊNCIAS E TECNOLOGIA
UNIVERSIDADE D COIMBRA

Ana Catarina Baptista de Sousa

SEX-DEPENDENT CHANGES IN BRAIN MICROSTRUCTURES ORGANIZATION AND NEUROCHEMICAL PROFILE IN TSC2 MOUSE MODEL

Thesis submitted to the University of Coimbra for the degree of Master in Biomedical Engineering

Supervisors:
Joana Teresa Ferreira Gonçalves (ICNAS)
João Filipe Martins (ICNAS)

Coimbra, 2021

ABSTRACT

Tuberous sclerosis complex (TSC) is a hereditary disorder, resulting from a mutation in either *Tsc1* or *Tsc2*. This disorder is characterized by benign tumours in several organ systems, such as the skin, brain and kidneys. TSC individuals also present high comorbidity with other disorders, often referred to as TSC-associated neuropsychiatric disorders (TAND), which include hyperactivity, aggression, autism spectrum disorders (ASD), epilepsy and intellectual impairments.

Diffusion tensor imaging (DTI) is an MRI-based technique that quantifies the anisotropic movement of water molecules, providing relevant structural information in the brain tissue. Other techniques, namely generalized q-sampling imaging (GQI), that quantify anisotropy was also used in this thesis. Moreover, proton magnetic resonance spectroscopy (^{1}H-MRS) was performed to investigate neurochemical profile of *Tsc2*$^{+/-}$ mouse model.

Here, we observed that in prefrontal cortex there is a reduction of fractional anisotropy (FA) in male *Tsc2*$^{+/-}$ mice, together with an increase in axial diffusion (AD) and mean diffusivity (MD) in the amygdala. On the other hand, female *Tsc2*$^{+/-}$ mice displayed augmentation of cortical FA and AD. Concerning ^{1}H-MRS data, we found that transgenic males exhibited lower levels of cortical alanine (Ala) and glutathione (GSH), while in transgenic females, detected a down-regulation of gamma-amino butyric acid (GABA) levels were detected. In the hippocampus, male *Tsc2*$^{+/-}$ mice showed higher lactate, taurine, and inositol levels, without changes in females.

Our results lead us to postulate that brain structural organization and neurochemical profile of *Tsc2*$^{+/-}$ mouse model are sex-dependent. Furthermore, our results agree with the male bias described in autism spectrum disorders. This work may contribute to better understand the neural effects of *Tsc2*$^{+/-}$ disorder and potential therapeutic targets, and therefore possibly aid the development of therapeutic approaches.

Key words: Diffusion tensor imaging, Tractography, Generalized q-space imaging, Proton magnetic resonance spectroscopy, Tuberous sclerosis complex

RESUMO

O Complexo de Esclerose Tuberosa (CET) é uma doença hereditária, resultado de uma mutação num ou ambos os genes *Tsc1 e Tsc2*. Clinicamente, as manifestações incluem tumores benignos em diversos órgãos, como a pele, o cérebro e os rins. Esta doença apresenta elevada comorbidade com outros distúrbios, conhecidos como distúrbios neuropsiquiátricos associados ao CET (TAND), que incluem hiperatividade, agressão, transtornos do espectro do autismo (TEA) e deficiências intelectuais.

A imagem por tensor de difusão (DTI) é uma técnica de ressonância magnética (MRI) que quantifica o movimento anisotrópico de moléculas de água, oferecendo informação estrutural relevante sobre o tecido cerebral. Outras técnicas, nomeadamente a imagem por amostra q generalizada (GQI), que quantifica anisotropia foi também aplicada nesta tese. Para além disto, a espectroscopia de protões por ressonância magnética (1H-MRS) foi utlizada para investigar o perfil neuroquímico cerebral do modelo de murganho *Tsc2*$^{+/-}$.

No presente estudo, observámos no córtex pré-frontal uma redução da anisotropia fracional (AF) em murganhos machos *Tsc2*$^{+/-}$, acompanhada de um aumento na difusividade axial (DA) e difusividade média (DM) na amígdala. No sentido oposto, em fêmeas *Tsc2*$^{+/-}$ mostraram um aumento de AF e DA cortical. Relativamente aos dados de ^{1}H-MRS, machos transgénicos apresentaram menores níveis de alanina (Ala) e glutationa (GSH) corticais, enquanto em fêmeas transgénicas, foi detetada uma sub-regulação em níveis de ácido gama-aminobutírico (GABA). No hipocampo, murganhos machos *Tsc2*$^{+/-}$ apresentaram níveis mais elevados de lactato, taurina e inositol.

Os nossos resultados levam-nos a assumir que a organização estrutural do cérebro e o perfil neuroquímico do modelo de murganho *Tsc2*$^{+/-}$ é dependente do sexo. Para além disto, os resultados estão de acordo com o viés masculino nos distúrbios do espetro do autismo. Esta investigação ajuda um melhor entendimento dos efeitos neuronais deste distúrbio, e potencialmente auxilia o desenvolvimento de terapêuticas.

Palavras-chave: Imagem por tensor de difusão, Tractografia, Imagem por amostra q generalizada, Espetroscopia, Complexo de esclerose tuberosa.

CONTENT

LIST OF TABLES

LIST OF FIGURES

LIST OF ACRONYMS

^{1}H-MRS	Proton magnetic resonance spectroscopy
4E-BP1	Eukaryotic translation initiation factor 4E-binding protein 1
AD	Axial diffusivity
ADHD	Attention deficit/Hyperactivity disorder
Ala	Alanine
ASD	Autism spectrum disorder
Cho	Choline
CNS	Central nervous system
CSF	Cerebrospinal fluid
DSI	Diffusion spectrum imaging
DTI	Diffusion tensor imaging
DWI	Diffusion weighted imaging
FA	Fractional anisotropy
FACT	Fiber assignment by continuous tracking
GABA	Gamma amino butyric acid
GFA	Generalized fractional anisotropy
Gln	Glutamine
Glu	Glutamate
Glx	Glutamine+ Glutamate
GPC	Glycerophosphocholine
GQI	Generalized q-sampling imaging
GSH	Gluthatione
Ins	Inositol
ISO	Isotropic component
Lac	Lactate
MD	Median diffusivity
MRSI	Magnetic resonance spectroscopy imaging

mTORC1	Mechanistic target of rapamycin complex 1
mI	Myo-inositol
NAA	N-acetyl aspartate
NAAG	N-Acetyl Aspartyl Glutamate
NQA	Normalized quantitative anisotropy
ODF	Orientation distribution function
PCh	Phosphocholine
PFA	Paraformaldehyde
PRESS	Point-resolved spectroscopy
QA	Quantitative anisotropy
QBI	Q-ball imaging
RD	Radial diffusivity
RHEB	RAS homologue enriched in brain
S6K1	S6 kinase 1
SDF	Spin distribution function
SEGAs	Subependymal giant cell astrocytomas
SENs	Subependymal nodules
STEAM	Stimulated echo acquisition mode
SVS	Single voxel spectroscopy
TAND	TSC-associated neuropsychiatric disorders
Tau	Taurine
TBC1D7	TBC1 domain family member 7
TSC	Tuberous sclerosis complex

1 INTRODUCTION

TSC is an autosomal, dominant disease that affects approximately 2 million people worldwide. This disease is caused by an abnormal cellular proliferation and growth, thus affecting several organs, such as the brain. TSC presents a high comorbidity with ASD, a neurodevelopmental disease characterized by deficits in social interaction, communication and repetitive/restrictive behaviours. Here, we evaluated diffusion tensor imaging (DTI) to explore brain structural alterations in juvenile *Tsc2*$^{+/-}$ mice. DTI is a relatively new imaging technique that can be used to evaluate white matter in the brain. Its application can provide visualization and quantification of the orientation and directions of white matter fiber tracts. The generalized q-sampling imaging (GQI) technique will also be used to aid the exploration of possible brain alterations, by providing additional metrics of the water diffusion in fiber tracts. Furthermore, data from proton magnetic resonance spectroscopy (^{1}H-MRS) was analysed to study how *Tsc2*$^{+/-}$ mutation interferes with the neurochemical profile.

1.1 Objectives and hypothesis

This thesis aimed the following objectives:

1) Investigating alterations in DTI and GQI metrics looking to the influence of both *Tsc2*$^{+/-}$mutation and sex;
2) Exploring changes in metabolic profiles induced by genotype and sex;
3) Examining possible correlations between imaging metrics and neurochemical profile.

This thesis presents in Chapter 2 a compiled overview of the relevant theory on the physiology of TSC2 condition, a comprehensive description of DTI and GQI as non-invasive imaging techniques used to study the brain, and an introduction about ^{1}H-MRS as a technique to study neurochemical profile. The current state-of-the-art for DTI, GQI and neurometabolism in the TSC disorder is addressed in Chapter 3. The following chapter – Chapter 4 – is dedicated to the materials and methods used for data acquisition, image processing, tractography, spectroscopy and statistical analysis. In Chapter 5, the results of the described processes are presented according to each aforementioned goal. Finally, in Chapter 6, the discussion, limitations and future work are presented.

2 BACKGROUND

2.1 Tuberous Sclerosis Complex disorder

Tuberous sclerosis complex (TSC) is an autosomal-dominant disorder, which features include cellular hyperplasia and tissue dysplasia, and known to affect multiple organ systems (Gomez et al., 1999). Its name originates from the composition of the Latin word *tuber* (root-shaped growths) and the Greek word *skleros* (hard), referring to 'tubers'. These thick, firm and pale gyri were first described in depth by Bourneville in 1880, and can be found post-mortem in brains of patients with this pathology (Henske et al., 2016).

Epidemiologically, TSC is not ethnically or sex dependent in terms of incidence. Studies showed a prevalence of 1 in 60000 to 90000 people, estimating at least 2 million people affected worldwide (Hyman et al., 2000).

The TSC protein complex includes TSC1, known as hamartin, and TSC2, known as tuberin. All TSC patients carry loss-of-function mutations in either of the corresponding genes, with TSC1 accounting for 10% to 30% of families diagnosed (Henske et al., 2016; Rosset, 2017). Despite being an autosomal-dominant inherited disorder, 65% to 75% of TSC patients report spontaneous mutations (DiMario et al., 2015). The TSC complex also includes the TBC1 domain family member 7 (TBC1D7), which loss-of-function has been associated with macrocephaly and intellectual disability but without other typical features of TSC (Capo-chichi et al., 2013, Alfaiz et al., 2014).

Clinically, individuals with the TSC2 mutation tend to have a more severe manifestation of the disorder, such as more hypomelanotic macules and learning disabilities, and, in the case of male individuals, higher frequency of neurologic and ophthalmologic signs, renal cysts, and ungueal fibromas (Au et al., 2007).

The most established pathway for the disorder is the TSC– RHEB–mTORC1 pathway. The protein complex inhibits mTORC1 (mechanistic target of rapamycin complex 1), a serine/threonine kinase involved in the control and mediation of several cellular processes (Henske et al., 2016; DiMario et al., 2017). This inhibition is achieved via RAS homologue enriched in brain (RHEB), the target of the GTPase-activating domain of TSC2. The TSC1/TSC2 complex acts as a GTPase-activating protein (GAP) for RHEB, stimulating the RHEB-GTP to GDP-bound state conversion, and inactivating RHEB signalling used to stimulate mTORC1. Accordingly, the loss-of-function mutations found

in the TSC disorder lead to a hyperactive RHEB-GTP signalling and mTORC1 activation (Figure 1) (DiMario et al., 2015).

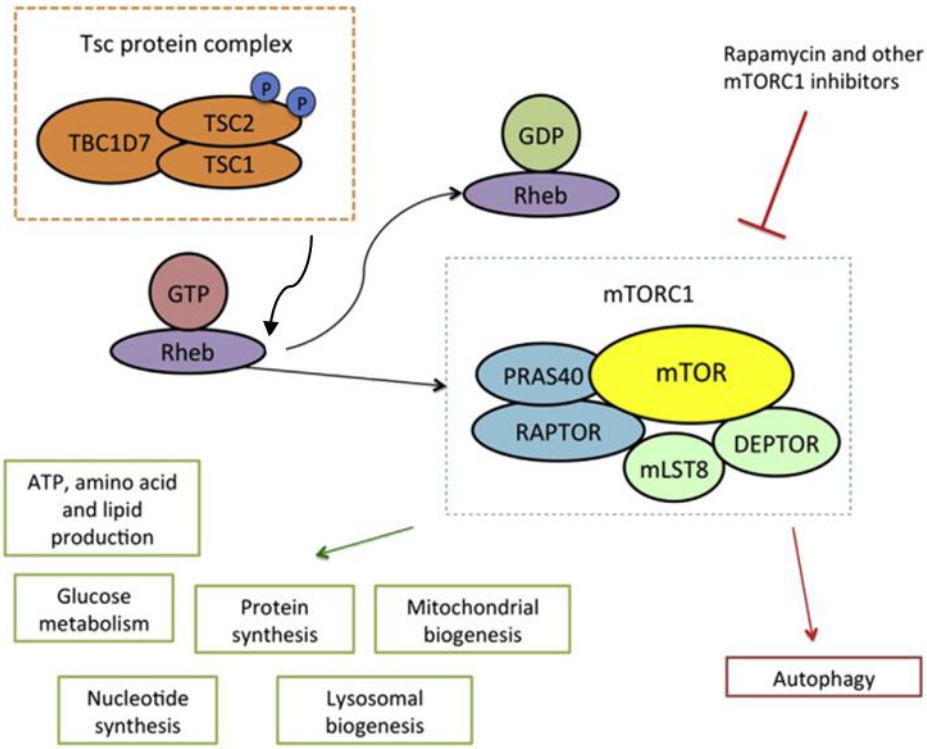

Figure 1. *TSC protein complex and mTOR signaling and its functional consequences - TSC1, TSC2 and TBC1D7 form the TSC protein complex that acts as a critical negative regulator of the mechanistic target of mTORC1. Rheb is a specific GTPase downstream of the TSC protein complex that links TSC1/TSC2 to mTORC1. mTORC1 signalling consequently impacts several biological processes. Adapted from DiMario et al., 2015. Abbreviations: TSC1 - Tuberous Sclerosis Complex 1, TSC2 - Tuberous Sclerosis Complex 2, TBC1D7 - TBC1 domain family member 7, GDP - Guanosine diphosphate ,GTP - Guanosine triphosphate, Rheb - RAS homologue enriched in brain, mTOR - mechanistic target of rapamycin, mTORC1 - mechanistic target of rapamycin complex 1, PRAS40 - proline-rich AKT substrate of 40 kDa, RAPTOR - regulatory associated protein of TOR, mLST8 - MTOR Associated Protein, LST8 Homolog, DEPTOR - DEP-domain containing mTOR-interacting protein.*

Protein synthesis is stimulated by mTORC1 in its active state, through the phosphorylation of translational regulators 4E-BP1 (eukaryotic translation initiation factor 4E-binding protein 1) and S6K1 (S6 kinase 1). Cell growth is also influenced by mTORC1, through the regulation of anabolic pathways that facilitate an adaptation to several external stimuli. Various other processes such as the biosynthesis of ribosomes, lipid biogenesis, glucose metabolism, nucleotide synthesis, mitochondrial and lysosomal biogenesis, ATP, and amino acid production are also stimulated by active mTORC1. Contrarily, it also functions as a negative autophagy regulator, a known implicated process in many neurodegenerative and neurodevelopmental diseases (DiMario et al., 2015).

In addition, other pathways were also discovered, even if currently less understood. These pathways include TSC2-indepentent targets of TSC1, RHEB-independent targets of both TSC1 and TSC2, as well as mTORC1-independent targets of RHEB (Figure 2) (Henske et al., 2016).

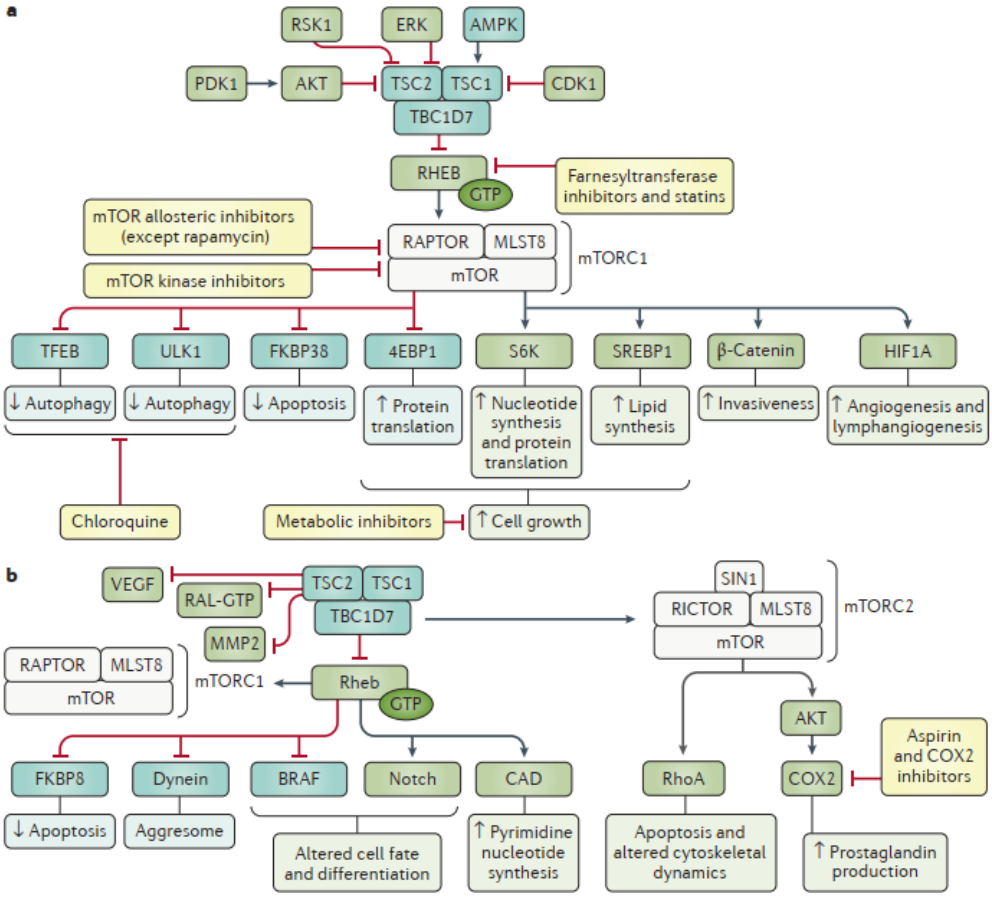

***Figure 2**. TSC signaling pathways – (a) Canonical TSC signaling pathways include RHEB activation of mTORC1 signaling network, resulting in increased protein translation and cell growth, as well as decreased autophagy and apoptosis, among other effects. (b) Non-canonical signaling pathways, include regulation by the TSC protein complex in an mTORC2-mediated manner and regulation by RHEB that seem to be independent of mTORC1. Yellow boxes represent potential therapeutic agents, green boxes, represent protein promoters or that are promoted by mTOR, and blue boxes, protein inhibitors or that are inhibited by of mTOR. Adapted from Henske et al., 2016. Abbreviations: TSC1 - Tuberous Sclerosis Complex 1, TSC2 - Tuberous Sclerosis Complex 2, RHEB - RAS homologue enriched in brain, mTOR - mechanistic target of rapamycin, mTORC1 - mechanistic target of rapamycin complex 1, 4EBP1 - eukaryotic translation initiation factor 4E-binding protein 1, AMPK - AMP-activated protein kinase, CAD - carbamoyl-phosphate synthetase 2, aspartate transcarbamylase and dihydroorotase, CDK1 cyclin-dependent kinase 1, COX2 - cyclooxygenase 2, HIF1A - hypoxia-inducible factor 1α, MLST8 - target of rapamycin complex subunit LST8, MMP2 - matrix metalloproteinase 2, PDK1 - pyruvate dehydrogenase kinase isoform 1, RAL - RAS-related protein, RAPTOR - regulatory-associated protein of TOR, RICTOR - rapamycininsensitive companion of mTOR, RSK1 - ribosomal S6 kinase 1, S6K - S6 kinase, SIN1 - stress-activated map kinaseinteracting protein 1, SREBP1 - sterol regulatory element-binding protein 1, TBC1D7 - TBC1 domain family member 7, TFEB - transcription factor EB, ULK1 - unc-51-like kinase 1, VEGF - vascular endothelial growth factor.*

2.1.1 TSC and the brain

TSC is often accompanied by neurological manifestations such as epilepsy, mental retardation and autistic behaviour.

Epilepsy

Up to 80%-90% of TSC patients report epilepsy as a symptom, although the origin of this relation is still not well understood (Henske et al., 2016; Holmes et al., 2007). Neuropathological features thought to be related include cortical tubers, subependymal nodules (SENs), and subependymal giant cell astrocytomas (SEGAs) (Holmes et al., 2007).

Cortical tubers, abnormal cortex cells with neural and glial marker proteins, constitute the hallmark of TSC, formed during fetal development (Barkovich et al., 2005). The variation in number and localization of these tubers is a possible explanation for the variability of the neurological phenotype of TSC patients. Often localized at the border between grey and white matter, a posterior localization may be an indication of an aggravation in seizure control and development outcome (Holmes et al., 2007). However, increasing evidence suggests the perituberal cortex is of equal importance (Ruppe et al., 2014). Overactivation of mTORC1 as a result of TSC mutations has shown to cause altered cellular morphology with cytomegalic neurons, altered synaptogenesis and an imbalance between excitation and inhibition. In the brain, many γ-aminobutyric acid type A receptor ($GABA_AR$) subunits are downregulated, including α1-$GABA_AR$, α4-$GABA_AR$ and α5-$GABA_AR$ (Curatolo et al., 2016). The aforementioned mTORC1 overactivation is also thought of as the cause of alterations in migration and orientation of neural cells, that results in abnormal cortical lamination and dendritic arborisation (Aronica et al., 2014).

SENs, present in 80% to 90% of TSC patients, are benign proliferative lesions lining the surface of the cerebral ventricles. They are thought to develop from progenitor cells and, unlike tubers, have the potential to change over time. SEGAs can originate from SENs and are most often located under the ependymal lining of the ventricular wall, typically in the region of the foramen of Monro, containing cells with astrocytic and neural characteristics. Neurological dysfunction can happen by SEGA-induced occlusion of cerebrospinal fluid flow, causing hydrocephalus, as well as cortical (transmantle) dysplasia, demyelination, radial migration lines, cerebral cysts, hemimegalencephaly,

chordomas, and meningiomas (Shepherd et al., 1991; Rott et al., 2002). Unlike cortical tubers and the perituberal cortex, SENs and SEGAs are not currently considered epileptogenic, though interaction with adjacent tissue leading to heighten excitability is possible (Holmes et al., 2007).

Autism

TSC displays high comorbidity with autism spectrum disorder (ASD), with a prevalence in the latter of 1% to 4% and features of ASD being present in 25% to 50% of TSC individuals with a formal diagnosis (Curatolo et al., 2008; Asato et al., 2004; Bolton et al., 2004; Wiznitzer et al., 2004). Children with a TSC2 mutation are more likely to develop ASD than children with a mutation in the TSC1 gene instead. The probability of developing an ASD is also greater in the presence of early-onset infantile spasms, especially if there is an epileptiform focus in the temporal lobes. Therefore, early onset electrophysiological disturbances within the temporal lobes seem to have a damaging effect on social and cognitive process related to social information processing, and possibly facial recognition (Bolton et al., 2004).

Tuber location is a possible explanation for the ASD presence in TSC patients, with temporal areas reporting a higher number of tubers in ASD patients compared to non-autistic individuals (Bolton et al., 1997; Bolton et al., 2002). However, although TSC combined with early on-set spasms and temporal deficits has shown to correlate with communication deficits, it is not necessarily associated with autism, suggesting that cortical tubers are not the sole cause of ASD in TSC patients (Asano et al., 2001).

Other cognitive and neurobehavioral issues

TSC individuals showed up to 50% of some degree of intellectual disability, with the possibility of impairment being associated with a history of seizures, especially early-on set spasms (Joinson et al., 2003).

In addition, mental health issues are very common in TSC such as ADHD, depression and particularly anxiety, that affects 30% to 60% of TSC individuals (De Vries et al., 2015).

However, neither the relationship between cognitive impairment and the neuroanatomical features of TSC (such as cortical tubers and SENs) or the

pathophysiological link between mental health disorders and TSC are yet very well understood.

2.2 Diffusion Tensor Imaging

Some studies have used diffusion tensor imaging to obtain macroscopic information on the anatomical characterization of mouse models (Wu et al., 2013; Mori et al., 2003; Müller et al., 2019). This section aims to provide a theoretical overview of this technique, as well as a brief introduction to tractography methods, a method used to reconstruct and visualize fibers in 3D.

2.2.2 Technical background

Biological diffusion

Diffusion describes the transfer of material, such as water molecules, between different spatial locations over time.

In three dimensions, Einstein concluded that the diffusion coefficient D (in mm^2 /s) is proportional to the mean squared displacement (Δr^2) divided by the number of dimensions, n, and the diffusion time, Δt (Equation 1) (Einstein, 1956).

$$D = \frac{<\Delta r^2>}{2n\Delta t} \qquad (1)$$

If boundaries are absent, the Gaussian probability density describes the molecular water displacement (Equation 2).

$$P(\Delta r, \Delta t) = \frac{1}{\sqrt{2\pi D \Delta t^3}} exp\left(\frac{-\Delta r^2}{4D\Delta t}\right) \qquad (2)$$

In biological tissues, water diffuses inside, outside, around and through cellular structures, primarily by thermal changes. Cellular membranes difficult water diffusion, causing a decrease of the mean squared displacement. Cellular swelling or density

increase may also pose obstacles to diffusion. On the other hand, necrosis, characterized by membrane breakdowns, aids the water displacement. Accordingly, cellular membranes tend to restrict intracellular water, also decreasing the apparent diffusivity, but only until a plateau with the increasing of the diffusion time (Le Bihan, 1995). Fibrous tissues, such as white matter, present a relatively unimpaired parallel water diffusion, whereas perpendicular diffusion is highly restricted and hindered. This difference in diffusion in fibrous tissues is labelled as anisotropic.

Anisotropic diffusion can be modelled as a multivariate normal distribution (Equation 3, 4) (Basser et al., 1994).

$$P(\Delta\vec{r}, \Delta t) = \frac{1}{\sqrt{(4\pi\Delta t)^3|D|}} exp\left(\frac{-\Delta\vec{r}^T D^{-1}\overrightarrow{\Delta r}}{4\Delta t}\right) \qquad (3),$$

where the diffusion tensor is a 3x3 covariance matrix

$$D = \begin{bmatrix} D_{xx} & D_{xy} & D_{xz} \\ D_{yx} & D_{yy} & D_{yz} \\ D_{zx} & D_{zy} & D_{zz} \end{bmatrix} \qquad (4)$$

The diffusion tensor describes the diffusion displacement in 3D, normalized by the diffusion time. The diagonal elements ($D_{ii} > 0$) represent the variances along the tree axes, and the rest, symmetric about the diagonal ($D_{ij} = D_{ji}$), the covariance terms. Tensor diagonalization produces the eigenvalues and corresponding eigenvectors of the tensor, representing the directions and apparent diffusivities along the axes of the principal diffusion.

The tensor can be represented by an ellipsoid, whose directions of the principal axes are defined by the eigenvectors, and ellipsoidal radii by the corresponding eigenvalues (Figure 3).

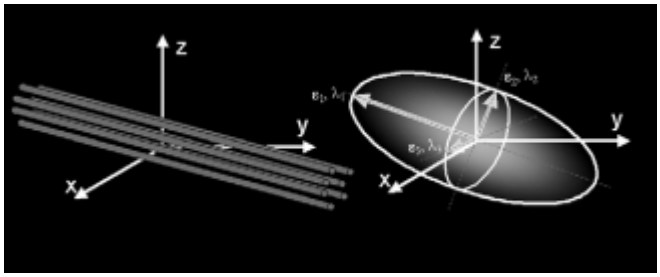

Figure 3. *Schematic representation of diffusion displacement distributions for the diffusion tensor, represented by ellipsoids. Adapted from Alexander et al., 2007.*

Anisotropy is expressed when the eigenvalues differ significantly in magnitude. The magnitudes can be influenced by alterations in tissue microstructure caused by biological processes such as aging, disease or tissue injury. These sensitivities make the diffusion tensor a good characterizer of tissue microstructure.

In the context of the central nervous system (CNS), water usually diffuses in an anisotropic fashion in white matter regions, and isotropic in grey matter and cerebrospinal fluid (CSF) (Alexander et al., 2007).

Diffusion-weighted imaging (DWI)

The DWI technique is most often based on a pulse sequence that includes two large-gradient pulses placed on both sides of a 180º refocusing pulse (Alexander et al., 2007). These gradients are applied before and after the refocusing pulse, known as the Stejskal-Tanner diffusion encoding. The first pulse dephases the magnetization across the sample, meaning there is a phase shift in proton spins, whereas the second rephases it. This second phase shift can only completely cancel the first for stationary molecules, since diffusing molecules keep changing position throughout the entire process, resulting in a non-zero net phase difference (Stejskal et al., 1965).

Because faster molecules travel a wider distance, signal loss occurs. This is represented by darker image voxels, meaning that image contrast is based on the differences between diffusion magnitudes (O'Donnell et al., 2011).

The signal attenuation caused by phase dispersion for a simple isotropic Gaussian diffusion can be described as

$$S = S_0 e^{-bD} \qquad (5)$$

In which, S is the diffusion-weighted signal, S_0 the signal without diffusion-weighted gradients, D the apparent diffusion coefficient, and b the Le Bihan's factor. The b value describes the diffusion sequence, gradient strength and physical constant. For rectangular gradient pulses, b can be defined by

$$b(\gamma G\delta)^2[\Delta - (\delta/3)] \quad (6),$$

where γ is the gyromagnetic ratio, G the pulse's amplitude, δ the duration of each diffusion, and Δ the duration between the two pulses (Alexander et al., 2007).

An increased b-value consequently increases the degree of diffusion weighting, influencing a signal loss along the direction of the gradients applied.

Diffusion tensor imaging (DTI)

DTI is a non-invasive MRI-based technique that utilizes the diffusion tensor to model diffusion. It is highly sensitive to changes in diffusion, therefore being a great tool for indirect characterization of both micro and macrostructures of tissues, as well as their orientation (Van Hecke et al., 2016). Maps of DTI measures are estimated from the raw diffusion weighted images.

To facilitate the interpretation of the image information, is optimal to utilize simpler scalar maps distilled from the image data. As previously mentioned, the eigenvectors represent the direction of the diffusion, while the corresponding eigenvalues the length of the diffusion. The axial diffusivity (AD) is the principal eigenvalue (λ_1), defining the magnitude of greatest diffusion (Equation 7)

$$AD = \lambda_{\parallel} = \lambda_1 \quad (7)$$

The radial diffusivity (RD) is obtained by averaging the second and third eigenvalues (λ_2 and λ_3), representing the contribution of diffusion transversely (Equation 8).

$$RD = \lambda_{\perp} = \frac{\lambda_2 + \lambda_3}{2} \quad (8)$$

Mean diffusivity (MD) can be expressed as the mean of the three eigenvalues, describing the total amount of diffusion for each voxel (Equation 9).

$$MD = \frac{1}{3}\sum \lambda_i \quad (9)$$

Finally, the fractional anisotropy (FA) varies between 0 (maximal isotropic diffusion) and 1 (maximal anisotropic diffusion) (Equation 10), and expresses the how far the tensor is from a sphere (Figure 4).

$$FA = \sqrt{\frac{3}{4}} \frac{\sqrt{(\lambda_1 - MD)^2 + (\lambda_2 - MD)^2 + (\lambda_3 - MD)^2}}{\sqrt{\sum \lambda_i^2}} \qquad (10)$$

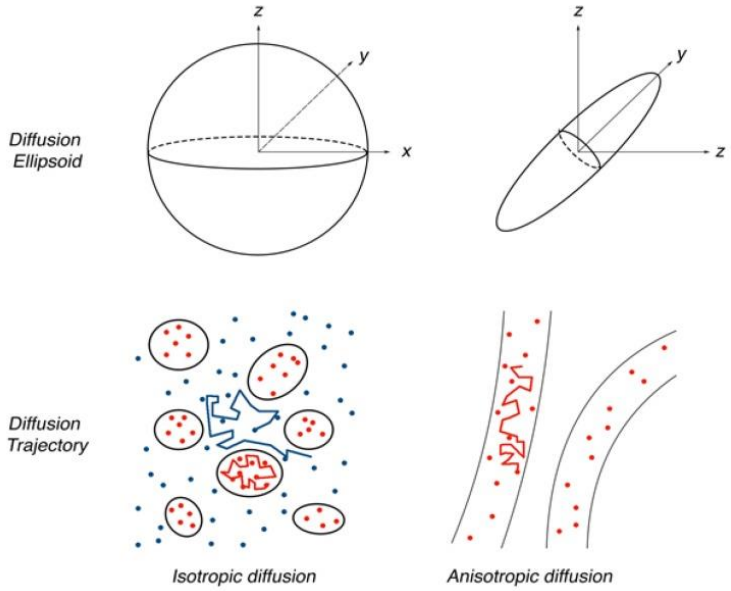

Figure 4. *Schematic representation of different diffusion tensor shapes for different diffusion types – Isotropic and anisotropic diffusion representation differs depending on the type of trajectory and diffusion tensor shape. Adapted from Rodrigues et al., 2018.*

2.2.2 Tractography

Tractography allows for the visualization of connection patterns in 3D (Mori, 2001). Patterns are estimated by the specification of a *seed* region, a starting location, followed by estimating the direction of propagation (often the major eigenvector), and moving a small distance in the same direction. The direction is then re-evaluated and another step is taken. This incremental loop is constricted by the use of regions of interest (ROI), that encompass the tracts (Mori et al., 2002; Catani et al., 2002).

The propagation step can be done using different types of algorithms, either probabilistic or deterministic (Figure 5).

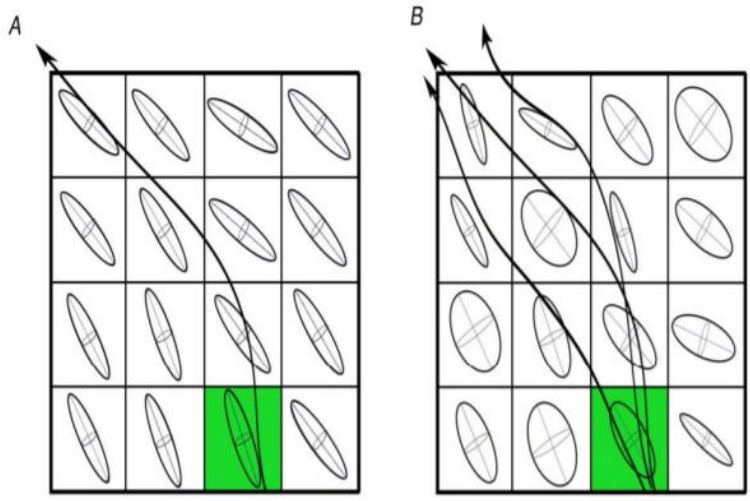

Figure 5. *Schematic representation of tractography propagation methods – Panel A Illustrates a deterministic tractography method, while B represents a probabilistic tractography method. Adapted from Rodrigues et al., 2018.*

Deterministic tractography, also known as streamline tractography, generates discrete trajectories through computational methods, such as Euler's method, Runge-Kutta method of the second or fourth order, and fiber assignment by continuous tracking (FACT). The FACT algorithm is the most commonly used by the commercially available DTI software, and utilizes user defined initiation voxels and stopping criteria, by tracking in the direction of the main eigenvector of the next voxel until the stopping criteria is met (Rodrigues, 2018). On the other hand, probabilistic tractography already accounts for the uncertainty of the tracking, caused by noise and other distortions. A deterministic approach is best suited for the calculation of the most likely path of a fiber, whereas a probabilistic method is more beneficial to aster all the possible paths and the likelihood of a voxel being included in a fiber (Soares et al., 2016).

2.3 Generalized q-sampling imaging (GQI)

2.3.1 Theoretical background

Q-space imaging methods, also known as model-free methods, have the Fourier transform relation between the Fourier transform as the diffusion MR signals and the underlying diffusion displacement as their basis. The orientation distribution function (ODF) is acquired from the diffusion displacement, and from this one can infer the underlying crossing patterns of the fibers as well as evaluate the microstructure property

in terms of generalized fractional anisotropy (GFA) or diffusion anisotropy. Given that the measuring of diffusion ODF comes with some limitations, the generalized q-sampling imaging method uses a new derived relation between spin distribution function (SDF) and the MR signals. While, the diffusion ODF represents a probability distribution of the diffusion displacement, the SDF measure defines a quantitative distribution of the spins undergoing diffusion and can be compared across different voxels (Yeah et al., 2010; Tuch, 2004).

Metrics

GQI provides several types of diffusion measures. Extending on the FA metric

$$FA = \frac{std(\psi)}{rms(\psi)} \quad (11),$$

where ψ is the ODF, the generalized fractional anisotropy (GFA) can be defined by

$$GFA = \frac{std(\psi)}{rms(\psi)} = \sqrt{\frac{n\sum_{i=1}^{n}\left((\psi(u_i)-\langle\psi\rangle\right)^2}{(n-1)\sum_{i=1}^{n}\psi(u_i)^2}} \quad (12)$$

in which,

$$\langle\psi\rangle = (1/n)\sum_{i=1}^{n}\psi(u_i) = (1/n) \quad (13)$$

is the mean of the ODF. Like the FA metric for DTI, the GFA metric is also normalized, ranging between 0 and 1.

The quantitative anisotropy (QA) can also be defined, as a way to quantify the spin population in a given direction. Unlike FA and GFA, this metric is not for each voxel but fiber population instead. The QA metric defined by the SDF value at the resolved fiber orientation â minus the background isotropic diffusion component $\mathrm{I}(\psi_Q)$ (Yeh et al., 2010) is

$$QA(\hat{a}) = Z_0\left(\psi_Q(\hat{a}) - I(\psi_Q)\right) \quad (14),$$

in which Z_0 is the SDF scaling constant. The QA metric scales with spin density and MRI signals, consisting therefore of an "arbitrary unit". This causes consistency problem in

comparing QA values between scans. To overcome this limitation, QA can also be expressed in the normalized form (NQA) in which scales the maximum QA value of a subject to 1. NQA assumes that all subjects share the same compactness of the white matter bundle.

The aforementioned isotropic component can also be a metric (ISO), and it is defined as the minimum distribution value of an ODF. It encompasses the background isotropic diffusion contributed from CSF or non-directional restricted diffusion, including diffusion within or between cells.

2.3.2 Tractography

Tract reconstruction is also possible with this imaging technique, by the use of tracking algorithms also used in DTI.

The reconstruction process of GQI does not require deconvolution procedures and may offer a comparison of the SDF values amongst voxels. In other methods, such as q-ball imaging (QBI) and diffusion spectrum imaging (DSI) reconstruction, comparing ODFs among voxels is not possible, since each ODF is locally normalized, and the same ODF value in different voxels does not necessarily represent the same physical quantity. The SDF values are obtained from the scaling of the average propagator with the density function, unifying the scale of SDF across different voxels. Thus, GQI gives the SDF a consistent physical meaning over all the voxels and allows inter-voxel comparison (Yeah et al., 2010).

2.3.3 GQI vs DTI

Restricted diffusion vs overall diffusion

DTI metrics express a plethora of biological alterations, as this technique does not specify restricted diffusion from axonal myelination.

On the other hand, GQI uses the diffusion sampling length ratio, which is a length parameter, to account for restricted diffusion at a specific scalar distance. This means, that the GQI metric QA expresses the anisotropy of restricted diffusion, making the

quantification more robust and resulting in a more reliable tractography method (Zhang et al., 2013).

Diffusion rate vs diffusion density

The two techniques also differ in which diffusion characteristic is the basis. DTI metrics are based on diffusivity, or rate of diffusion, which includes both none-restricted and restricted diffusion. GQI quantifies the density of restricted and less-restricted diffusion instead, which means that QA measures the density of anisotropic diffusing water.

Fiber-specific vs voxel based

As previously mentioned, the GQI specific QA metric is obtained for each fiber population, and by contrast DTI specific FA encompasses a voxel shared by several fiber populations. This statement explains why GQI is often used to study crossing fiber areas.

Sensitivity

In practical terms, DTI metrics show to be more sensitive to pathological conditions, given that diffusivity is good for determining structure intactness, whereas GQI metrics better capture individual/physiological difference, since density measurement is good for "connectivity" quantification.

2.4 Magnetic Resonance Spectroscopy

Magnetic resonance spectroscopy (MRS) is a non-invasive, *in vivo* technique, complementary to MRI and capable to provide information about neuropathologies by generating a spectrum of brain metabolites. In principle, any change from the normal spectrum can indicate abnormal tissue function (Currie et al., 2012).

2.4.1 Theoretical background

MRS uses magnetic resonance images as a guide to specify the tissue region from where the spectrum is obtained. This technique encompasses different methods, such

as single voxel spectroscopy (SVS) and magnetic resonance spectroscopic imaging (MRSI).

The water signal, being more abundant, is much larger than the metabolite's signal, which commonly leads to the application of water signal suppression methods, though an intact spectrum could also be useful for quantification or corrections (Faghihi et al., 2017).

Exposure to a magnetic field leads to the polarization of the resonance of the atomic spins within nuclei. Radio frequency pulses cause spins within molecules to absorb energy and polarize the field. When terminated, the spins process along the magnet's axis. Consequently, a rotating magnetic field is created, inducing oscillating voltage in the radio frequency receiver coil analysed by the MR spectrometer (Ford et al., 2016).

Because each molecule has a unique molecular environment, frequency shifts differ among them. A chemical shift of a particular metabolite is the change of the atomic nucleus' MR frequency due to the shielding provided by the surrounding electrons (Equation 15) and can be presented as a spectrum. It is independent of the applied external magnetic field, and reported in parts per million (Ford et al., 2016).

$$\delta = \frac{\omega - \omega_{ref}}{\omega_{ref}} \qquad (15)$$

Single voxel spectroscopy (SVS)

In single voxel spectroscopy (SVS), the signal is received from a volume limited to a single voxel, where the metabolism may be damaged. The most commonly SVS methods used in proton magnetic resonance spectroscopy (^{1}H-MRS), an MRS technique that uses the proton resonance of hydrogen (^{1}H) atoms to quantify metabolites, are point-resolved spectroscopy (PRESS) and stimulated echo acquisition mode (STEAM) (Faghihi et al., 2017; Ford et al., 2016).
PRESS uses a slice-selective radio frequency pulse sequence, composed of a 90º pulse and two 180º refocusing pulses (Figure 6).

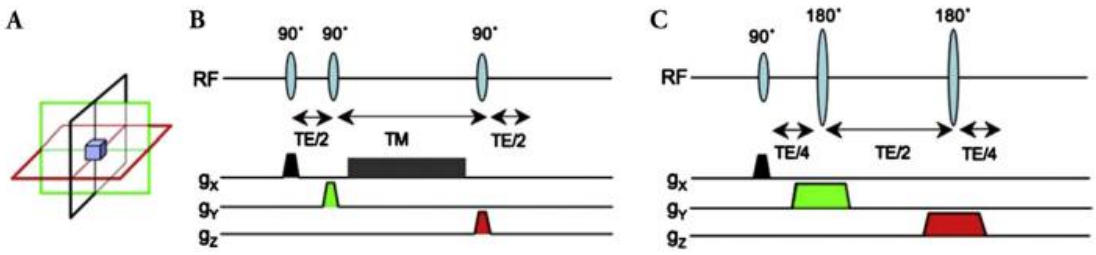

Figure 6. *Localization gradients and SVS, STEAM sequence and PRESS sequence – Panel A illustrates the localization gradients in space, B represents the STEAM technique, and C represents the PRESS technique. Adapted from Faghihi et al., 2017. Abbreviations: PRESS - point-resolved spectroscopy, RF – radio frequency, STEAM - stimulated echo acquisition mode, SVS - single voxel spectroscopy, TE – echo time, TM - mixing time.*

STEAM uses sequence of three slice-selective 90° radio frequency pulses (Figure 6). The amplitude of the obtained stimulated echo is two times less than the double spin echo from the PRESS technique, being a less sensitive method. However, in general, echo times are shorter, making it a better tool for metabolite detection with short T2 (measure relating to the decay of magnetization component in the plane transversal to the static magnetic field) (Frahim et al., 1989).

Magnetic resonance spectroscopic imaging (MRSI)

In MRSI, also called chemical shift imaging, a large volume composed of several smaller voxels is able to produce all voxel's spectrum at the same time. It is based on the application of phase-encoding gradients followed by the collection of a series of free induction decays. The data can be presented as a spatial distribution of the obtained metabolic signals. Compared to SVS, MRSI requires a longer acquisition time, but shows higher resolution (Hsu et al., 2001; Chan et al., 2001).

Usually, SVS is the preferred MRS technique when an accurate quantification is a must, a MRSI is commonly used to visualize the spatial distributions of the metabolites (Faghihi et al., 2017).

Metabolites

MRS can be used to determine the relative concentrations and physical properties of a variety of biochemicals frequently referred to as "metabolites" due to their role in metabolism, though many more can also provide relevant information (Figure 7).

NAA is only found in the brain and is the metabolite that generates the most prominent peak. It is suggested to have roles that include: water removal from neurons and

counteraction against the anion deficit in neurons. This metabolite is the precursor for the production of N-acetyl aspartyl glutamate (NAAG), a neuromodulator with inhibitory functions. Indeed, it provided acetate for myelin lipid synthesis in oligodendrocytes and assistant in the removal of nitrogen from the brain (Currie et al., 2012). Concentration appears higher in grey matter compared to white matter (Hajek et al., 2008).

Creatine detection is often acquired as the combination of creatine (Cr) and phosphocreatine (PCr). Both are involved in ATP reserves, and the peak signals energetic metabolism. Concentration is generally uniform across the brain (Currie et al., 2012).

The choline (Cho) also denoted as total choline - glycerophosphocholine + phosphocholine (GPC + PCh) -, peak is thought to represent alterations in membrane turnover (Ross et al., 2001), which explains choline concentration increases in the presence of cell proliferation or membrane disruption (e.g. malignancy and demyelination) (Miller, 1991). Choline is heavily concentrated in glial cells and astrocytes, compared to neurons. Concentration in the white matter also appears slightly greater than in grey matter (Currie et al., 2012).

Myoinositol (mI), a simple sugar absent from neurons, is primarily synthesised in glial cells and cannot cross the blood-brain barrier. Therefore, it marks glial proliferation and growth (possibly indicating inflammation). It can also be an indicator of myelin breakdown (Soares et al., 2009). It can be referred as the more general inositol (Ins), that helps control chemical imbalances, including the ones involved in mood control (Harris et al., 2017).

Glutamine (Gln) and glutamate (Glu) are usually analysed as a combination. Glutamine is an astrocyte marker, viewed as a crucial neurotoxin when in exceeding concentrations and participant in the redox cycle. Glutamate is the most abundant neurotransmitter in the brain, and has an excitatory role. Both are involved in the detoxification and regulation of neurotransmitters (Currie et al., 2012; Soares et al., 2009).

Lactate (Lac) does not appear to be detectable by MRS in healthy tissues, with its peak being superimposed on the lipid band. It is associated with glycolytic metabolism, alterations in mitochondrial metabolism, and activation of macrophages. When present, it can suggest brain injury when hypoxia is part of the diagnostic (Currie et al., 2012; Soares et al., 2009).

Gamma amino butyric acid (GABA) is the primary inhibitory neurotransmitter, involved in the control of cortical responses and cerebral plasticity (Harris et al., 2017).

Taurine (Tau) is a protein that helps stabilizing the neuronal structure and one the most widely established biomarkers of Alzheimer's disease.

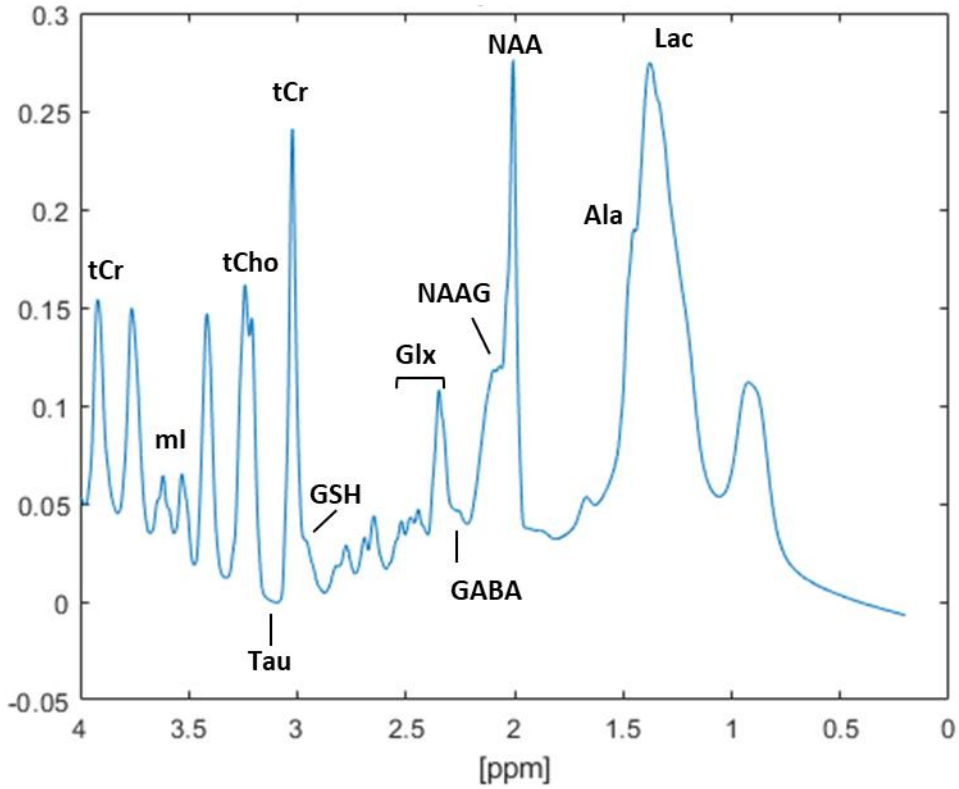

Figure 7. *Example of a magnetic resonance spectroscopy – Resonance frequency (ppm) spectrum of metabolic peaks, with each metabolite identified. Abbreviations: tCr – total creatine, mI – myo-inositol, tCho – total choline, Tau – taurine, GSH – glutathione, Glx – glutamate+glutamine, GABA - Gamma amino butyric acid, NAAG - N-acetyl aspartyl glutamate, NAA - N-acetyl aspartate, Ala – alanine, Lac – lactate.*

3 STATE-OF-THE-ART

3.1 Diffusion tensor imaging of the mouse brain

DTI is a useful tool for the study of brain anatomy and pathology (Figure 8). Its utility in clinic is not exclusive as it has also been used in basic research, including in the mouse brain (Mori et al., 2006). Applications include the characterization of white matter injuries in mouse models of neurological diseases, such as traumatic brain injury (MacDonald et al., 2007), multiple sclerosis (Budde et al., 2007), and stroke (Wang et al., 2009).

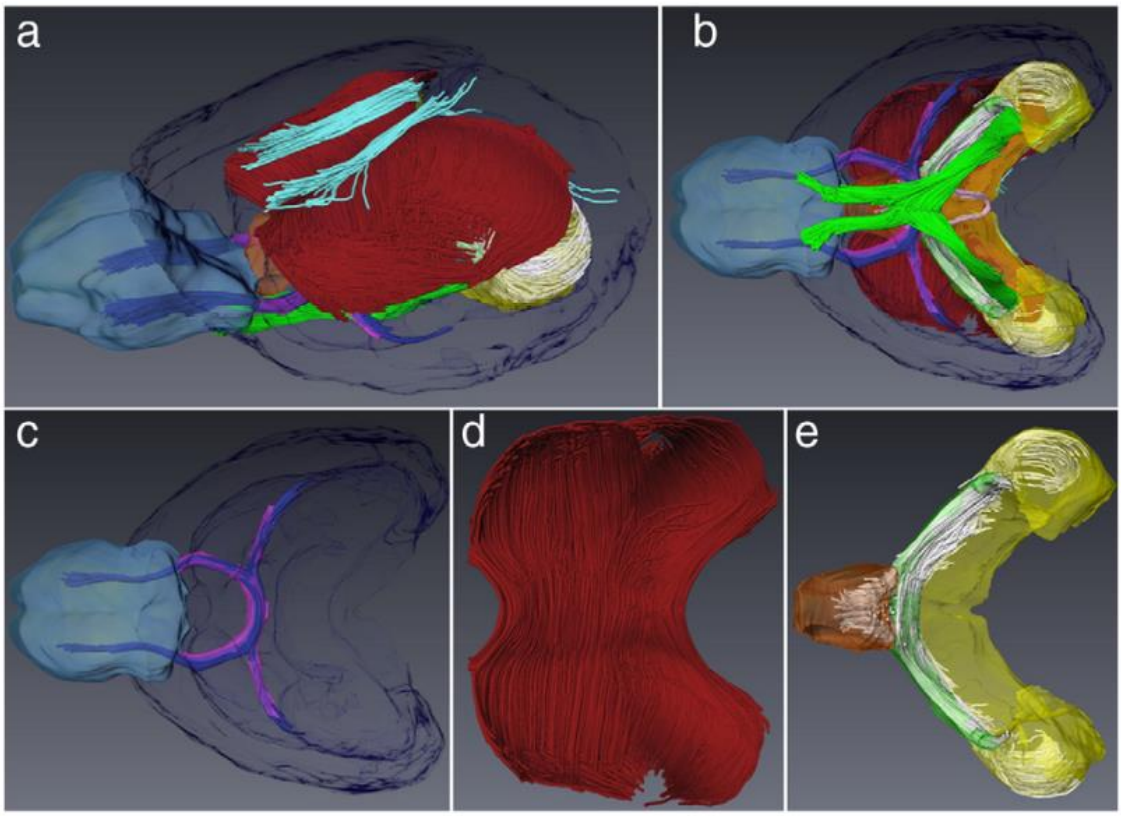

Figure 8. *Example of different views of a 3D reconstruction of some exemplary fiber tracts for a mouse model – Side view (a) and ventral view (b) of defined white matter regions. The displayed structures are: corpus callosum (red), cingulum (cyan), anterior commissure (blue), fimbria (white), optic tract (green), and habenular commissure (pink). In transparent colour are: olfactory bulbs (light blue), anterior commissure (purple), fimbria (green), hippocampus (yellow), septal nuclei (brown), and cerebral cortex (dark blue). Panels c to e show a magnified ventral view of the anterior commissure (c), corpus callosum (d), and fimbria (e). Adapted from Jiang et al., 2010.*

Reports on DTI of animal models demonstrate that axial diffusivity is sensitive to axonal injury, and radial diffusivity to myelin injury in certain models (Song et al., 2002; Song et al., 2003). A relation between DTI-based measurements and histology-based

measurements of axon and myelin pathology has also been found in mouse models (Budde et al., 2009), demonstrating the potential of this imaging technique in both the detection and monitoring of white matter pathology beyond the basic research.

In vivo mouse brain DTI can be performed, even having been successfully applied to the study of microstructures of embryonic and early postnatal mouse brains (Mori et al., 2001). However, its application is still limited in terms of range of mouse models. This is explained by the fact that several complex structures, including small white matter tracts in the thalamus, require a higher resolution imaging technique to be visualized. Furthermore, high resolution DTI of the *in vivo* brain calls for lengthier acquisition times, limiting the acquired data and making it more difficult for the mice to survive the MRI scans. *In vivo* DTI has therefore limited imaging resolution and is susceptible to subject motion (Wu et al., 2013; Zhang et al., 2011).

Ex vivo DTI, on the other hand, allows higher imaging resolution than in vivo DTI and is free of motion artefacts, even if less sensitive. While diffusivity seems to be reduced in *ex vivo* compared to *in vivo*, diffusion anisotropy in normal white matter structures did not seem to be affected by fixation. For white matter under pathological conditions however, paraformaldehyde (PFA) fixation can affect the DTI measurements' ability to detect pathology in certain models (Zhang et al., 2011).

The DTI tractography method has been validated with post-mortem anatomic and animal studies, showing compatibility (Jiang et al., 2010; Wakana et al., 2004).

3.2 Diffusion tensor imaging of the *Tsc2*$^{+/-}$ mouse model brain

In mouse models of TSC, loss-of-function mutations are associated with abnormal neuronal connectivity, including neuronal polarity, axon formation and guidance (Nie et al., 2010; Meikle et al., 2007; Choi et al., 2008). Regarding cell growth, mouse models have also shown the importance of TSC proteins in axonal, dendritic and synaptic development and function (Sahin, 2012). mTOR inhibitors have also shown to prevent, improve and stop seizures (Wong et al., 2010; Zheng et al., 2008), as well as improve learning and prevent autistic features (Ehninger et al., 2008; Tsai et al., 2012).

Social behaviour tests of *Tsc2*$^{+/-}$ mice demonstrated that loss of *Tsc2* in Purkinje cells (GABAergic inhibitory neurons located in the cerebellum) in a Tsc2-haploinsufficient

background causes autistic-like behavioural deficits. Hence, Purkinje cell loss and/or dysfunction may constitute a link between TSC and ASD (Reith et al., 2013).

Altered FA and MD in the anterior cingulate cortex and the hippocampus of the *Tsc2*$^{+/-}$ mice have been reported, suggesting an altered neural circuit. In addition, mTORC1 has also showed to be hyperactive in the cortex and hippocampus, which is in accordance with abnormal cortical myelination and increased glial fibrillary acidic protein expression in the hippocampal CA1 of *Tsc2*$^{+/-}$ mice. Thus, DTI has demonstrated to be sensitive to subtle alterations, namely in the *Tsc2*$^{+/-}$ mouse model (Hsieh et al., 2020).

The application of the DTI technique in a *Tsc2*$^{+/-}$ mouse model in more studies could aid the discovery of more links between the TSC pathology and brain alterations.

3.3 TSC2 neurochemical metabolism

In the human TSC2 mutation, both the DTI and the MRS were complementarily used to assess the relation between tubers and TSC (Ishikawa et al., 2018).

Metabolically, TSC patients have been shown to have altered levels of certain metabolites. In adults, a decrease of white matter NAA, as well an increase in Cho has been reported in TSC patients compared with reported values for healthy adults (Wu et al., 2013).

Changes in metabolic levels also seem to be related to the altered structural implications TSC. Cortical tubers have revealed increased mI/Cr ratio, and slightly decreased NAA/Cr and NAA/Cho ratios in TSC patients. Lac peaks may also be present in cortical tubers (Urkiewicz et al., 2006). A reduced level of NAA in cortical tuber seems to be common, possibly as a consequence of immature neurons and glia in tubers that do not express NAA, or perhaps caused by gliosis, a histological component of tubers (Mukonoweshuro et. al, 2001). SEGAs may show high Cho/Cr and low NAA/Cr ratios (Carvalho Neto et al., 2006).

Concerning the GABA neurotransmitter, dysfunction of tonic $GABA_BR$-mediated inhibition in the medial prefrontal cortex is hypothesized as a contributing factor to the development of ASD symptoms in TSC2 mice (Bassetti et al., 2020).

These findings demonstrate the utility of MRS as a non-invasive tool to investigate brain neurochemistry.

4 MATERIALS AND METHODS

The present study focuses on different brain regions. Imaging data were collected for six regions: prefrontal cortex, parieto-temporal cortex, amygdala, striatum, hippocampus, and cerebellum. Metabolic data were only available for four of these regions: prefrontal cortex, striatum, hippocampus, and cerebellum.

4.1 Study dataset

The image analyses portion of this study includes data from a total of 51 subjects. The mice differed among themselves in both sex and phenotype, resulting in four different subsets (Figure 9).

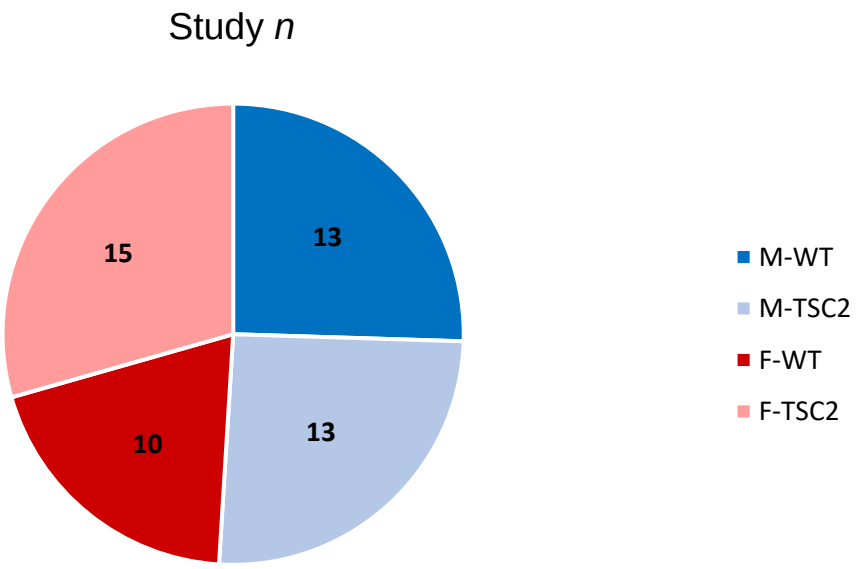

***Figure 9**. Distribution of the total of subjects in study among the different subsets – The subsets represented are: male wild-type mice (M-WT), male Tsc2$^{+/-}$ mice (M-TSC2), female wild-type mice (F-WT), and female Tsc2$^{+/-}$ mice (F-TSC2).*

For the data from ^{1}H-MRS, we analysed:

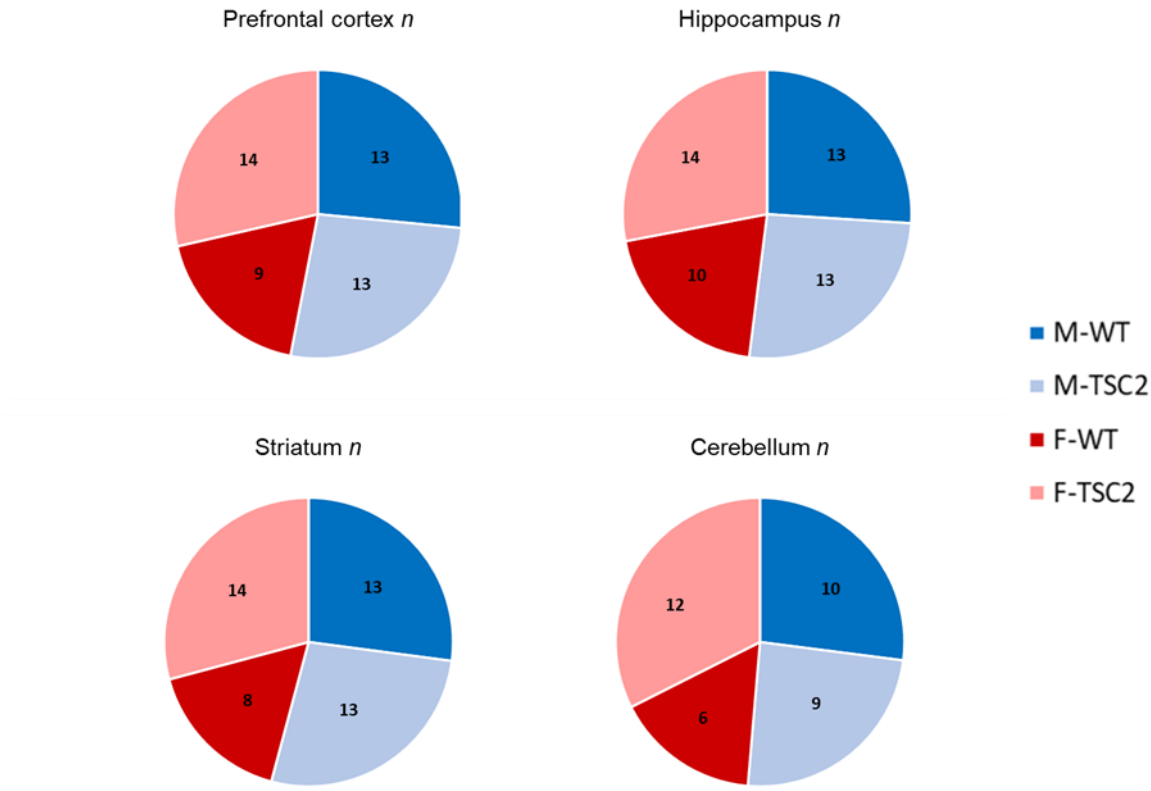

Figure 10. *Distribution of the total subjects in study in the prefrontal cortex, hippocampus, striatum, and cerebellum among the different subsets - The subsets represented are: male wild-type mice (M-WT), male Tsc2$^{+/-}$ mice (M-TSC2), female wild-type mice (F-WT), and female Tsc2$^{+/-}$ mice (F-TSC2).*

4.2 DTI data acquisition

4.2.1 DTI

The diffusion images were acquired using a 9.4T Bruker Biospin MR imaging system (with Paravision 6.0.1 software). Each DTI acquisition consisted of 22 slices, 0.5 mm thick encompassing the entire brain. The echo time was of 19.7806 ms and the repetition time 3000 ms. A HARDI scheme was used, and a total of 120 diffusion sampling directions were acquired. The in-plane resolution was 0.125 mm. The b-value was 686.225 s/mm2, and the b-table was checked by an automatic quality control routine to ensure its accuracy.

4.2.2 GQI

The restricted diffusion was quantified using restricted diffusion imaging. The diffusion data were reconstructed using generalized q-sampling imaging with a diffusion sampling length ratio of 1.

4.3 DTI processing and Tractography

DTI data were post-processed using DSI Studio (http://dsi-studio.labsolver.org). The raw data acquired were imported into DSI Studio.

The reconstruction from the acquired images was preceded by the setup of a mask, so as to filter out the background region, increase the reconstruction efficacy, and facilitate visualization. For each file, the mask was generated by several built-in functions, including: “thresholding”, generating an initial selection; “smoothing”, smoothing the mask contour; and “defragment”, filtering out small fragments. DTI reconstruction was then performed.

The obtained *.fib* file was imported to the Fiber Tracking part of the software. As no compatible atlas of the mouse model was available, each brain region was manually drawn. DTI statistics were exported for each region of interest (ROI) drawn. To execute the fiber tracking, additional complementary regions of avoidance (ROA) as well as *seed* regions were also defined. By selecting the ROI, ROA and seed for each region, fiber tracking was then performed. The ROI region filters in the tracts that pass through it, the ROA filters out, and the seed region places starting points that were chosen to be more at the centre of the desired region to ensure that tractography is only performed for the wanted region and not the entire brain. The statistics for the tracts were also exported.

4.4 GQI processing and Tractography

The protocol for GQI processing was the same as for the DTI processing, except GQI reconstruction was selected and a diffusion sampling length ratio of 1 was defined. This process is separate from the first DTI, as new regions had to be hand drawn because the previous ones could not be properly exported. For this reason, a parallel DTI based

on the same regions, and provided by the software simultaneously to the GQI, is used to compare metrics.

4.5 Spectroscopy

For localized ^{1}H magnetic resonance spectroscopy (^{1}H-MRS), data were collected in a volume of interest placed on the hippocampus, prefrontal cortex, striatum and cerebellum. B_0 map was acquired before spectroscopy, and shims were optimized through a mapshim voxel. Spectra were acquired using a point-resolved spectroscopy (PRESS) sequence with outer volume suppression (OVS) and VAPOR water suppression (Bottomley, 1987; Tkác et al., 1999). The following parameters were used: TR = 2500 ms, TE = 16,225 ms, number of averages = 720, 3 flip angles = 90°, 142°, 142°, bandwidth = 5000 Hz, number of acquired points = 2048 yielding a spectral resolution of 1.22 Hz/pt. Total acquisition time was 30 min. Before each spectrum, we acquired an unsuppressed water spectrum at the same voxel location (TE = 16,225 ms, TR = 2500 ms, 16 averages, scanning time = 40 s).

Data analysis of ^{1}H-MRS spectra was performed using linear combination modeling LCModel (Stephen Provencher Inc., Toronto, Canada) (Provencher, 2001). Metabolite quantification was performed applying the internal water reference method. Concentrations in millimole units were calculated for metabolites, and results are presented in institutional units (i.u.). Only metabolites with Cramér–Rao bounds < 20% were considered for statistical analysis.

4.7 Statistical analysis

4.7.1 Imaging data

After the data processing, outliers were identified and removed. The criteria used was the exclusive inclusion of data between the range of Mean ± 2*SD.

Subsequent statistical analysis was performed using the GraphPad Prism Software Version 9.2.0 (GraphPad Software, Inc., La Jolla, CA, USA). The data analysis concerning the four groups was done in a exploratory manner, for each region.

The Mann-Whitney's U-test was applied, and statistical significance was defined to $P<0.05$.

4.7.2 Metabolic data

For each region and each subject type, the mean and standard deviations for each metabolite were calculated, and values outside the Mean ± 2*SD were excluded.

Using the GraphPad Prism Software Version 9.2.0 (GraphPad Software, Inc., La Jolla, CA, USA), the Mann-Whitney's U-test was applied, and statistical significance was defined to $P<0.05$.

Combining the imaging data and the metabolic data, correlation was checked for each subset, for each region, in an exploratory manner. Through the aforementioned software, Pearson (or Spearman, if normality is absent) r values and two-tailed P-values were collected. Variable pairs with both significant P-value ($P<0.05$) and strong correlation ($|Pearson\ r|>0.7$) were selected.

5 RESULTS

5.1 DTI tables

In this section, the main findings of the analysis on the region and tract-based DTI are presented. Regional DTI uses the defined region to sample the voxels, whereas tractional uses tracts.

Table 1. *DTI metrics in the prefrontal cortex - Median and interquartile range (Median ± IQR) values on the regional-based and tract-based DTI metrics for the prefrontal cortex of the four subsets: male wild-type mice (M-WT), male Tsc2$^{+/-}$ mice (M-TSC2), female wild-type mice (F-WT), and female Tsc2$^{+/-}$ mice (F-TSC2). Diffusivity measures - AD, MD and RD - in 10^{-3} mm^2/s; FA is dimensionless.*

PFC	**M-WT**	**M-TSC2**	**F-WT**	**F-TSC2**
FA-reg	0.22 ± 0.01	0.21 ± 0.02	0.21 ± 0.01	0.23 ± 0.02
MD-reg	0.69 ± 0.02	0.68 ± 0.03	0.68 ± 0.02	0.68 ± 0.02
AD-reg	0.84 ± 0.03	0.83 ± 0.03	0.83 ± 0.02	0.83 ± 0.01
RD-reg	0.60 ± 0.02	0.60 ± 0.02	0.60 ± 0.02	0.60 ± 0.02
FA-tracts	0.24 ± 0.03	0.22 ± 0.03	0.23 ± 0.03	0.24 ± 0.02
MD-tracts	0.68 ± 0.04	0.67 ± 0.02	0.68 ± 0.02	0.66 ± 0.01
AD-tracts	0.84 ± 0.02	0.84 ± 0.02	0.82 ± 0.03	0.84 ± 0.01
RD-tracts	0.58 ± 0.04	0.59 ± 0.03	0.59 ± 0.02	0.58 ± 0.02

Table 2. *DTI metrics in the hippocampus - Median and interquartile range (Median ± IQR) values on the regional-based and tract-based DTI metrics for the hippocampus of the four subsets: male wild-type mice (M-WT), male Tsc2$^{+/-}$ mice (M-TSC2), female wild-type mice (F-WT), and female Tsc2$^{+/-}$ mice (F-TSC2). Diffusivity measures - AD, MD and RD - in 10^{-3} mm^2/s; FA is dimensionless.*

HIP	**M-WT**	**M-TSC2**	**F-WT**	**F-TSC2**
FA-reg	0.26 ± 0.03	0.25 ± 0.01	0.25 ± 0.02	0.26 ± 0.03
MD-reg	0.85 ± 0.09	0.86 ± 0.03	0.82 ± 0.03	0.86 ± 0.07
AD-reg	1.08 ± 0.08	1.08 ± 0.04	1.05 ± 0.03	1.08 ± 0.08
RD-reg	0.73 ± 0.09	0.75 ± 0.03	0.71 ± 0.03	0.74 ± 0.06
FA-tracts	0.23 ± 0.03	0.30 ± 0.02	0.29 ± 0.04	0.30 ± 0.02
MD-tracts	1.01 ± 0.09	1.01 ± 0.02	0.97 ± 0.05	0.96 ± 0.08
AD-tracts	1.37 ± 0.08	1.36 ± 0.08	1.27 ± 0.07	1.29 ± 0.11
RD-tracts	0.81 ± 0.09	0.84 ± 0.07	0.81 ± 0.04	0.80 ± 0.07

Table 3. *DTI metrics in the striatum - Median and interquartile range (Median ± IQR) values on the regional-based and tract-based DTI metrics for the striatum of the four subsets: male wild-type mice (M-WT), male Tsc2$^{+/-}$ mice (M-TSC2), female wild-type mice (F-WT), and female Tsc2$^{+/-}$ mice (F-TSC2). Diffusivity measures - AD, MD and RD - in 10^{-3} mm^2/s; FA is dimensionless.*

STR	**M-WT**	**M-TSC2**	**F-WT**	**F-TSC2**
FA-reg	0.26 ± 0.01	0.24 ± 0.01	0.23 ± 0.01	0.25 ± 0.03
MD-reg	0.70 ± 0.02	0.72 ± 0.03	0.70 ± 0.03	0.70 ± 0.03
AD-reg	0.88 ± 0.02	0.90 ± 0.02	0.87 ± 0.04	0.88 ± 0.05
RD-reg	0.61 ± 0.02	0.62 ± 0.02	0.61 ± 0.01	0.61 ± 0.03
FA-tracts	0.25 ± 0.03	0.24 ± 0.02	0.23 ± 0.02	0.25 ± 0.04
MD-tracts	0.69 ± 0.03	0.70 ± 0.03	0.69 ± 0.03	0.69 ± 0.02
AD-tracts	0.87 ± 0.04	0.87 ± 0.03	0.85 ± 0.04	0.85 ± 0.03
RD-tracts	0.61 ± 0.02	0.61 ± 0.04	0.61 ± 0.03	0.61 ± 0.03

Table 4. *DTI metrics in the cerebellum - Median and interquartile range (Median ± IQR) values on the regional-based and tract-based DTI metrics for the cerebellum of the four subsets: male wild-type mice (M-WT), male Tsc2$^{+/-}$ mice (M-TSC2), female wild-type mice (F-WT), and female Tsc2$^{+/-}$ mice (F-TSC2). Diffusivity measures - AD, MD and RD - in 10^{-3} mm^2/s; FA is dimensionless.*

CRBL	**M-WT**	**M-TSC2**	**F-WT**	**F-TSC2**
FA-reg	0.27 ± 0.04	0.27 ± 0.03	0.27 ± 0.01	0.27 ± 0.02
MD-reg	0.71 ± 0.06	0.71 ± 0.06	0.69 ± 0.02	0.68 ± 0.02
AD-reg	0.90 ± 0.07	0.91 ± 0.07	0.87 ± 0.04	0.88 ± 0.03
RD-reg	0.61 ± 0.04	0.61 ± 0.05	0.59 ± 0.03	0.59 ± 0.02
FA-tracts	0.25 ± 0.02	0.26 ± 0.03	0.25 ± 0.01	0.26 ± 0.05
MD-tracts	0.65 ± 0.04	0.65 ± 0.03	0.64 ± 0.05	0.64 ± 0.06
AD-tracts	0.81 ± 0.05	0.82 ± 0.12	0.80 ± 0.05	0.80 ± 0.07
RD-tracts	0.58 ± 0.05	0.56 ± 0.06	0.56 ± 0.05	0.56 ± 0.07

Table 5. *DTI metrics in the parieto-temporal cortex - Median and interquartile range (Median ± IQR)values on the regional-based and tract-based DTI metrics for the parieto-temporal cortex of the four: male wild-type mice (M-WT), male Tsc2$^{+/-}$ mice (M-TSC2), female wild-type mice (F-WT), and female Tsc2$^{+/-}$ mice (F-TSC2). Diffusivity measures - AD, MD and RD - in 10^{-3} mm^2/s; FA is dimensionless.*

PAR	**M-WT**	**M-TSC2**	**F-WT**	**F-TSC2**
FA-reg	0.23 ± 0.04	0.21 ± 0.01	0.21 ± 0.01	0.21 ± 0.01
MD-reg	0.66 ± 0.04	0.67 ± 0.01	0.67 ± 0.01	0.67 ± 0.01
AD-reg	0.81 ± 0.03	0.82 ± 0.02	0.81 ± 0.01	0.81 ± 0.02
RD-reg	0.59 ± 0.04	0.60 ± 0.01	0.60 ± 0.00	0.60 ± 0.02
FA-tracts	0.22 ± 0.05	0.20 ± 0.02	0.21 ± 0.03	0.21 ± 0.02
MD-tracts	0.66 ± 0.05	0.66 ± 0.01	0.67 ± 0.02	0.66 ± 0.03
AD-tracts	0.79 ± 0.03	0.80 ± 0.03	0.80 ± 0.05	0.80 ± 0.03
RD-tracts	0.58 ± 0.07	0.59 ± 0.01	0.59 ± 0.02	0.59 ± 0.02

Table 6. *DTI metrics in the amygdala - Median and interquartile range (Median ± IQR) values on the regional-based and tract-based DTI metrics for the amygdala of the four subsets: male wild-type mice (M-WT), male Tsc2$^{+/-}$ mice (M-TSC2), female wild-type mice (F-WT), and female Tsc2$^{+/-}$ mice (F-TSC2). Diffusivity measures - AD, MD and RD - in 10^{-3} mm^2/s; FA is dimensionless.*

AMYG	**M-WT**	**M-TSC2**	**F-WT**	**F-TSC2**
FA-reg	0.28 ± 0.02	0.28 ± 0.01	0.28 ± 0.01	0.29 ± 0.02
MD-reg	0.67 ± 0.05	0.73 ± 0.02	0.73 ± 0.01	0.74 ± 0.02
AD-reg	0.86 ± 0.05	0.94 ± 0.02	0.94 ± 0.02	0.96 ± 0.03
RD-reg	0.62 ± 0.02	0.62 ± 0.02	0.63 ± 0.00	0.63 ± 0.03
FA-tracts	0.27 ± 0.03	0.27 ± 0.03	0.27 ± 0.03	0.27 ± 0.01
MD-tracts	0.67 ± 0.05	0.70 ± 0.03	0.71 ± 0.02	0.70 ± 0.03
AD-tracts	0.86 ± 0.05	0.89 ± 0.08	0.90 ± 0.03	0.89 ± 0.02
RD-tracts	0.58 ± 0.05	0.60 ± 0.03	0.61 ± 0.03	0.60 ± 0.03

5.2 Significant DTI changes analysis

For each region, Mann-Whitney statistical test results of the comparison of DTI metrics between the four subsets, applied in pairs, are presented using boxplots. Significant differences are marked with the respective P-values.

Prefrontal cortex

In the prefrontal cortex, region-based DTI showed altered FA (P=0.0002) between male wild-type mice (n=7) and female wild-type mice (n=9), as well as between female wild-type mice and female *Tsc2*$^{+/-}$ mice (n=14), with P=0.0106 (Figure 11a). Tract-based DTI showed significance (P=0.0222) between male *Tsc2*$^{+/-}$ mice (n=13) and female *Tsc2*$^{+/-}$

mice (n=14), as well as between female wild-type (n=9) and female *Tsc2*$^{+/-}$ mice, with P=0.0130 (Figure 11b).

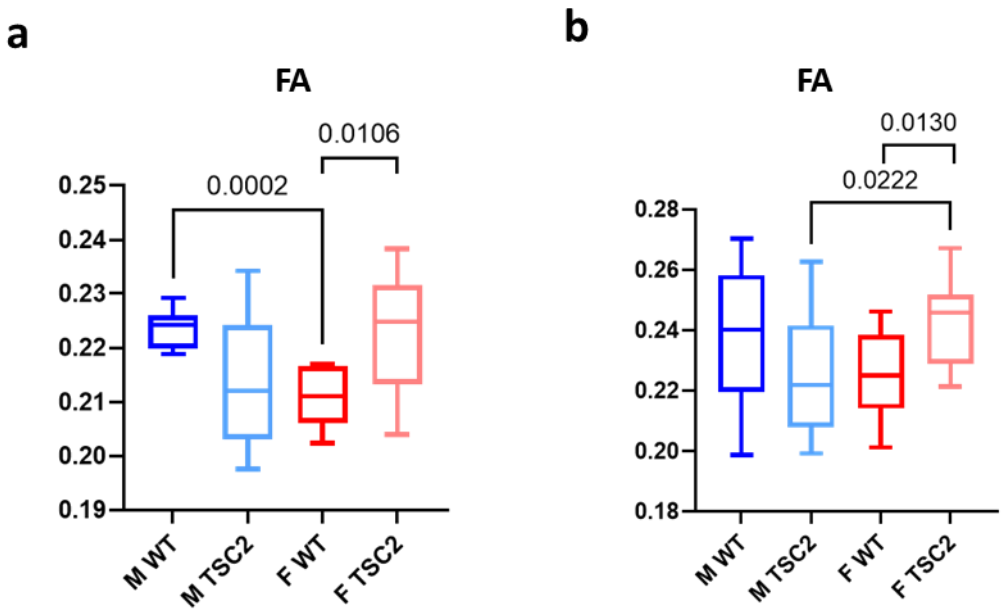

***Figure 11**. DTI changes in the prefrontal cortex - Region-based (a) and tract-based (b) FA boxplots for the prefrontal cortex. Mann-Whitney significant changes are marked with the respective P-value.*

Hippocampus

In the hippocampus, tract-based DTI showed MD and AD alterations (P=0.0266 and P=0.0117, respectively) between male wild-type (n=10) and female wild-type mice (n=9) (Figure 12a and 12b).

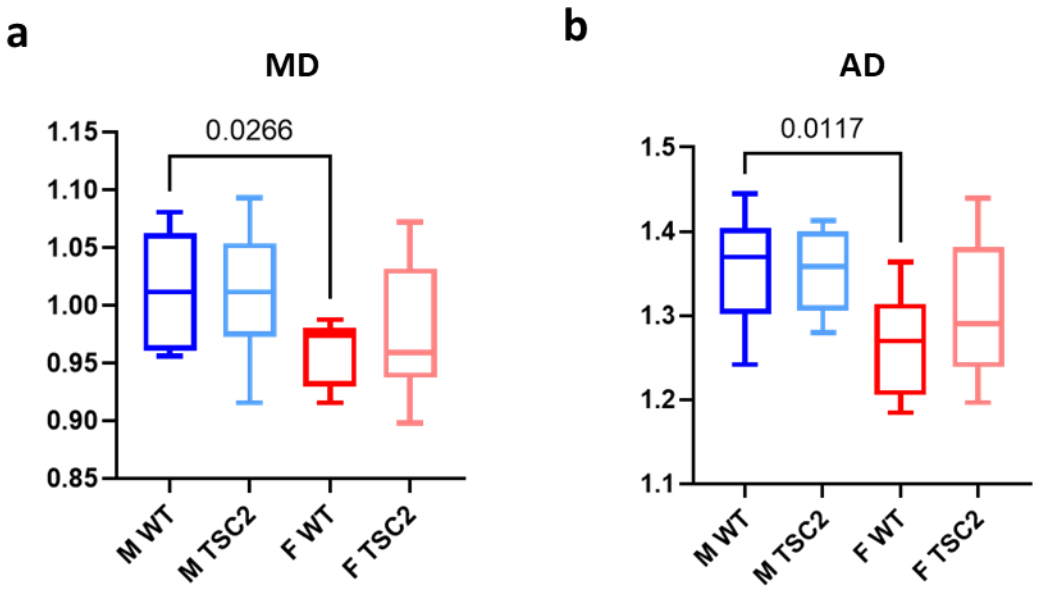

***Figure 12**. DTI changes in the hippocampus - Tract-based MD (a) and AD (b) boxplots for the hippocampus. Mann-Whitney significant changes are marked with the respective P-value.*

Striatum

In the striatum, altered region-based FA (P=0.0060) appeared between male wild-type (n=13) and female wild-type mice (n=8) (Figure 13), without changes in others parameters analysed.

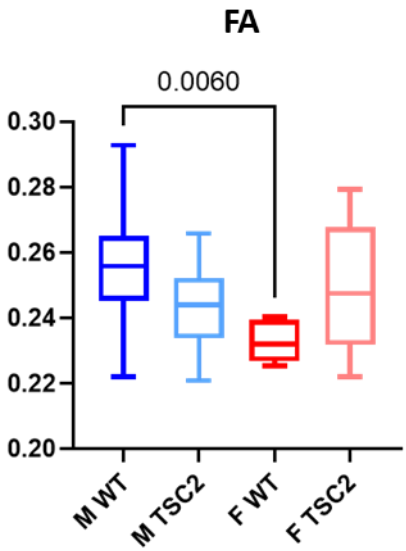

***Figure 13**. DTI changes in the striatum - Region-based FA boxplots for the striatum. Mann-Whitney significant changes are marked with the respective P-value.*

Cerebellum

In the cerebellum, region-based MD and RD appeared significant (P=0.0298 and P=0.0345, respectively) between male *Tsc2*$^{+/-}$ mice (n=12) and female *Tsc2*$^{+/-}$ mice (n=13) (Figure 14a and 14b).

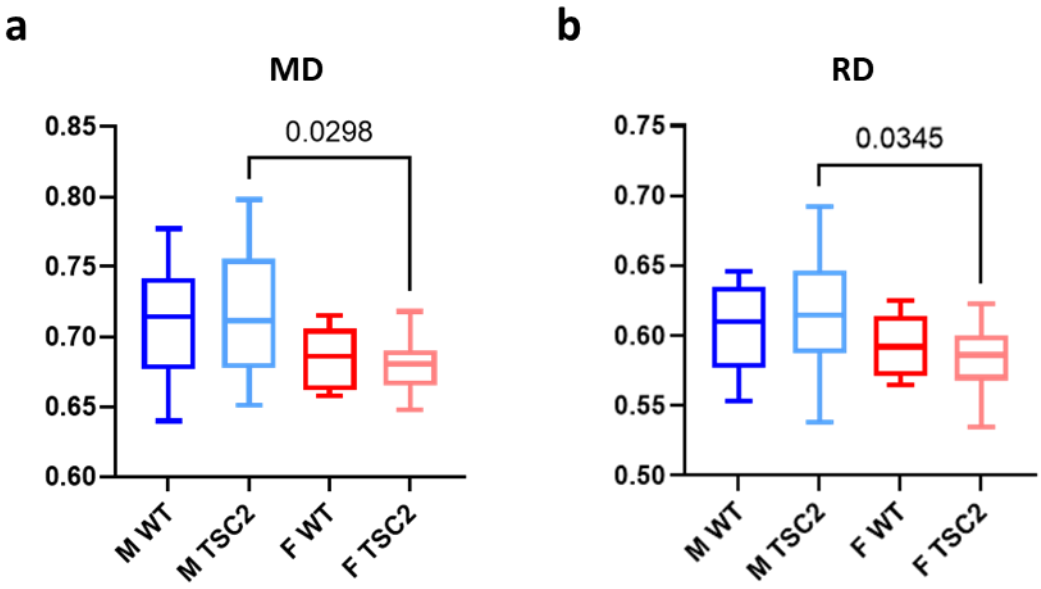

Figure 14. *DTI changes in the cerebellum - Region-based MD (a) and RD (b) boxplots for the striatum. Mann-Whitney significant changes are marked with the respective P-value.*

Parieto-temporal cortex

In the parieto-temporal cortex, tract-based FA was altered (P=0.0202) between male *Tsc2*$^{+/-}$ (n=12) and female *Tsc2*$^{+/-}$ mice (n=14) (Figure 15).

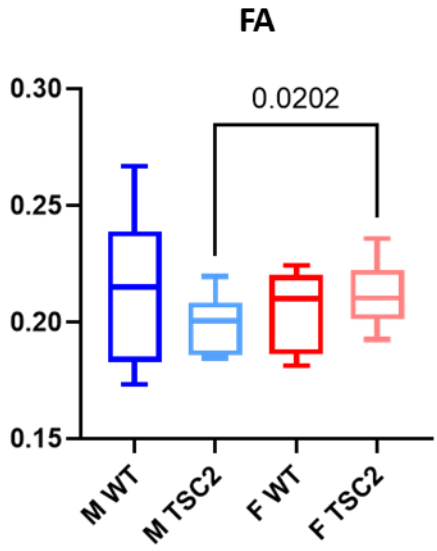

***Figure 15**. DTI changes in the parieto-temporal cortex - Tract-based FA boxplots for the striatum. Mann-Whitney significant changes are marked with the respective P-value.*

Amygdala

In the amygdala, region-based MD showed to be altered (P<0.0001) between male wild-type (n=11) and *Tsc2*$^{+/-}$ mice (n=9), between male wild-type and female wild-type mice (n=9), with P<0.0001, and between male *Tsc2*$^{+/-}$ and female *Tsc2*$^{+/-}$ mice (n=15), with P=0.0349 (Figure 16a). Tract-based MD showed alterations (P=0.0225) between male wild-type (n=11) and male *Tsc2*$^{+/-}$ mice (n=12), as well as between male wild-type and female wild-type mice (n=9), with P=0.0031 (Figure 16b).

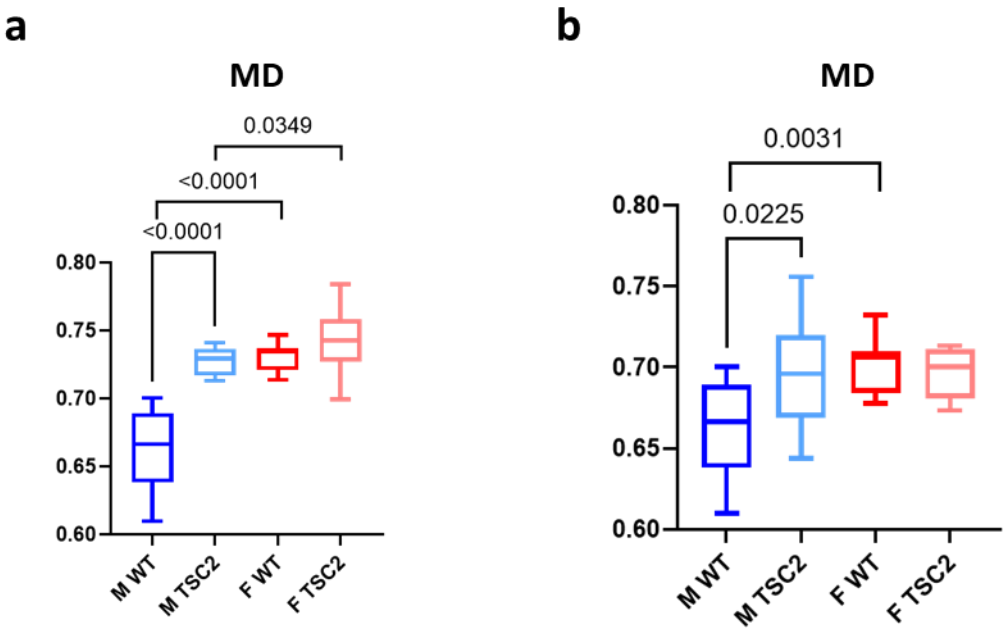

***Figure 16**. MD changes in the amygdala - Region-based (a) and tract-based (b) MD boxplots for the amygdala. Mann-Whitney significant changes are marked with the respective P-value.*

Region-based AD showed also changes (P<0.0001) between male wild-type (n=11) and *Tsc2*$^{+/-}$ mice (n=11) and between male wild-type and female wild-type mice (n=9), with P<0.0001 (Figure 17a). On the other hand, RD between male *Tsc2*$^{+/-}$ (n=9) and female *Tsc2*$^{+/-}$ mice (n=15) was altered (P=0.0409) (Figure 17c). Tract-based AD showed alterations (P=0.0430) between male wild-type (n=11) and female wild-type mice (n=10) (Figure 17b).

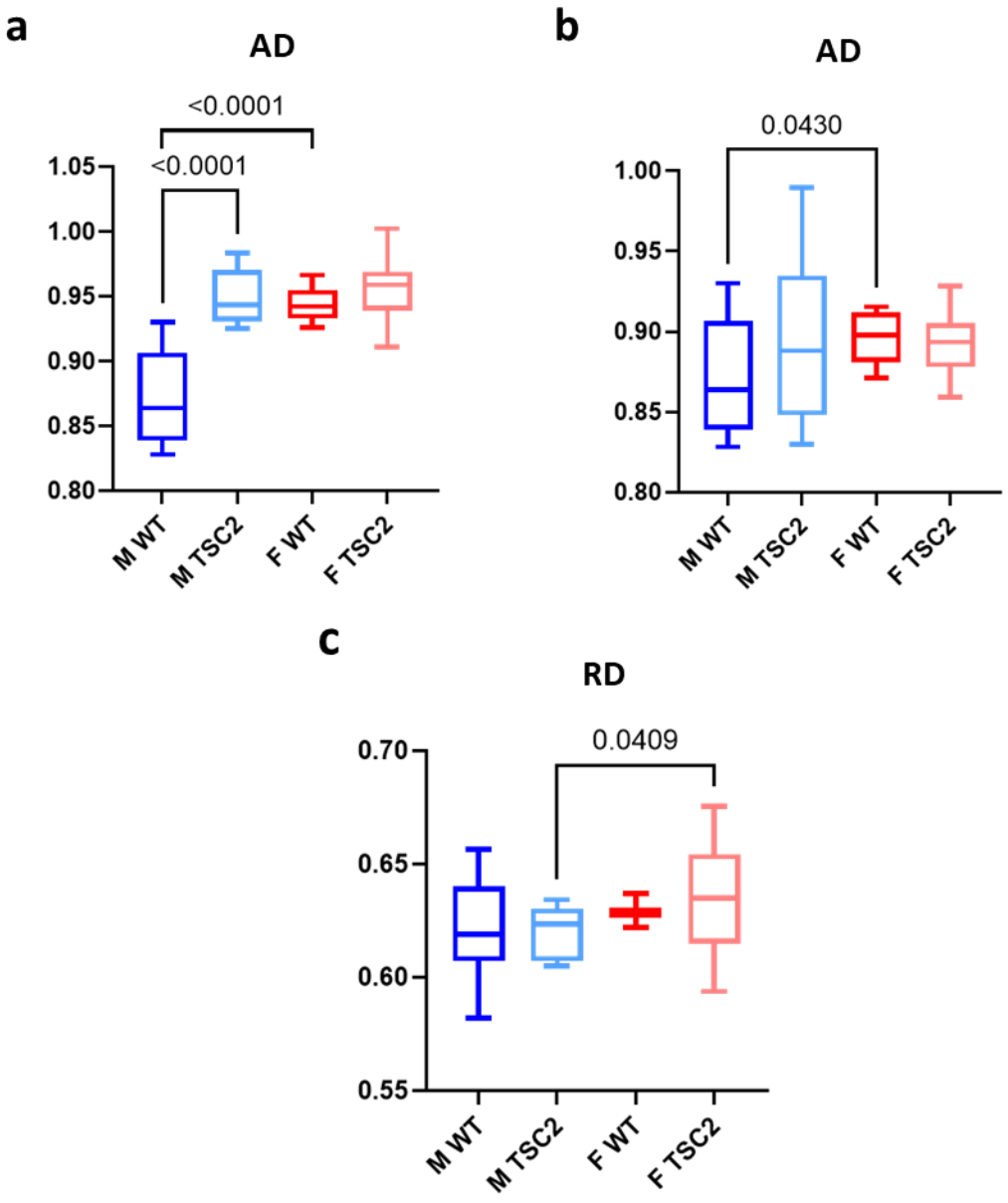

***Figure 17**. AD and RD changes in the amygdala - Region-based (a) and tract-based (b) AD boxplots, and region-based RD boxplot (c) for the amygdala. Mann-Whitney significant changes are marked with the respective P-value.*

5.3 GQI measures tables

Following, the main findings of the analysis on the tract-based GQI analysis, as well as the tract-based DTI performed in parallel, are presented.

Table 7. *GQI and DTI metrics in the prefrontal cortex - Median and interquartile range (Median ± IQR) values on the tract-based DTI and GQI metrics for the prefrontal cortex of the four subsets: male wild-type mice (M-WT), male Tsc2$^{+/-}$ mice (M-TSC2), female wild-type mice (F-WT), and female Tsc2$^{+/-}$ mice (F-TSC2). Diffusivity measures - AD, MD and RD - in 10^{-3} mm^2/s; NQA, GFA, ISO and FA are dimensionless.*

PFC	**M-WT**	**M-TSC2**	**F-WT**	**F-TSC2**
NQA	0.20 ± 0.06	0.19 ± 0.04	0.19 ± 0.05	0.20 ± 0.05
GFA	0.01 ± 0.00	0.01 ± 0.00	0.01 ± 0.00	0.01 ± 0.00
ISO	0.27 ± 0.15	0.27 ± 0.33	0.20 ± 0.01	0.23 ± 0.04
FA	0.24 ± 0.02	0.22 ± 0.03	0.22 ± 0.03	0.24 ± 0.02
MD	0.67 ± 0.03	0.67 ± 0.01	0.67 ± 0.02	0.67 ± 0.01
AD	0.83 ± 0.04	0.83 ± 0.02	0.82 ± 0.02	0.84 ± 0.02
RD	0.58 ± 0.03	0.59 ± 0.02	0.59 ± 0.02	0.58 ± 0.02

Table 8. *GQI and DTI metrics in the hippocampus - Median and interquartile range (Median ± IQR) values on the tract-based DTI and GQI metrics for the hippocampus of the four subsets: male wild-type mice (M-WT), male Tsc2$^{+/-}$ mice (M-TSC2), female wild-type mice (F-WT), and female Tsc2$^{+/-}$ mice (F-TSC2). Diffusivity measures - AD, MD and RD - in 10^{-3} mm^2/s; NQA, GFA, ISO and FA are dimensionless.*

HIP	M-WT	M-TSC2	F-WT	F-TSC2
NQA	0.22 ± 0.09	0.22 ± 0.04	0.23 ± 0.07	0.22 ± 0.10
GFA	0.02 ± 0.00	0.02 ± 0.00	0.02 ± 0.00	0.02 ± 0.00
ISO	0.23 ± 0.10	0.19 ± 0.26	0.15 ± 0.02	0.17 ± 0.02
FA	0.28 ± 0.05	0.28 ± 0.02	0.29 ± 0.04	0.30 ± 0.02
MD	1.02 ± 0.10	1.02 ± 0.09	1.00 ± 0.06	1.02 ± 0.10
AD	1.35 ± 0.14	1.39 ± 0.12	1.37 ± 0.13	1.36 ± 0.08
RD	0.84 ± 0.10	0.88 ± 0.09	0.84 ± 0.02	0.83 ± 0.09

Table 9. *GQI and DTI metrics in the striatum - Median and interquartile range (Median ± IQR) values on the tract-based DTI and GQI metrics for the striatum of the four subsets: male wild-type mice (M-WT), male Tsc2$^{+/-}$ mice (M-TSC2), female wild-type mice (F-WT), and female Tsc2$^{+/-}$ mice (F-TSC2). Diffusivity measures - AD, MD and RD - in 10^{-3} mm^2/s; NQA, GFA, ISO and FA are dimensionless.*

STR	M-WT	M-TSC2	F-WT	F-TSC2
NQA	0.14 ± 0.05	0.20 ± 0.09	0.14 ± 0.04	0.14 ± 0.04
GFA	0.01 ± 0.00	0.01 ± 0.00	0.01 ± 0.00	0.01 ± 0.00
ISO	0.19 ± 0.07	0.20 ± 0.25	0.15 ± 0.01	0.18 ± 0.04
FA	0.20 ± 0.03	0.22 ± 0.04	0.21± 0.07	0.21 ± 0.05
MD	0.66 ± 0.02	0.66 ± 0.02	0.65 ± 0.07	0.66 ± 0.03
AD	0.82 ± 0.05	0.81 ± 0.07	0.80 ± 0.05	0.81 ± 0.06
RD	0.66 ± 0.03	0.56 ± 0.06	0.55 ± 0.04	0.56 ± 0.08

***Table 10**. GQI and DTI metrics in the cerebellum - Median and interquartile range (Median ± IQR) values on the tract-based DTI and GQI metrics for the prefrontal cortex of the four subsets: male wild-type mice (M-WT), male Tsc2$^{+/-}$ mice (M-TSC2), female wild-type mice (F-WT), and female Tsc2$^{+/-}$ mice (F-TSC2). Diffusivity measures - AD, MD and RD - in 10^{-3} mm^2/s; NQA, GFA, ISO and FA are dimensionless.*

Cerebellum	M-WT	M-TSC2	F-WT	F-TSC2
NQA	0.15 ± 0.05	0.15 ± 0.04	0.15 ± 0.00	0.15 ± 0.06
GFA	0.01 ± 0.00	0.01 ± 0.00	0.01 ± 0.00	0.01 ± 0.00
ISO	0.19 ± 0.07	0.16 ± 0.03	0.15 ± 0.04	0.14 ± 0.04
FA	0.20 ± 0.03	0.22 ± 0.04	0.21 ± 0.07	0.21 ± 0.05
MD	0.66 ± 0.02	0.66 ± 0.02	0.65 ± 0.06	0.66 ± 0.03
AD	0.82 ± 0.05	0.81 ± 0.07	0.80 ± 0.05	0.81 ± 0.06
RD	0.56 ± 0.03	0.56 ± 0.06	0.55 ± 0.04	0.56 ± 0.08

***Table 11.** GQI and DTI metrics in the parieto-temporal cortex - Median and interquartile range (Median ± IQR) values on the tract-based DTI and GQI metrics for the parieto-temporal cortex of the four subsets: male wild-type mice (M-WT), male Tsc2$^{+/-}$ mice (M-TSC2), female wild-type mice (F-WT), and female Tsc2$^{+/-}$ mice (F-TSC2). Diffusivity measures - AD, MD and RD - in 10^{-3} mm^2/s; NQA, GFA, ISO and FA are dimensionless.*

Par	M-WT	M-TSC2	F-WT	F-TSC2
NQA	0.15 ± 0.06	0.17 ± 0.03	0.14 ± 0.05	0.17 ± 0.05
GFA	0.01 ± 0.00	0.01 ± 0.00	0.01 ± 0.00	0.01 ± 0.00
ISO	0.31 ± 0.15	0.26 ± 0.31	0.20 ± 0.01	0.22 ± 0.07
FA	0.21 ± 0.04	0.19 ± 0.02	0.20 ± 0.03	0.20 ± 0.01
MD	0.65 ± 0.04	0.66 ± 0.16	0.66 ± 0.02	0.66 ± 0.02
AD	0.79 ± 0.03	0.80 ± 0.03	0.80 ± 0.05	0.80 ± 0.02
RD	0.59 ± 0.06	0.59 ± 0.01	0.59 ± 0.02	0.59 ± 0.02

Table 12. *GQI and DTI metrics in the amygdala - Median and interquartile range (Median ± IQR) values on the tract-based DTI and GQI metrics for the amygdala the four subsets: male wild-type mice (M-WT), male Tsc2$^{+/-}$ mice (M-TSC2), female wild-type mice (F-WT), and female Tsc2$^{+/-}$ mice (F-TSC2). Diffusivity measures - AD, MD and RD - in 10^{-3} mm^2/s; NQA, GFA, ISO and FA are dimensionless.*

Amygdala	M-WT	M-TSC2	F-WT	F-TSC2
NQA	0.16 ± 0.07	0.15 ± 0.02	0.15 ± 0.05	0.14 ± 0.05
GFA	0.02 ± 0.00	0.02 ± 0.00	0.01 ± 0.00	0.01 ± 0.00
ISO	0.16 ± 0.07	0.15 ± 0.24	0.12 ± 0.02	0.14 ± 0.00
FA	0.26 ± 0.03	0.26 ± 0.02	0.27 ± 0.03	0.27 ± 0.01
MD	0.67 ± 0.02	0.68 ± 0.03	0.71 ± 0.03	0.70 ± 0.02
AD	0.87 ± 0.05	0.88 ± 0.04	0.90 ± 0.02	0.89 ± 0.02
RD	0.58 ± 0.05	0.59 ± 0.03	0.61 ± 0.04	0.59 ± 0.02

5.4 Significant changes analysis

Mann-Whitney statistical test results of the comparison of GQI and DTI metrics between the four subsets are presented using boxplots. Significant differences are marked with the respective P-values.

Prefrontal cortex

In the prefrontal cortex, FA showed significant differences (P=0.0160) between male wild-type (n=13) and male *Tsc2*$^{+/-}$ mice (n=12), between male wild-type and female wild-type (n=9; P=0.0184), between male (n=12) and female *Tsc2*$^{+/-}$ mice (n=14; P=0.0145) and changes (P=0.0158) between female wild-type and female *Tsc2*$^{+/-}$ mice (Figure 18a). Concerning AD, it was changed (P=0.0491) between female wild-type (n=9) and female *Tsc2*$^{+/-}$ mice (n=12) (Figure 18b). GFA showed also significant differences between male wild-type (n=10) and male *Tsc2*$^{+/-}$ mice (n=13; P=0.0015), between male wild-type and female wild-type (n=9; P=0.0041), between male (n=13) and female *Tsc2*$^{+/-}$ mice (n=14; P=0.00255) and between female wild-type and female *Tsc2*$^{+/-}$ mice (P=0.0327) (Figure 18c). Further, changes in ISO it was observed between male (n=12) and female wild-

type mice (n=10; P=0.0071) between male (n=13) and female *Tsc2*$^{+/-}$ mice (n=14), with P=0.0377 and between female wild-type and *Tsc2*$^{+/-}$ mice, P=0.0185 (Figure 18d).

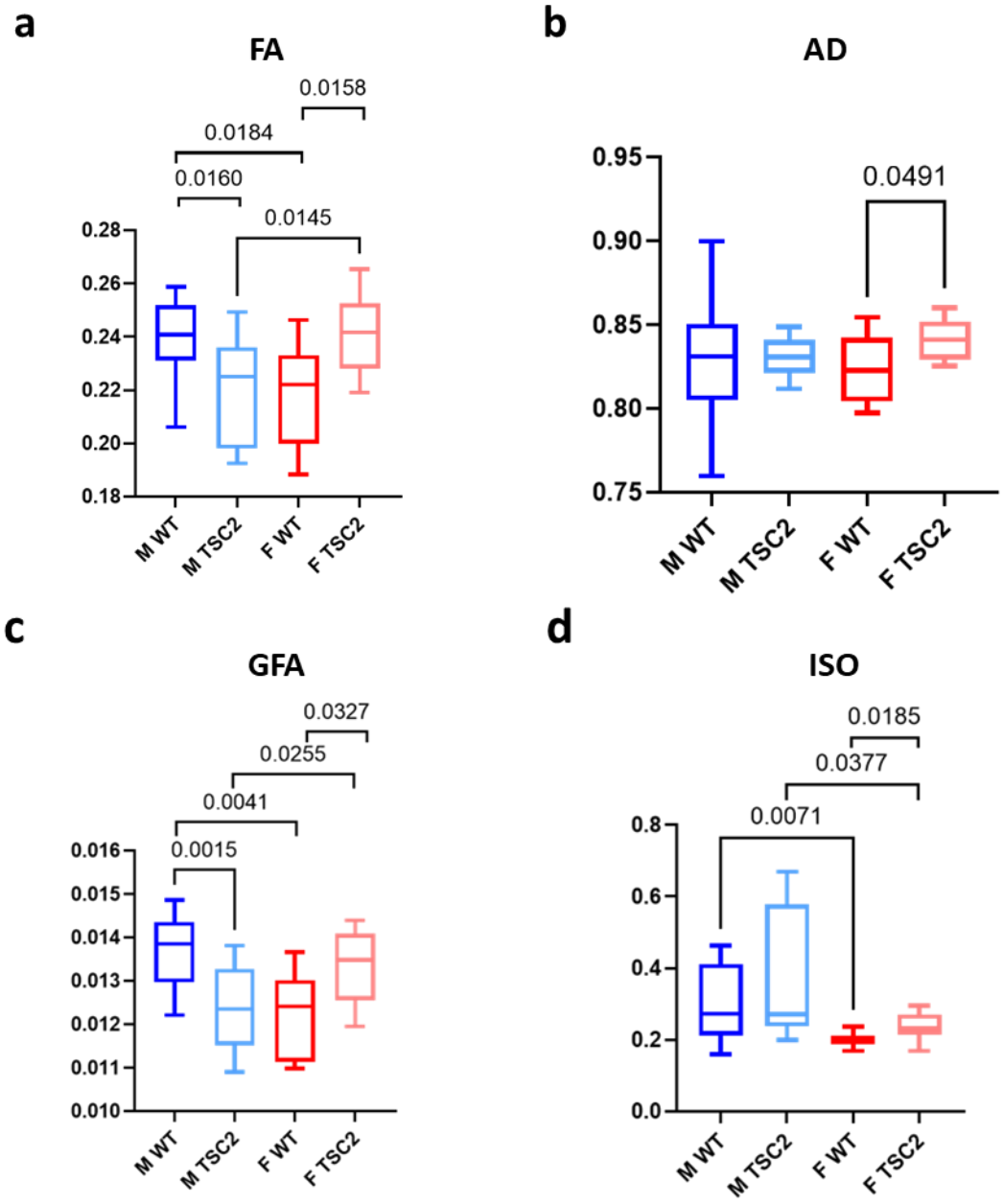

***Figure 18**. DTI and GQI changes in the prefrontal cortex - FA (a), AD (b), GFA (c) and ISO (d) boxplots for the prefrontal cortex. Mann-Whitney significant changes are marked with the respective P-value.*

Hippocampus

In the hippocampus, changes occurred only in ISO between male (n=13) and female wild-type mice (n=10; P=0.0147) and between male (n=13) and female *Tsc2*$^{+/-}$ mice (n=14), P=0.0168 (Figure 19).

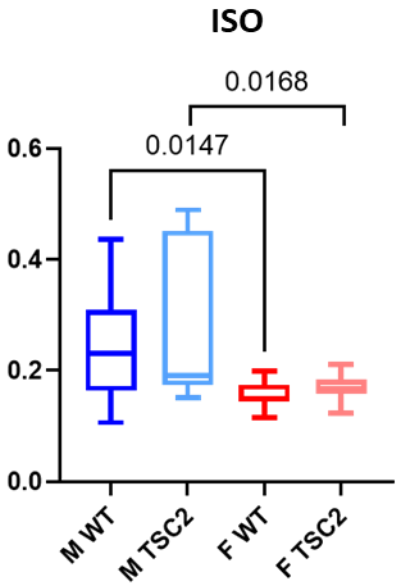

***Figure 19**. GQI changes in the hippocampus - ISO boxplots for the hippocampus. Mann-Whitney significant changes are marked with the respective P-value.*

Striatum

In the striatum, NQA is significant (P=0.0073) between male wild-type (n=13) and *Tsc2*$^{+/-}$ mice (n=11); and between male and female *Tsc2*$^{+/-}$ mice (n=14), P=0.0018 (Figure 20a). ISO showed changes (P=0.0465) between male (n=11) and female wild-type mice (n=9); and between male (n=13) and female *Tsc2*$^{+/-}$ mice (n=14), with P=0.0222 (Figure 20b).

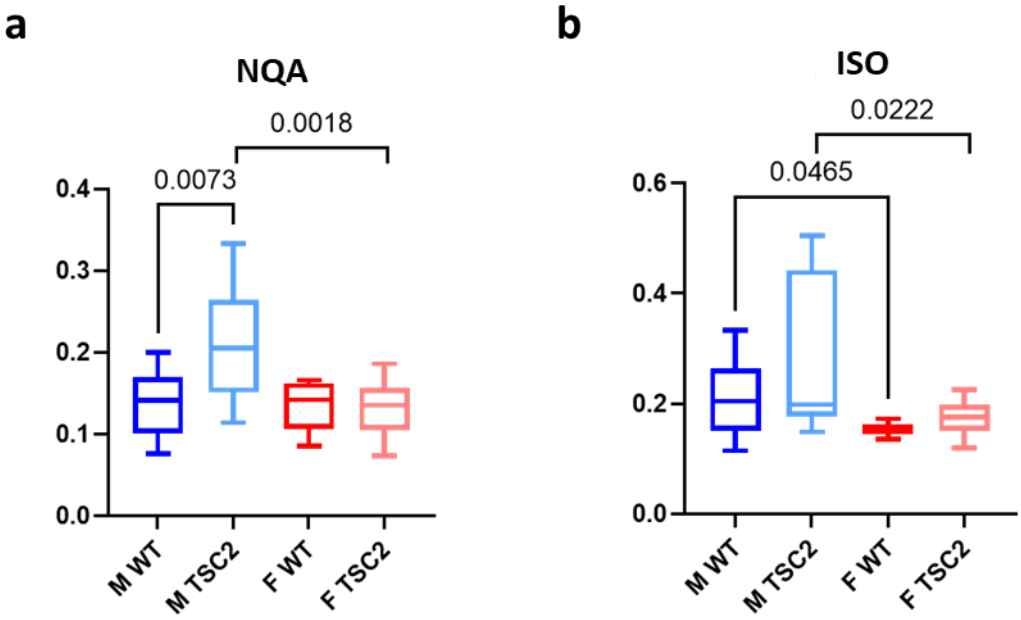

***Figure 20**. GQI changes in the striatum - NQA (a) and ISO (b) boxplots for the striatum. Mann-Whitney significant changes are marked with the respective P-value.*

Cerebellum

In the cerebellum, changes were shown (P=0.0184) between male (n=12) and female wild-type mice (n=19) in ISO parameter (Figure 21).

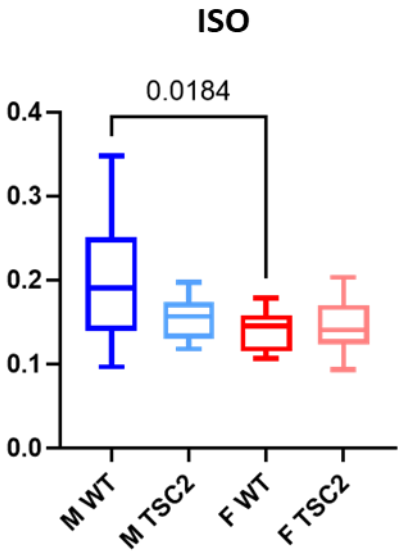

***Figure 21**. GQI changes in the cerebellum - ISO boxplots for the cerebellum. Mann-Whitney significant changes are marked with the respective P-value.*

Parieto-temporal cortex

In the parieto-temporal cortex, differences were detected (P=0.0111) between male (n=13) and female wild-type mice (n=7); and between male (n=13) and female *Tsc2*$^{+/-}$ mice (n=15), P=0.0253, again only in ISO measure (Figure 22).

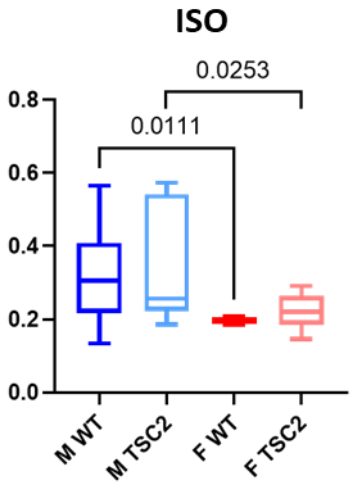

***Figure 22**. GQI changes in the parieto-temporal cortex - ISO boxplots for the parieto-temporal cortex. Mann-Whitney significant changes are marked with the respective P-value.*

Amygdala

In the amygdala, MD seemed to change (P=0.0101) between male (n=10) and female wild-type mice (n=9) (Figure 23a). AD revealed alterations (P=0.0465) between male (n=11) and female wild-type mice (n=9) (Figure 23b). In addition, ISO showed alterations (P=0.433) between male (n=10) and female wild-type mice (n=10) and between male (n=13) and female *Tsc2*$^{+/-}$ mice (n=7), with P=0.0456 (Figure 23c).

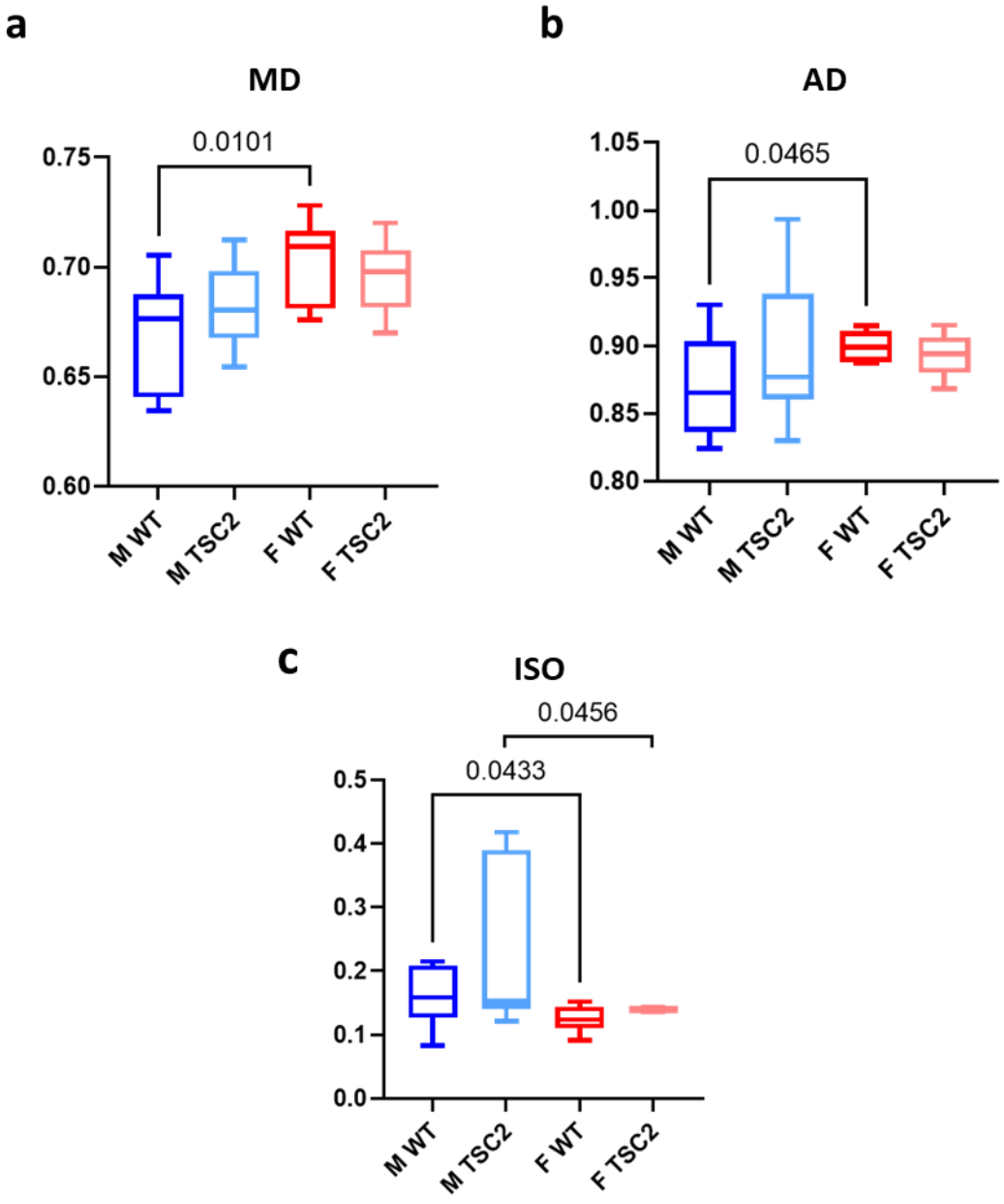

***Figure 23**. DTI and GQI changes in the amygdala - MD (a), AD (b) and ISO (c) boxplots for the amygdala. Mann-Whitney significant changes are marked with the respective P-value.*

5.5 Metabolic spectrums

For each region, metabolic spectrums (normalized in parts per million) were obtained for each subject type (Figures 24-31).

Prefrontal cortex

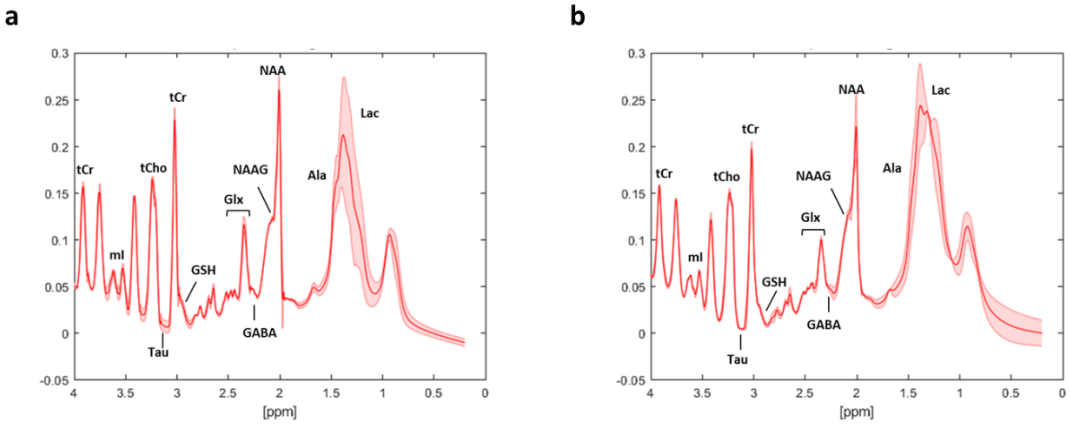

***Figure 24**. Male spectrum, for the prefrontal cortex – Metabolic spectrum with the identified peaks for each metabolite, for wild-type (a) and Tsc2$^{+/-}$ mice (b). Abbreviations: Abbreviations: tCr – total creatine, mI – myo-inositol, tCho – total choline, Tau – taurine, GSH – glutathione, Glx – glutamate+glutamine, GABA - Gamma amino butyric acid, NAAG - N-acetyl aspartyl glutamate, NAA - N-acetyl aspartate, Ala – alanine, Lac – lactate.*

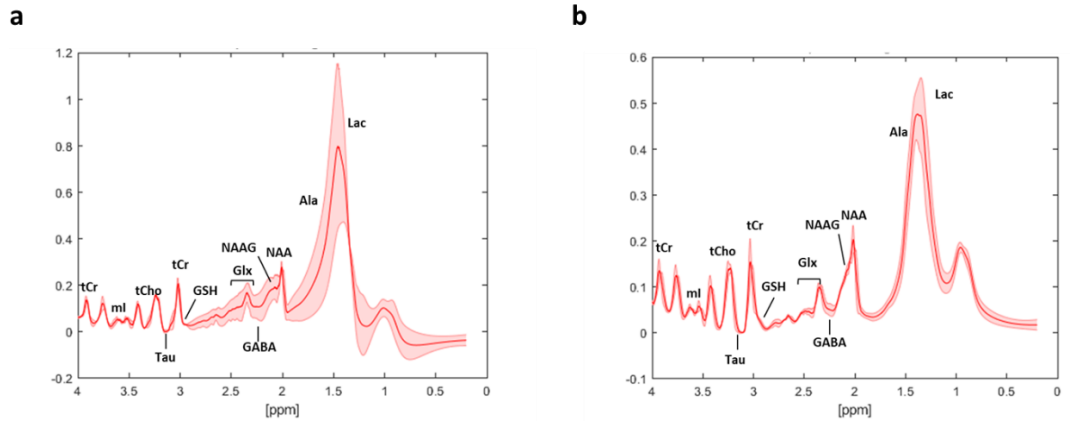

***Figure 25.** Female spectrum, for the prefrontal cortex – Metabolic spectrum with the identified peaks for each metabolite, for wild-type (a) and Tsc2$^{+/-}$ mice (b). Abbreviations: Abbreviations: tCr – total creatine, mI – myo-inositol, tCho – total choline, Tau – taurine, GSH – glutathione, Glx – glutamate+glutamine, GABA - Gamma amino butyric acid, NAAG - N-acetyl aspartyl glutamate, NAA - N-acetyl aspartate, Ala – alanine, Lac – lactate.*

Hippocampus

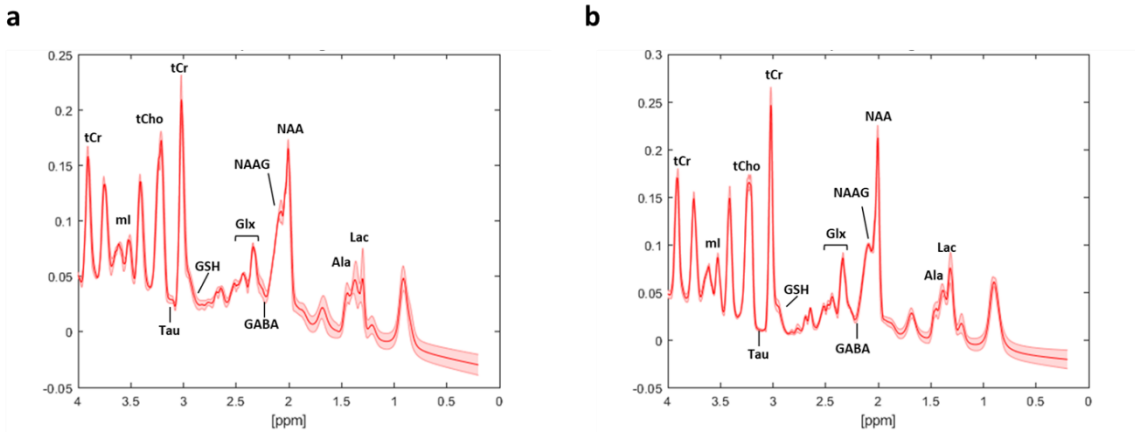

Figure 26. *Male spectrum, for the hippocampus – Metabolic spectrum with the identified peaks for each metabolite, for wild-type (a) and Tsc2$^{+/-}$ mice (b). Abbreviations: Abbreviations: tCr – total creatine, mI – myo-inositol, tCho – total choline, Tau – taurine, GSH – glutathione, Glx – glutamate+glutamine, GABA - Gamma amino butyric acid, NAAG - N-acetyl aspartyl glutamate, NAA - N-acetyl aspartate, Ala – alanine, Lac – lactate.*

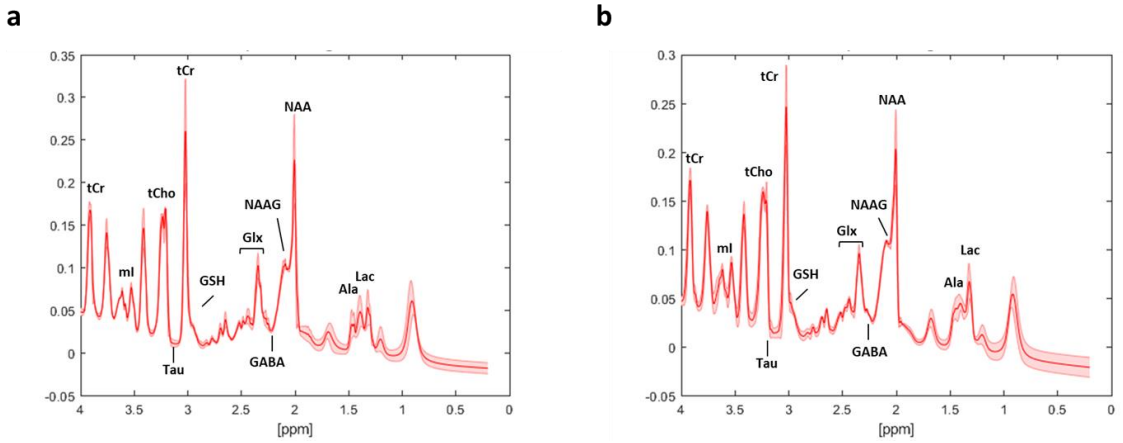

Figure 26. *Female spectrum, for the hippocampus – Metabolic spectrum with the identified peaks for each metabolite, for wild-type (a) and Tsc2$^{+/-}$ mice (b). Abbreviations: Abbreviations: tCr – total creatine, mI – myo-inositol, tCho – total choline, Tau – taurine, GSH – glutathione, Glx – glutamate+glutamine, GABA - Gamma amino butyric acid, NAAG - N-acetyl aspartyl glutamate, NAA - N-acetyl aspartate, Ala – alanine, Lac – lactate.*

Striatum

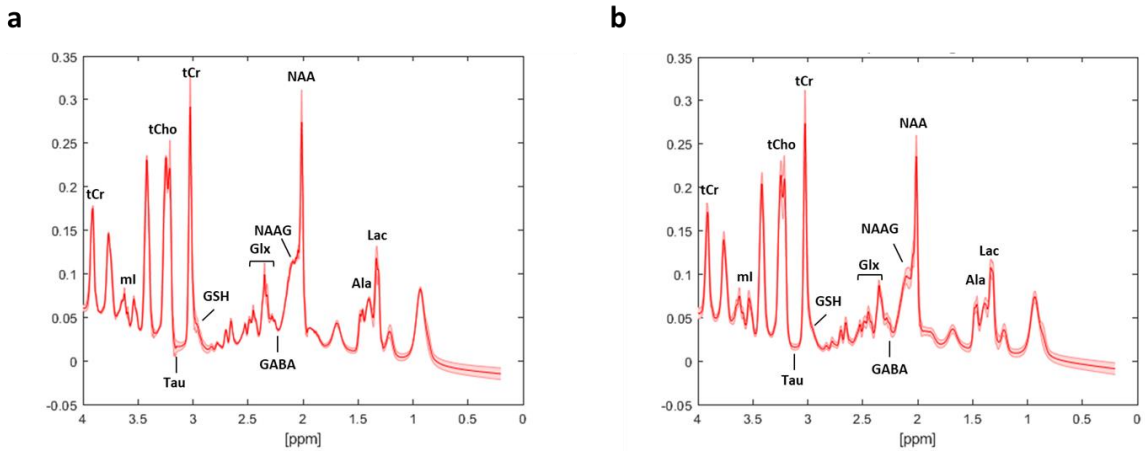

Figure 27. *Male spectrum, for the striatum – Metabolic spectrum with the identified peaks for each metabolite, for wild-type (a) and Tsc2$^{+/-}$ mice (b). Abbreviations: Abbreviations: tCr – total creatine, mI – myo-inositol, tCho – total choline, Tau – taurine, GSH – glutathione, Glx – glutamate+glutamine, GABA - Gamma amino butyric acid, NAAG - N-acetyl aspartyl glutamate, NAA - N-acetyl aspartate, Ala – alanine, Lac – lactate.*

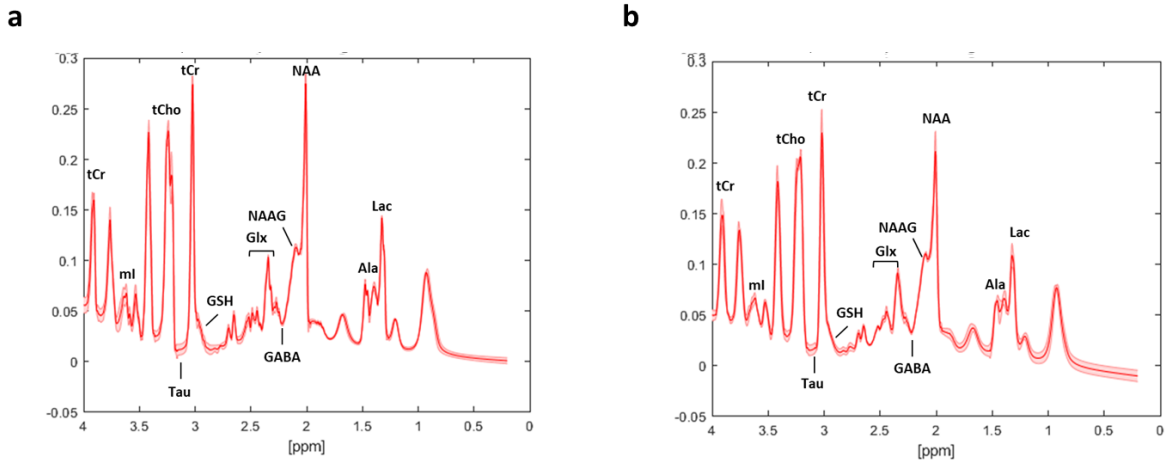

Figure 28. *Female spectrum, for the striatum – Metabolic spectrum with the identified peaks for each metabolite, for wild-type (a) and Tsc2$^{+/-}$ mice (b). Abbreviations: Abbreviations: tCr – total creatine, mI – myo-inositol, tCho – total choline, Tau – taurine, GSH – glutathione, Glx – glutamate+glutamine, GABA - Gamma amino butyric acid, NAAG - N-acetyl aspartyl glutamate, NAA - N-acetyl aspartate, Ala – alanine, Lac – lactate.*

Cerebellum

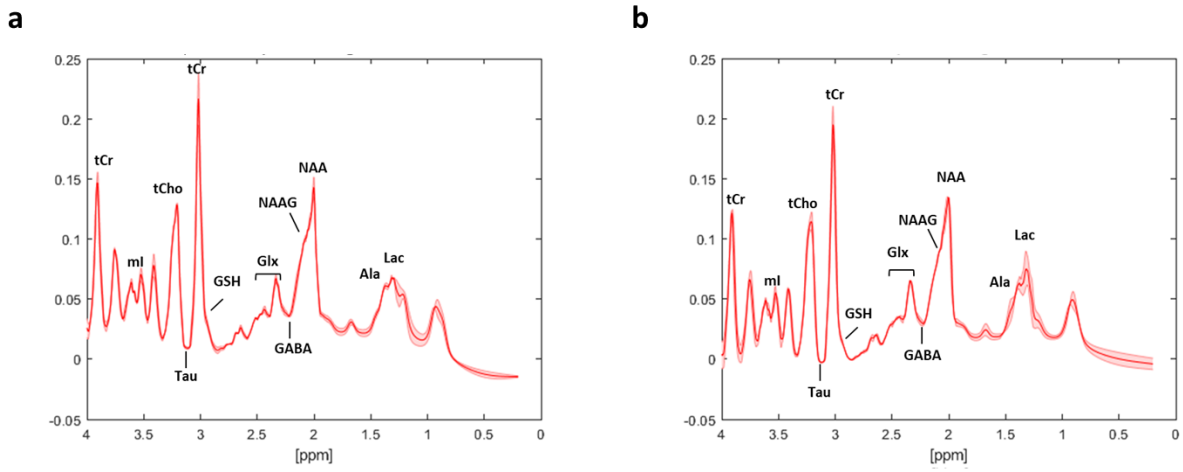

Figure 29. *Male spectrum, for the cerebellum – Metabolic spectrum with the identified peaks for each metabolite, for wild-type (a) and Tsc2$^{+/-}$ mice (b). Abbreviations: Abbreviations: tCr – total creatine, mI – myo-inositol, tCho – total choline, Tau – taurine, GSH – glutathione, Glx – glutamate+glutamine, GABA - Gamma amino butyric acid, NAAG - N-acetyl aspartyl glutamate, NAA - N-acetyl aspartate, Ala – alanine, Lac – lactate.*

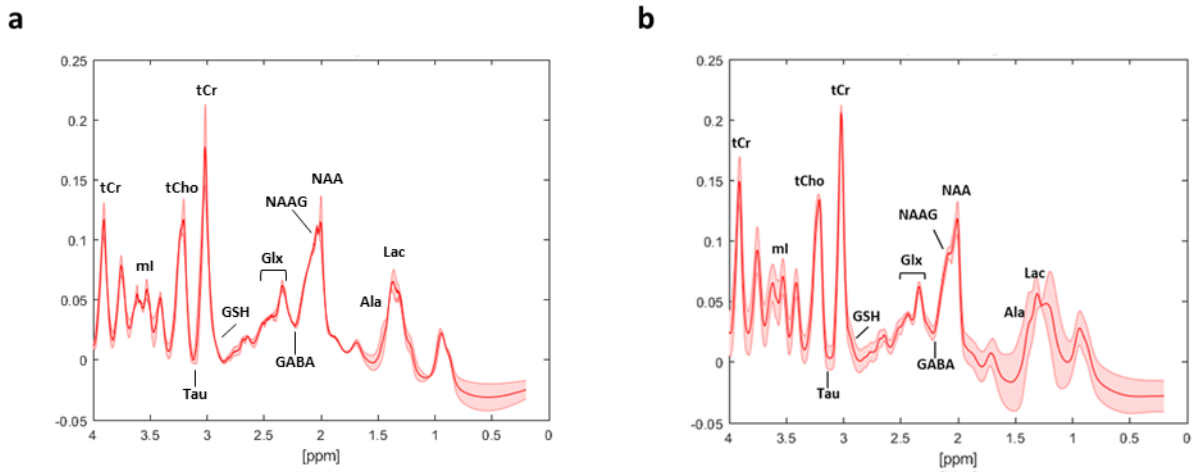

Figure 30. *Female spectrum, for the cerebellum – Metabolic spectrum with the identified peaks for each metabolite, for wild-type (a) and Tsc2$^{+/-}$ mice (b). Abbreviations: Abbreviations: tCr – total creatine, mI – myo-inositol, tCho – total choline, Tau – taurine, GSH – glutathione, Glx – glutamate+glutamine, GABA - Gamma amino butyric acid, NAAG - N-acetyl aspartyl glutamate, NAA - N-acetyl aspartate, Ala – alanine, Lac – lactate.*

5.6 Metabolic levels

As for the metabolic analysis, the metabolic levels acquired by MRS are presented as Median ± IQR, for each subset and each region.

Table 13. *Metabolic values in the prefrontal cortex - Median and interquartile range (Median ± IQR) values on metabolic concentrations (mM) for the prefrontal cortex of the four subsets: male wild-type mice (M-WT), male Tsc2$^{+/-}$ mice (M-TSC2), female wild-type mice (F-WT), and female Tsc2$^{+/-}$ mice (F-TSC2).*

PFC	**M-WT**	**M-TSC2**	**F-WT**	**F-TSC2**
NAA + NAAG	10.39 ± 0.37	10.34 ± 1.93	10.27 ± 0.78	9.92 ± 1.41
Total choline	3.90 ± 0.23	1.74 ± 0.22	1.57 ± 0.30	1.82 ± 0.08
Glx	17.20 ± 0.69	16.61 ± 1.22	15.75 ± 3.26	16.51 ± 1.32
Total creatine	8.90 ± 0.56	8.97 ± 0.52	8.93 ± 1.09	9.40 ± 0.71
GABA	2.65 ± 0.37	2.64 ± 0.51	3.26 ± 0.82	2.38 ± 0.22
GSH	2.49 ± 0.51	2.15 ± 0.32	2.73 ± 0.42	2.41 ± 0.58
Tau	12.26 ± 1.66	11.64 ± 0.41	11.87 ± 2.16	12.84 ± 2.09
Ala	4.24 ± 2.10	2.72 ± 0.87	4.69 ± 2.79	5.62 ± 1.50
Ins	4.65 ± 0.88	4.98 ± 0.61	5.21 ± 1.94	6.36 ± 1.22
Lac	3.68 ± 2.22	3.06 ± 0.64	6.40 ± 3.11	6.44 ± 2.87

Table 14. *Metabolic levels in the hippocampus - Median and interquartile range (Median ± IQR) values on metabolic concentrations (mM) for the hippocampus of the four subsets: male wild-type mice (M-WT), male Tsc2$^{+/-}$ mice (M-TSC2), female wild-type mice (F-WT), and female Tsc2$^{+/-}$ mice (F-TSC2).*

HIP	M-WT	M-TSC2	F-WT	F-TSC2
NAA + NAAG	8.89 ± 0.98	9.62 ± 0.73	8.95 ± 0.67	8.83 ± 0.98
Total choline	1.64 ± 0.02	1.74 ± 0.28	1.98 ± 0.25	1.85 ± 0.20
Glx	15.40 ± 1.10	15.36 ± 1.16	16.02 ±0.62	15.79 ± 1.96
Total creatine	9.59 ± 1.11	9.81 ± 0.66	9.25 ± 0.37	9.25 ± 0.23
GABA	2.53 ± 0.62	2.65 ± 0.33	2.88 ± 0.43	2.76 ± 0.52
GSH	2.38 ± 0.37	2.35 ± 0.60	2.35 ± 0.70	2.04 ± 0.30
Tau	10.78 ± 1.26	11.97 ± 0.82	11.05 ± 0.71	11.04 ± 1.22
Ala	2.75 ± 0.16	2.90 ± 1.19	2.51 ± 0.30	2.46 ± 0.24
Ins	4.84 ± 0.45	5.72 ± 0.60	5.46 ± 1.30	5.35 ± 0.87
Lac	3.42 ± 0.82	4.41 ± 0.19	3.63 ± 0.82	3.48 ± 0.57

Table 15. *Metabolic levels in the striatum - Median and interquartile range (Median ± IQR) values on metabolic concentrations (mM) for the striatum of the four subsets: male wild-type mice (M-WT), male Tsc2$^{+/-}$ mice (M-TSC2), female wild-type mice (F-WT), and female Tsc2$^{+/-}$ mice (F-TSC2).*

STR	M-WT	M-TSC2	F-WT	F-TSC2
NAA + NAAG	8.98 ± 0.54	9.49 ± 0.71	8.84 ± 0.55	9.06 ± 0.35
Total choline	2.25 ± 0.08	2.19 ± 0.40	2.23 ± 0.14	2.34 ± 0.23
Glx	13.86 ± 1.59	13.99 ± 0.27	13.65 ± 1.15	14.15 ± 0.78
Total creatine	8.55 ± 0.64	8.48 ± 0.72	8.49 ± 0.17	8.60 ± 0.68
GABA	3.40 ± 0.96	3.32 ± 0.52	3.61 ± 0.33	3.26 ± 0.43
GSH	1.68 ± 0.56	1.82 ± 0.47	1.91 ± 0.34	1.94 ± 0.22
Tau	16.56 ± 1.22	16.61 ± 1.24	16.08 ± 1.39	15.77 ± 1.60
Ala	2.85 ± 1.17	2.72 ± 0.22	3.44 ± 0.43	3.23 ± 0.64
Ins	3.45 ± 0.68	3.92 ± 0.85	3.75 ± 0.69	3.27 ± 0.73
Lac	5.54 ± 1.25	5.22 ± 1.16	6.45 ± 0.69	6.85 ± 0.69

Table 16. *Metabolic levels in the cerebellum - Median and interquartile range (Median ± IQR) values on metabolic concentrations (mM) for the cerebellum of the four subsets: male wild-type mice (M-WT), male Tsc2$^{+/-}$ mice (M-TSC2), female wild-type mice (F-WT), and female Tsc2$^{+/-}$ mice (F-TSC2).*

CRBL	**M-WT**	**M-TSC2**	**F-WT**	**F-TSC2**
NAA + NAAG	7.10 ± 0.87	7.04 ± 0.64	7.62 ± 1.37	7.02 ± 1.36
Total choline	2.00 ± 0.13	1.98 ± 0.17	2.30 ± 0.09	2.23 ± 0.11
Glx	11.99 ± 1.35	11.92 ± 0.81	11.77 ± 3.80	12.33 ± 1.82
Total creatine	11.01 ± 1.05	11.01 ± 0.73	11.82 ± 1.37	11.38 ± 0.27
GABA	2.31 ± 0.47	2.40 ± 0.25	2.57 ± 0.40	2.54 ± 0.25
GSH	1.95 ± 0.67	2.04 ± 0.48	2.73 ± 0.12	2.66 ± 0.52
Tau	6.52 ± 1.20	6.59 ± 0.77	7.51 ± 0.62	7.05 ± 1.14
Ala	2.08 ± 0.41	----	2.09 ± 0.95	----
Ins	7.00 ± 1.33	6.36 ± 1.22	7.39 ± 0.93	6.80 ± 0.33

5.7 Significant metabolic changes analysis

Similar to the DTI and GQI results, Mann-Whitney statistical test results of the comparison of the levels of each metabolite between the four subsets are presented using boxplots. Significant differences are marked with the respective P-values.

Prefrontal cortex

In the prefrontal cortex, Lac was altered (P=0.0381) between male (n=4) and female wild-type mice (n=6) (Figure 32a). Also, GABA revealed alterations (P=0.0317) between female wild-type (n=5) and *Tsc2*$^{+/-}$ mice (n=5) (Figure 32b).

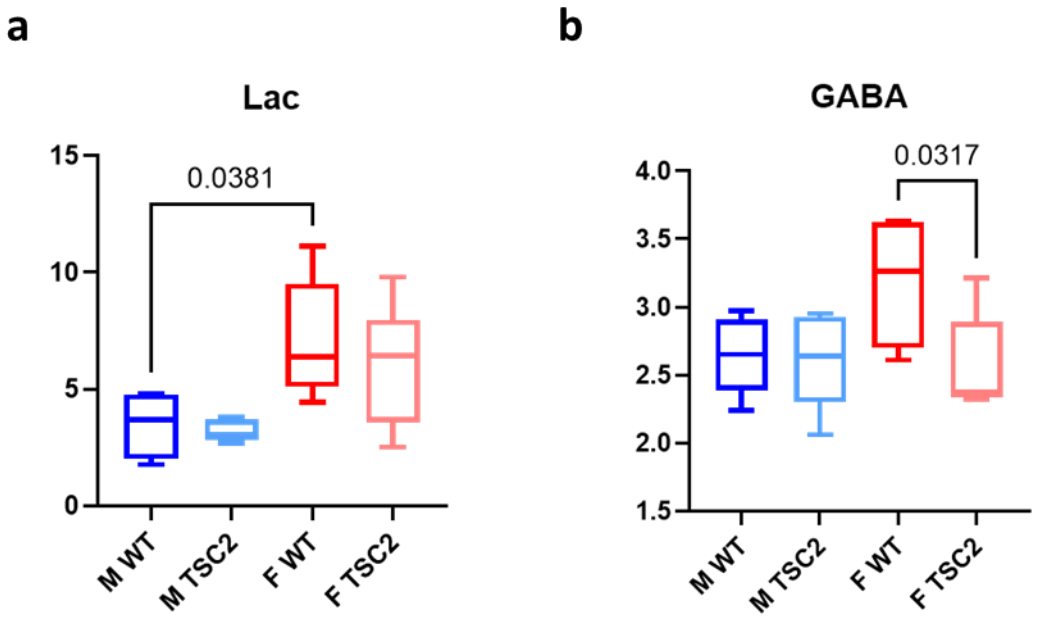

***Figure 31**. Lac and GABA changes in the prefrontal cortex - Lac (a) and GABA (b) boxplots for the prefrontal cortex. Mann-Whitney significant changes are marked with the respective P-value.*

Moreover, cortical Ins was changed (P=0.0010) between male (n=12) and female *Tsc2*$^{+/-}$ mice (n=11) (Figure 33a), and Tau revealed an increase (P=0.0026) between male (n=10) and female *Tsc2*$^{+/-}$ mice (n=12) (Figure 33b).

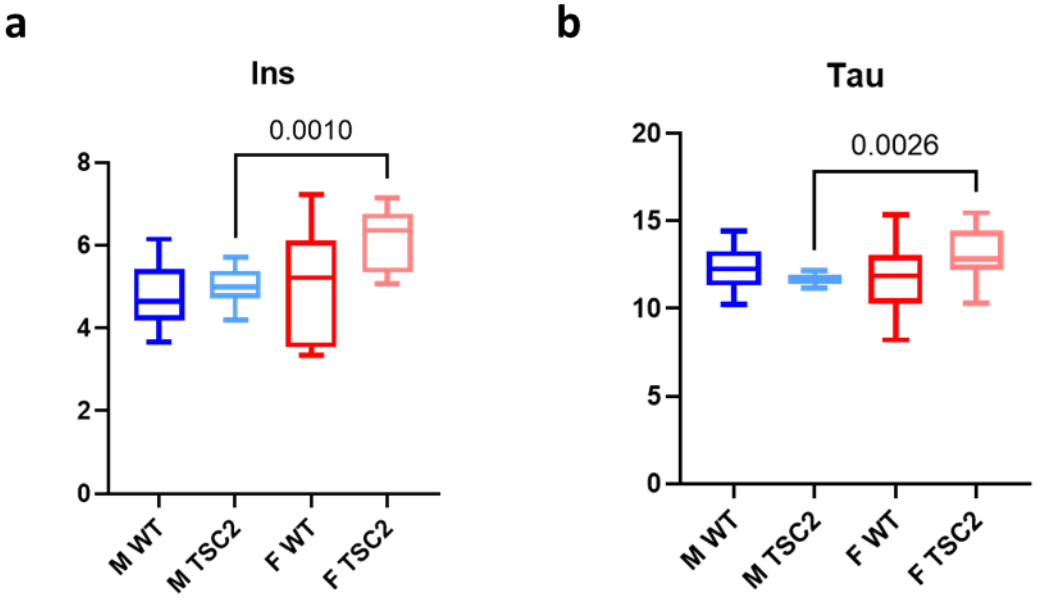

***Figure 32**. Ins and Tau changes in the prefrontal cortex - Ins (a) and Tau (b) boxplots for the prefrontal cortex. Mann-Whitney significant changes are marked with the respective P-value.*

In addition, we found a reduction in Ala levels (P=0.0205) in TSC2 males between male wild-type (n=17) and *Tsc2*$^{+/-}$ mice (n=8); and between male (n=7) and female *Tsc2*$^{+/-}$ mice (n=8) P=0.0011 (Figure 34a). Glutathione also revealed alterations (P=0.0352) between male wild-type (n=13) *Tsc2*$^{+/-}$ mice (n=11) (Figure 34b).

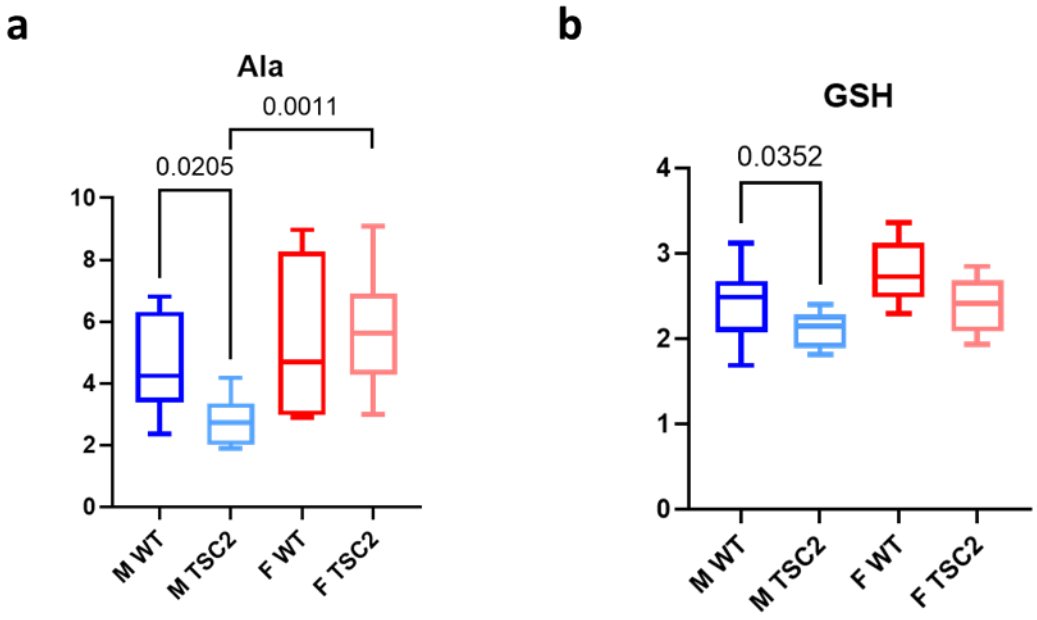

***Figure 33**. Ala and GSH changes in the prefrontal cortex - Ala (a) and GSH (b) boxplots for the prefrontal cortex. Mann-Whitney significant changes are marked with the respective P-value.*

Hippocampus

In the hippocampus, total choline changed (P=0.0108) between male (n=7) and female wild-type mice (n=9) (Figure 35a). Furthermore, NAA+NAAG revealed alterations (P=0.0130) between male (n=10) and female wild-type (n=14) mice (Figure 35b).

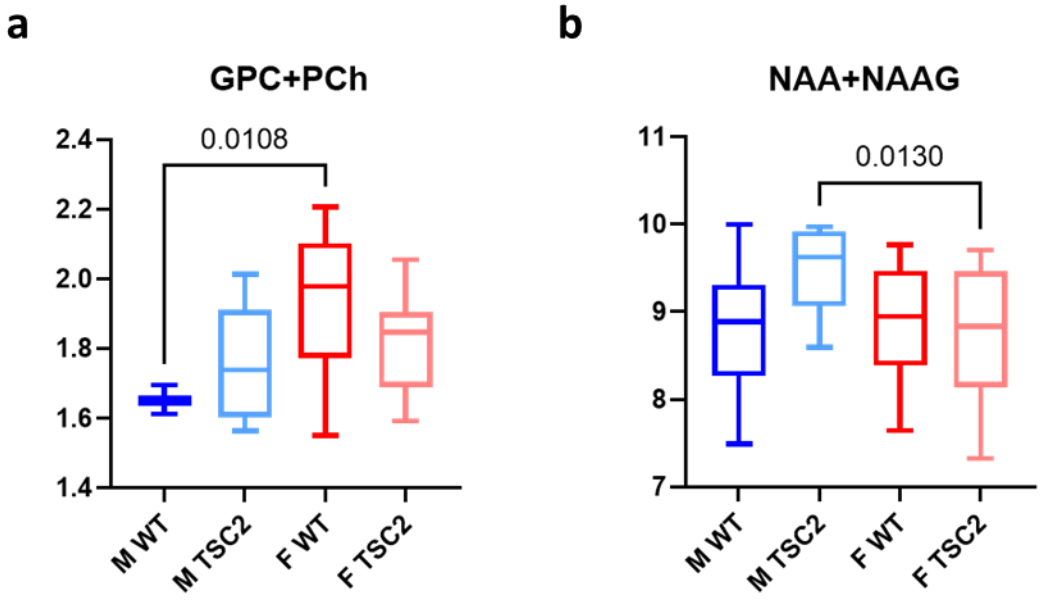

***Figure 34**. Total choline and NAA+NAAG changes in the hippocampus – Total choline (a) and NAA+NAAG (b) boxplots for the hippocampus. Mann-Whitney significant changes are marked with the respective P-value.*

Total creatine and Lac were altered (P=0.0214 and P=0.0040, respectively) between male (n=13) and female *Tsc2*$^{+/-}$ mice (n=10) (Figure 36a and 36b). Lac was also altered (P=0.0056) between male wild-type (n=9) and *Tsc2*$^{+/-}$ mice (n=9) (Figure 36b).

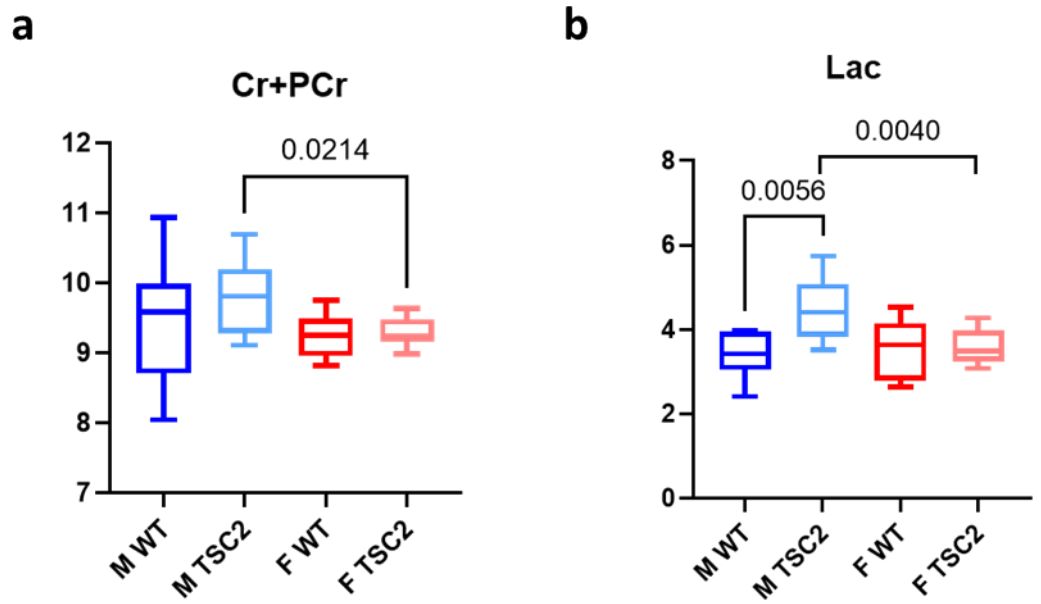

***Figure 35**. Total creatine and Lac changes in the hippocampus – Total creatine (a) and Lac (b) boxplots for the hippocampus. Mann-Whitney significant changes are marked with the respective P-value.*

The levels of Tau and Ins were up-regulated in transgenic males (P=0.0173 and P<0.0001, respectively) compared with male wild-type (n=12 and n=9, respectively) (Figure 37a and 37b). Additionally, compared female *Tsc2*$^{+/-}$ mice (n=13), Tau levels of males TSC2 was increased (P=0.0019) (Figure 37a).

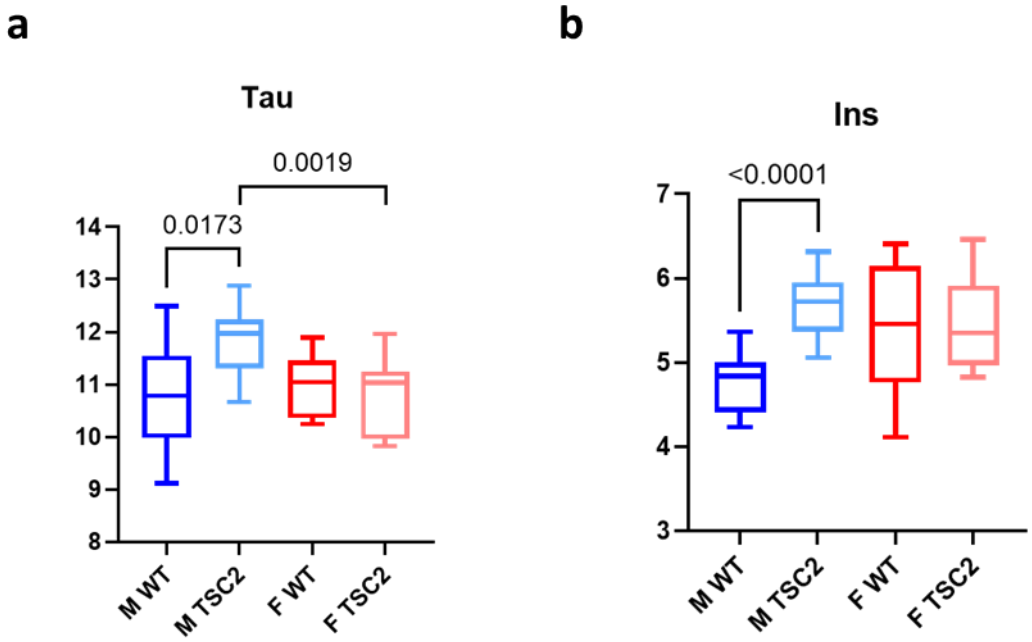

***Figure 36**. Tau and Ins changes in the hippocampus - Tau (a) and Ins (b) boxplots for the hippocampus. Mann-Whitney significant changes are marked with the respective P-value.*

Striatum

In the striatum, Ala was altered (P=0.0032) between male (n=10) and female *Tsc2*$^{+/-}$ mice (n=13) (Figure 38a). Moreover, Lac revealed alterations (P=0.0012) between male (n=11) and female wild-type (n=8) mice and between male (n=11) and female *Tsc2*$^{+/-}$ mice (n=13), P=0.0001 (Figure 38b).

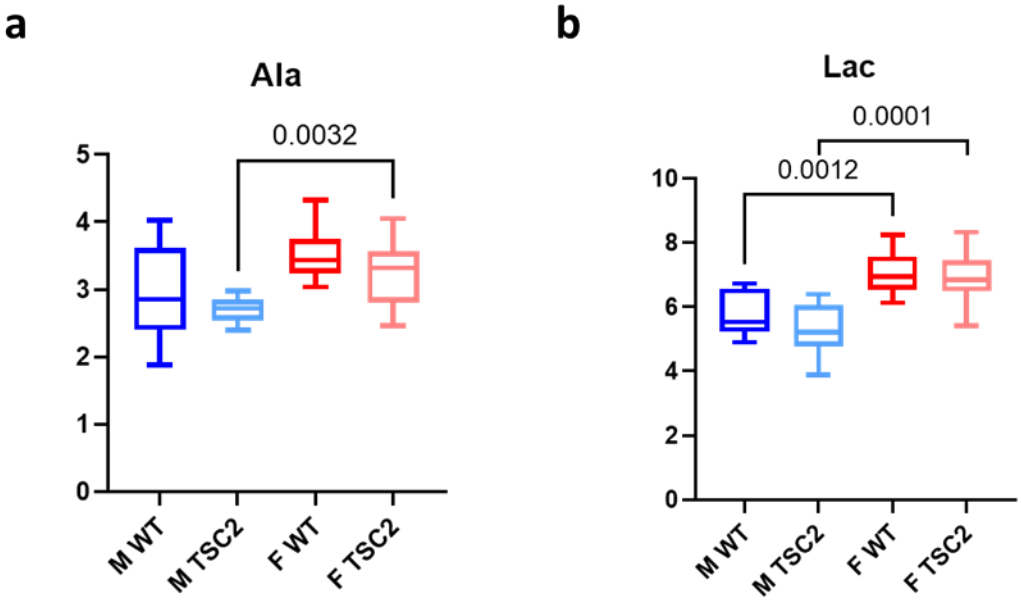

Figure 37. *Ala and Lac changes in the striatum - Ala (a) and Lac (b) boxplots for the striatum. Mann-Whitney significant changes are marked with the respective P-value.*

Cerebellum

In the cerebellum, total choline seemed to change significantly (P=0.0015) between male (n=9) and female *Tsc2*$^{+/-}$ mice (n=10) (Figure 39).

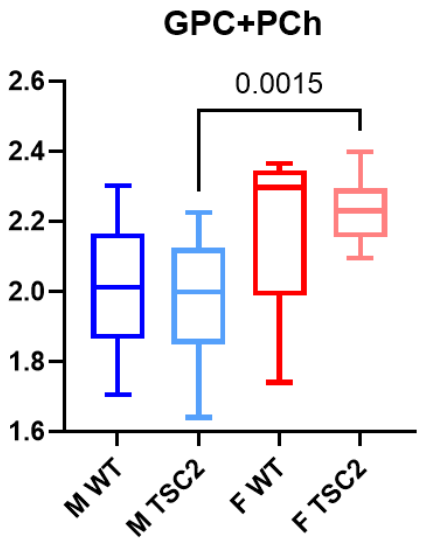

Figure 38. *Total choline changes in the cerebellum – Total choline boxplots for the cerebellum. Mann-Whitney significant changes are marked with the respective P-value.*

5.8 Correlation

All the acquired values of the DTI, GQ, and MRS procedures were tested for correlation (Appendix: Supplementary Tables 1-8).

Correlation heat-maps are also presented. For each map, Pearson (or Spearman when applicable) coefficient values are colour coded for both sexes (Figures 40-43).

Prefrontal cortex

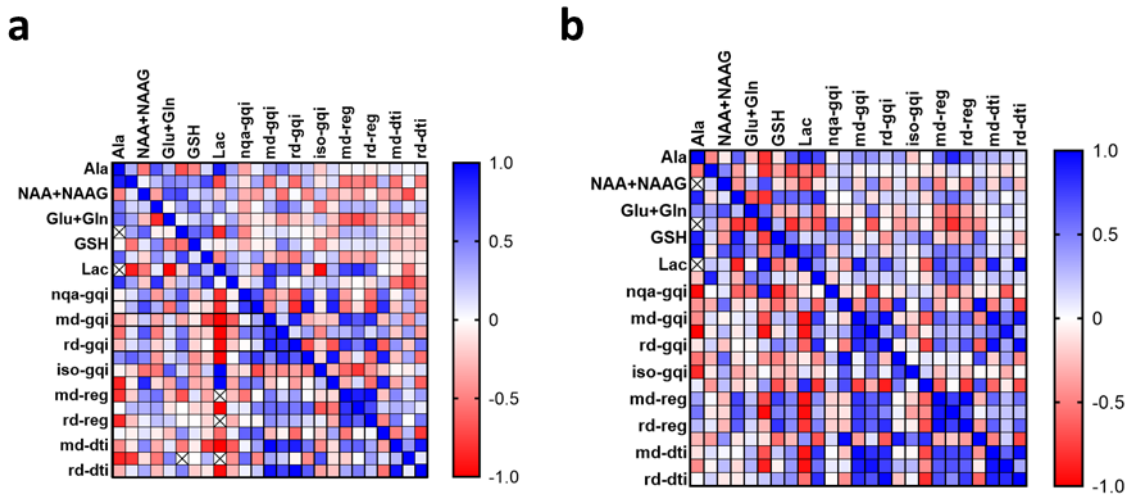

Figure 39. *Correlation assessment in the prefrontal cortex - Correlation heat-maps for males (a) and females (b), for the prefrontal cortex. In relation to the matrix diagonal, the bottom triangle represents the values for the wild-type subset and the top the Tsc2$^{+/-}$ condition.*

Hippocampus

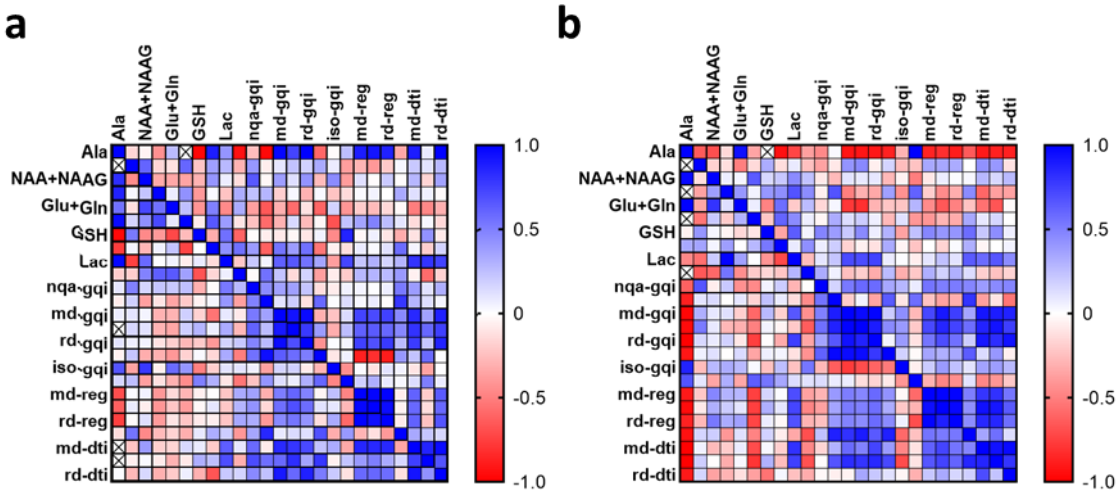

Figure 40.. *Correlation assessment in the hippocampus - Correlation heat-maps for males (a) and females (b), for the hippocampus. In relation to the matrix diagonal, the bottom triangle represents the values for the wild-type subset and the top the Tsc2$^{+/-}$ condition.*

Striatum

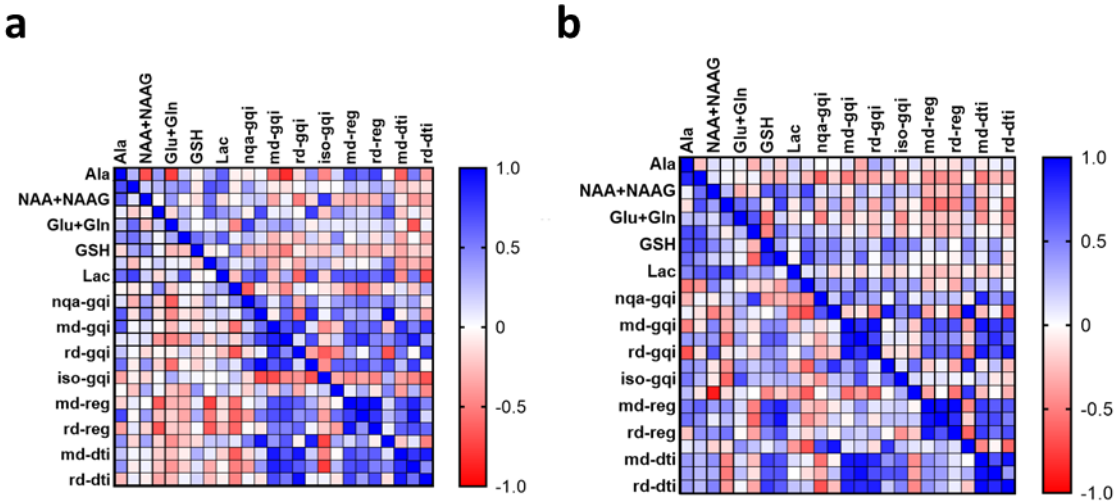

Figure 41. *Correlation assessment in the striatum - Correlation heat-maps for males (a) and females (b), for the striatum. In relation to the matrix diagonal, the bottom triangle represents the values for the wild-type subset and the top the Tsc2$^{+/-}$ condition.*

Cerebellum

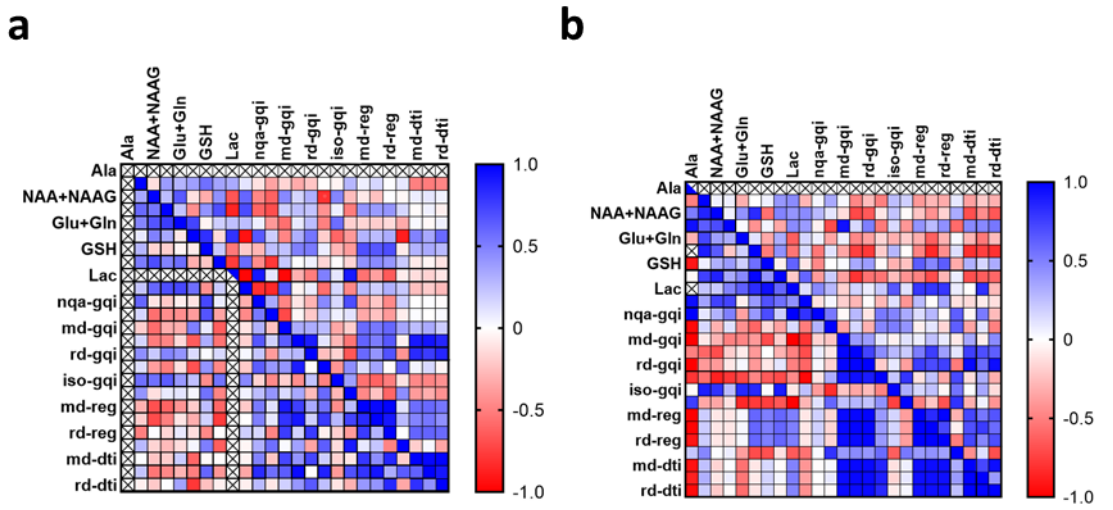

***Figure 42**. Correlation assessment in the cerebellum - Correlation heat-maps for males (a) and females (b), for the prefrontal cortex. In relation to the matrix diagonal, the bottom triangle represents the values for the wild-type subset and the top the $Tsc2^{+/-}$ condition.*

6 DISCUSSION

Tuberous sclerosis complex (TSC) is a disease model that may aid the development of new therapies for associated pathologies, such as epilepsy, autism spectrum disorders, and intellectual disabilities. As a genetic disorder with high comorbidity with ASD, it can help elucidate the neurobiology associated with ASD, as well as support the identification of potential therapeutic drugs and drug targets.

The diffusion tensor imaging (DTI) technique, an MRI-based technique that uses the diffusivity of water molecules to study fiber arrangements, seems to be a promising tool in the investigation of the TSC brain anatomy. By extracting a set of metrics of the region in study, it can reveal microstructural changes associated with the disorder, offering relevant information for potential therapies.

To our knowledge, the current study is the first to investigate the *Tsc2*$^{+/-}$ disorder in this mouse model by application of both DTI and GQI, as well as possible correlations with metabolic changes.

6.1 Investigating the TSC disorder on diffusion tensor metrics of the TSC2 mouse brain

Regarding the question that this thesis proposes to answer, it was found that for the 51 subjects analysed, some DTI metrics change significantly in the presence of the TSC phenotype.

For the prefrontal cortex, both region and tract-based DTI showed an increase of the FA in female *Tsc2*$^{+/-}$ subjects compared with the female wild-type (Figure 11). Although demyelination would explain a FA decrease instead, we can hypothesise that the increase could be associated with a more coherent myelination, which may represent a loss in neurite complexity (Hsieh et al., 2020). A coherence analysis of the region would be needed to verify this. This myelination strengthening would also explain the AD increase (Ding et al., 2021) between the same groups reported in the DTI that was made in parallel to the GQI (Figure 18).

Interestingly, the opposite trend was captured in males – FA decreased in *Tsc2*$^{+/-}$ compared with wild-type (Figure 18). This result is consistent with the reported lower FA levels for axonal damage pathologies, and the contrast with the female analysis could indicate a different pathological mechanism dependent on the sex.

GQI metrics reported a correlation between FA and GFA, as predicted, showing the same patterns of significant changes (Figure 18). The ISO increase in female *Tsc2*$^{+/-}$ mice over wild-type (Figure 18) can suggest altered white matter integrity with reduction in the number of neurons, as it has been reported (Edmonson et al., 2014).

In the amygdala, DTI displayed increases in both MD and AD values in male *Tsc2*$^{+/-}$ subjects (Figures 16-17), which might indicate lesions. These could result in increased water diffusion in axonal fibers with greater extracellular water content, and atrophy of white-matter fibers (Tsai et al., 2020; Habas et al., 2018).

For every region considered, the ISO metric showed to be higher in males compared with females, in one or both phenotypes. This may expose a sex identification power of the metric.

6.2 Investigating the TSC disorder on metabolic profiles of the TSC2 mouse brain

Analysing the spectrums, the prefrontal cortex showed higher Lac and/or Ala peaks in females compared to males (Figures 24-25), possibly suggesting an increase in anaerobic metabolism in this area.

Spectrums of the striatum also showed *Tsc2*$^{+/-}$ subjects having lower peaks of NAA compared to healthy ones (Figures 28-29), indicating possible myelination problems or injury.

In the prefrontal cortex of female *Tsc2*$^{+/-}$ subjects a decrease in GABA levels was observed in relation to healthy females (Figure 32). This result may be associated with the previously mentioned finding that faulty $GABA_BR$-mediated inhibition in this region might contribute to ASD like symptoms in TSC2 mice (Bassetti et al., 2020). Furthermore, for male *Tsc2*$^{+/-}$ subjects there is a decrease of both Ala and GSH (Figure 34), which can indicate an increase in oxidative stress (Hu et al., 2018).

In the hippocampal region, male *Tsc2*$^{+/-}$ mice showed increases in Lac, Tau and Ins measures when compared with their healthy counterparts (Figures 36-37). The increase of Lac can be positively correlated with anaerobic metabolism. Higher Tau quantities may report a loss of neuron structure and increased Ins levels reveal a chemical imbalance. These changes in the hippocampus of *Tsc2*$^{+/-}$ subjects can help make sense the correlation between the disorder and intellectual disabilities.

Although some variable pairs showed good correlation in terms of r (and associated p-values), such as Lac - iso in the prefrontal cortex of male wild-type mice (Appendix: Supplementary Table 1), or Lac - rd-reg in the cerebellum of male *Tsc2*$^{+/-}$ mice (Appendix: Supplementary Table 7), the linear regressions did not indicate strong correlation between structural metrics and metabolites.

6.3 Limitations and future work

Region selection in this study was limited both by the quality definition of the acquired images, where they were manually drawn, and the lack of a compatible atlas as an input reference. For these reasons, the study focused on regions as general representations of larger areas, instead of small brain structures.

Additional imaging techniques would also be of use, and a larger overall subject sample would provide confirmation of the preliminary findings identified in this study.

A more detailed statistical analysis, with the employment of subsequent ANOVA tests to the results for example, would also make the present study a more comprehensive one.

This thesis should provide new insights on the neuropathology of TSC, serving as a basis for more complex future studies on potential therapies.

7 REFERENCES

ALEXANDER, Andrew L., et al. Diffusion tensor imaging of the brain. Neurotherapeutics [online]. 2007. 4(3), 316–329. ISSN 1878-7479

ALFAIZ, Ali Abdullah, et al. TBC1D7 Mutations are associated with intellectual disability, macrocrania, patellar dislocation, and celiac disease. Human Mutation [online]. 2014, 35(4), 447–451. ISSN 1059-7794

ARONICA, Eleonora, and Peter B. CRINO. Epilepsy related to developmental tumors and malformations of cortical development. Neurotherapeutics [online]. 2014. 11(2). 251–268. ISSN 1878-7479

ASANO, E., et al. Autism in tuberous sclerosis complex is related to both cortical and subcortical dysfunction. Neurology [online]. 2001. 57(7), 1269–1277. ISSN 1526-632X

ASATO, Miya R., and Antonio Y. HARDAN. Topical review: neuropsychiatric problems in tuberous sclerosis complex. Journal of Child Neurology [online]. 2004. 19(4), 241–249. ISSN 1708-8283

AU, Kit Sing, et al. Genotype/phenotype correlation in 325 individuals referred for a diagnosis of tuberous sclerosis complex in the United States. Genetics in Medicine [online]. 2007. 9(2), 88–100. ISSN 1530-0366

BARKOVICH, A. J., et al. A developmental and genetic classification for malformations of cortical development. Neurology [online]. 2005. 65(12), 1873–1887. ISSN 1526-632X

BASSER, P. J., J. MATTIELLO, and D. LEBIHAN, MR diffusion tensor spectroscopy and imaging. Biophysical Journal [online]. 1994. 66(1), 259–267. ISSN 0006-3495

BASSETTI, Davide, et al. Haploinsufficiency of tsc2 leads to hyperexcitability of medial prefrontal cortex via weakening of tonic GABAB receptor-mediated inhibition. Cerebral Cortex [online]. 2020. 30(12), 6313–6324. ISSN 1460-2199

BIHAN, Denis Le. Molecular diffusion, tissue microdynamics and microstructure. NMR in Biomedicine [online]. 1995. 8(7), 375–386. ISSN 1099-1492

BOLTON, Patrick F. Neuroepileptic correlates of autistic symptomatology in tuberous sclerosis. Mental Retardation and Developmental Disabilities Research Reviews [online]. 2004. 10(2), 126–131. ISSN 1098-2779

BOLTON, Patrick F., and Paul D. GRIFFITHS. Association of tuberous sclerosis of temporal lobes with autism and atypical autism. The Lancet [online]. 1997. 349(9049), 392–395. ISSN 0140-6736

BOLTON, Patrick F., et al. Neuro-epileptic determinants of autism spectrum disorders in tuberous sclerosis complex. Brain [online]. 2002. 125(6), 1247–1255. ISSN 1460-2156

BOTTOMLEY, Paul A. Spatial localization in NMR spectroscopy in vivo. Annals of the New York Academy of Sciences [online]. 1987, 508(1 Physiological), 333–348. ISSN 1749-6632

BUDDE, M. D., et al. Axial diffusivity is the primary correlate of axonal injury in the experimental autoimmune encephalomyelitis spinal cord: a quantitative pixelwise analysis. Journal of Neuroscience [online]. 2009. 29(9), 2805–2813. ISSN 1529-2401

BUDDE, Matthew D., et al. Toward accurate diagnosis of white matter pathology using diffusion tensor imaging. Magnetic Resonance in Medicine [online]. 2007. 57(4), 688–695. ISSN 1522-2594

CAPO-CHICHI, José-Mario, et al. Disruption of TBC1D7, a subunit of the TSC1-TSC2 protein complex, in intellectual disability and megalencephaly. Journal of Medical Genetics [online]. 2013, 50(11), 740–744. ISSN 1468-6244

CARVALHO NETO Arnolfo de, Emerson L. GASPARETTO, and Isac BRUCK. Subependymal giant cell astrocytoma with high choline/creatine ratio on proton MR spectroscopy. Arquivos de Neuro-Psiquiatria [online]. 2006. 64(3b) 877–880. ISSN 0004-282X

CATANI. Marco, et al. Virtual in vivo interactive dissection of white matter fasciculi in the human brain. NeuroImage [online]. 2002. 17(1), 77–94. ISSN 1053-8119

CHAN, Yl, SCHLEMMER, H., YEUNG. DKW, et al. Comparison of Magnetic Resonance Spectroscopic Imaging and Single Voxel Magnetic Resonance Spectroscopy for Suspected Recurrent Brain Tumour or Radiation Necrosis J. Hong Kong Journal of Radiology. 2001. 4, 259-263.

CHOI, Y. J., et al. Tuberous sclerosis complex proteins control axon formation. Genes & Development [online]. 2008. 22(18), 2485–2495. ISSN 0890-9369

CURATOLO, Paolo, and Raffaella CUSMAI. Autism and infantile spasms in children with tuberous sclerosis. Developmental Medicine & Child Neurology [online]. 2008. 29(4), 551. ISSN 1469-8749

CURATOLO, Paolo, et al. Early onset epileptic encephalopathy or genetically determined encephalopathy with early onset epilepsy? Lessons learned from TSC. European Journal of Paediatric Neurology [online]. 2016. 20(2), 203–211. ISSN 1090-3798

CURRIE, Stuart, et al. Magnetic resonance spectroscopy of the brain. Postgraduate Medical Journal [online]. 2012. 89(1048), 94–106. ISSN 1469-0756

DE VRIES, Petrus J., et al. Tuberous sclerosis associated neuropsychiatric disorders (TAND) and the TAND checklist. Pediatric Neurology [online]. 2015. 52(1), 25–35. ISSN 0887-8994

DIMARIO, Francis J., Mustafa SAHIN. and Darius EBRAHIMI-FAKHARI. Tuberous sclerosis complex. Pediatric Clinics of North America [online]. 2015. 62(3), 633–648. ISSN 0031-3955

DING, Shuang, et al. Demyelination and remyelination detected in an alternative cuprizone mouse model of multiple sclerosis with 7.0 T multiparameter magnetic resonance imaging. Scientific Reports [online]. 2021, 11(1). ISSN 2045-2322

EDMONSON, Catherine, Mark N ZIATS. and Owen M RENNERT. Altered glial marker expression in autistic post-mortem prefrontal cortex and cerebellum. Molecular Autism [online]. 2014. 5(1), 3 ISSN 2040-2392

EHNINGER, Dan, et al. Reversal of learning deficits in a Tsc2+/− mouse model of tuberous sclerosis. Nature Medicine [online]. 2008. 14(8), 843–848. ISSN 1546-170X

EINSTEIN, Albert. Investigations on the theory of Brownian movement. New York. N.Y: Dover Publications. 1956. ISBN 9780486603049.

FAGHIHI, Reza, et al. Magnetic resonance spectroscopy and its clinical applications: a review. Journal of Medical Imaging and Radiation Sciences [online]. 2017. 48(3), 233–253. ISSN 1939-8654

FORD, Talitha C., and David P. CREWTHER. A comprehensive review of the 1H-MRS metabolite spectrum in autism spectrum disorder. Frontiers in Molecular Neuroscience [online]. 2016. 9. ISSN 1662-5099

FRAHM, J., et al. Localized high-resolution proton NMR spectroscopy using stimulated echoes: initial applications to human brain in vivo. Magnetic Resonance in Medicine [online]. 1989. 9(1), 79–93. ISSN 1522-2594

GOMEZ, Manuel Rodríguez, Julian R. SAMPSON, and Vicky Holets WHITTEMORE. eds. Tuberous sclerosis complex. 3rd ed. New York: Oxford University Press. 1999. ISBN 0195122100.

HABAS, Christophe, and Mario MANTO. Probing the neuroanatomy of the cerebellum using tractography. In: The cerebellum: from embryology to diagnostic investigations [online]. Elsevier. 2018. pp. 235–249. ISBN 9780444639561

HAJEK, Milan, and Monika DEZORTOVA. Introduction to clinical in vivo MR spectroscopy. European Journal of Radiology [online]. 2008. 67(2), 185–193. ISSN 0720-048X

HARRIS, Ashley D., Muhammad G. SALEH. and Richard A. E. EDDEN. Edited 1H magnetic resonance spectroscopy in vivo: methods and metabolites. Magnetic Resonance in Medicine [online]. 2017. 77(4), 1377–1389. ISSN 0740-3194

HENSKE, Elizabeth P., et al. Tuberous sclerosis complex. Nature Reviews Disease Primers [online]. 2016. 2(1) ISSN 2056-676X

HOLMES, Gregory L., and Carl E. STAFSTROM. Tuberous sclerosis complex and epilepsy: recent developments and future challenges. Epilepsia [online]. 2007. 48(4), 617–630. ISSN 1528-1167

HSIEH, Christine Chin-jung, et al. Detection of endophenotypes associated with neuropsychiatric deficiencies in a mouse model of tuberous sclerosis complex using diffusion tensor imaging. Brain Pathology [online]. 2020. ISSN 1750-3639

HSU, Yuan-Yu, et al. Reproducibility of hippocampal single-voxel proton MR spectroscopy and chemical shift imaging. American Journal of Roentgenology [online]. 2001. 176(2), 529–536. ISSN 1546-3141

HU, Qingchuan, et al. Metabolite-related antidepressant action of diterpene ginkgolides in the prefrontal cortex. Neuropsychiatric Disease and Treatment [online]. 2018. 14, 999–1011. ISSN 1178-2021

HYMAN, Mark H., and Vicky H. WHITTEMORE. National institutes of health consensus conference: tuberous sclerosis complex. Archives of Neurology [online]. 2000. 57(5), 662. ISSN 0003-9942

ISHIKAW, Hidehiro, et al. Diffusion tensor imaging and magnetic resonance spectroscopy in a patient with adult onset tuberous sclerosis complex. Journal of Clinical Neuroscience [online]. 2018. 48, 108–110. ISSN 0967-5868

JIANG, Yi, and G. Allan JOHNSON. Microscopic diffusion tensor imaging of the mouse brain. NeuroImage [online]. 2010. 50(2), 465–471. ISSN 1053-8119

JOINSON, C., et al. Learning disability and epilepsy in an epidemiological sample of individuals with tuberous sclerosis complex. Psychological Medicine [online]. 2003. 33(2), 335–344. ISSN 1469-8978

MAC DONALD, C. L., et al. Diffusion tensor imaging reliably detects experimental traumatic axonal injury and indicates approximate time of injury. Journal of Neuroscience [online]. 2007. 27(44), 11869–11876. ISSN 1529-2401

MEIKLE, L., et al. A mouse model of tuberous sclerosis: neuronal loss of tsc1 causes dysplastic and ectopic neurons. reduced myelination. seizure activity. and limited survival. Journal of Neuroscience [online]. 2007. 27(21), 5546–5558. ISSN 1529-2401

MILLER, Bruce L. A review of chemical issues in1H NMR spectroscopy:n-acetyl-l-aspartate. creatine and choline. NMR in Biomedicine [online]. 1991. 4(2), 47–52. ISSN 1099-1492

MORI, Susumu, and Jiangyang ZHANG. Principles of diffusion tensor imaging and its applications to basic neuroscience research. Neuron [online]. 2006. 51(5), 527–539. ISSN 0896-6273

MORI, Susumu, et al. Diffusion tensor imaging of the developing mouse brain. Magnetic Resonance in Medicine [online]. 2001. 46(1), 18–23. ISSN 1522-2594

MORI, Susumu, et al. Imaging cortical association tracts in the human brain using diffusion-tensor-based axonal tracking. Magnetic Resonance in Medicine [online]. 2002. 47(2), 215–223. ISSN 1522-2594

MUKONOWESHURO, W., WILKINSON, I.D., GRIFFITHS, P.D. Proton MR spectroscopy of cortical tubers in adults with tuberous sclerosis complex. AJNR. American journal of neuroradiology [online] 2001. 22 (10), 1920-1925.

MÜLLER, Hans-Peter, et al. Longitudinal diffusion tensor magnetic resonance imaging analysis at the cohort level reveals disturbed cortical and callosal microstructure with spared corticospinal tract in the TDP-43G298S ALS mouse model. Translational Neurodegeneration [online]. 2019. 8(1). ISSN 2047-9158

NIE, Duyu, et al. Tsc2-Rheb signaling regulates EphA-mediated axon guidance. Nature Neuroscience [online]. 2010. 13(2), 163–172. ISSN 1546-1726

O'DONNELL, Lauren J., and Carl-Fredrik WESTIN. An introduction to diffusion tensor image analysis. Neurosurgery Clinics of North America [online]. 2011. 22(2), 185–196. ISSN 1042-3680

PROVENCHER, Stephen W. Automatic quantitation of localizedin vivo1H spectra with LCModel. NMR in Biomedicine [online]. 2001, 14(4), 260–264. ISSN 1099-1492

REITH, R. Michelle. et al. Loss of Tsc2 in Purkinje cells is associated with autistic-like behavior in a mouse model of tuberous sclerosis complex. Neurobiology of Disease [online]. 2013. 51, 93–103. ISSN 0969-9961

RODRIGUES, Nelson. et al. The emerging role of tractography in deep brain stimulation: basic principles and current applications. Brain Sciences [online]. 2018. 8(2), 23. ISSN 2076-3425

ROSS, Brian, and Stefan BLUML. Magnetic resonance spectroscopy of the human brain. The Anatomical Record [online]. 2001. 265(2), 54–84. ISSN 1097-0185

ROSSET, Clévia, Cristina Brinckmann Oliveira NETTO. and Patricia ASHTON-PROLLA. TSC1 and TSC2 gene mutations and their implications for treatment in Tuberous Sclerosis Complex: a review. Genetics and Molecular Biology [online]. 2017. 40(1), 69–79. ISSN 1678-4685

ROTT, Hans-Dieter, et al. Cyst-like cerebral lesions in tuberous sclerosis. American Journal of Medical Genetics [online]. 2002. 111(4), 435–439. ISSN 1096-8628

RUPPE, Véronique, et al. Developmental brain abnormalities in tuberous sclerosis complex: a comparative tissue analysis of cortical tubers and perituberal cortex. Epilepsia [online]. 2014. 55(4), 539–550. ISSN 0013-9580

SAHIN, Mustafa. Targeted treatment trials for tuberous sclerosis and autism: no longer a dream. Current Opinion in Neurobiology [online]. 2012. 22(5), 895–901. ISSN 0959-4388

SHEPHERD, Charles W., et al. Subependymal giant cell astrocytoma: a clinical. pathological. and flow cytometric study. Neurosurgery [online]. 1991. 28(6), 864–868. ISSN 0148-396X

SOARES, D. P., and M. LAW. Magnetic resonance spectroscopy of the brain: review of metabolites and clinical applications. Clinical Radiology [online]. 2009. 64(1), 12–21. ISSN 0009-9260

SOARES, José M., et al. A hitchhiker's guide to functional magnetic resonance imaging. Frontiers in Neuroscience [online]. 2016. 10. ISSN 1662-453X

SONG, Sheng-Kwei, et al. Diffusion tensor imaging detects and differentiates axon and myelin degeneration in mouse optic nerve after retinal ischemia. NeuroImage [online]. 2003. 20(3), 1714–1722. ISSN 1053-8119

SONG, Sheng-Kwei, et al. Dysmyelination revealed through MRI as increased radial (but unchanged axial) diffusion of water. NeuroImage [online]. 2002. 17(3), 1429–1436. ISSN 1053-8119

STEJSKAL, E. O., and J. E. TANNER. Spin diffusion measurements: spin echoes in the presence of a time-dependent field gradient. The Journal of Chemical Physics [online]. 1965. 42(1), 288–292. ISSN 1089-7690

TSAI, Jeng-Dau, et al. Disrupted white matter connectivity and organization of brain structural connectomes in tuberous sclerosis complex patients with neuropsychiatric disorders using diffusion tensor imaging. Magnetic Resonance Materials in Physics. Biology and Medicine [online]. 2020. ISSN 1352-8661

TSAI, Peter T., et al. Autistic-like behaviour and cerebellar dysfunction in Purkinje cell Tsc1 mutant mice. Nature [online]. 2012. 488(7413). 647–651. ISSN 1476-4687

TUCH, David S. Q-ball imaging. Magnetic Resonance in Medicine [online]. 2004. 52(6), 1358–1372. ISSN 1522-2594

TKÁC, I., et al. In vivo1H NMR spectroscopy of rat brain at 1 ms echo time. Magnetic Resonance in Medicine [online]. 1999, 41(4), 649–656. ISSN 1522-2594

URKIEWICZ, Elżbieta, JÓŹWIAK, Sergiusz, BEKIESIŃSKA-FIGATOWSKA, Monika, WALECKI. Jerzy and PAKUŁA-KOŚCIESZA. Iwona. Single-voxel proton spectroscopy of cortical tubers in children with tuberous sclerosis complex. Polish Journal of Radiology [online]. 2006. 71 (3), 74–77.

VAN HECKE, Wim, Louise EMSELL, and Stefan SUNAERT. eds. Diffusion tensor imaging [online]. New York. NY: Springer New York. 2016. ISBN 9781493931170

WAKANA, Setsu, et al. Fiber tract–based atlas of human white matter anatomy. Radiology [online]. 2004. 230(1), 77–87. ISSN 1527-1315

WANG. S., et al. Mild hypoxic-ischemic injury in the neonatal rat brain: longitudinal evaluation of white matter using diffusion tensor MR imaging. American Journal of Neuroradiology [online]. 2009. 30(10), 1907–1913. ISSN 1936-959X

WIZNITZER, Max. Autism and tuberous sclerosis. Journal of Child Neurology [online]. 2004. 19(9), 675–679. ISSN 1708-8283

WONG, Michael. Mammalian target of rapamycin (mTOR) inhibition as a potential antiepileptogenic therapy: from tuberous sclerosis to common acquired epilepsies. Epilepsia [online]. 2010. 51(1), 27–36. ISSN 1528-1167

WU, Dan, et al. In vivo high-resolution diffusion tensor imaging of the mouse brain. NeuroImage [online]. 2013. 83, 18–26. ISSN 1053-8119

WU, William E., et al. Brain MR spectroscopic abnormalities in “MRI-negative” tuberous sclerosis complex patients. Epilepsy & Behavior [online]. 2013. 27(2), 319–325. ISSN 1525-5050

YEH, Fang-Cheng. Diffusion MRI metrics - DSI studio—a tractography software tool. DSI Studio—A Tractography Software Tool [online]

YEH, Fang-Cheng, WEDEEN, Van Jay, and TSENG, Wen-Yih Isaac. Generalized q-sampling imaging. IEEE Transactions on Medical Imaging [online]. 2010. 29(9), 1626–1635. ISSN 1558-254X

ZENG, Ling-Hui, et al. Rapamycin prevents epilepsy in a mouse model of tuberous sclerosis complex. Annals of Neurology [online]. 2008. 63(4), 444–453. ISSN 1531-8249

ZHANG, Hongliang, et al. Differences between generalized q-sampling imaging and diffusion tensor imaging in the preoperative visualization of the nerve fiber tracts within peritumoral edema in brain. Neurosurgery [online]. 2013. 73(6), 1044–1053. ISSN 1524-4040

ZHANG, Jiangyang, et al. In vivo and ex vivo diffusion tensor imaging of cuprizone-induced demyelination in the mouse corpus callosum. Magnetic Resonance in Medicine [online]. 2011. 67(3), 750–759. ISSN 0740-3194

APPENDIX

Supplementary Table 1. *R values for males, in the prefrontal cortex. Orange boxes represent strong positive correlation, and blue strong negative. Bolded values mean a significant P-value (P<0.05). In relation to the table diagonal, the bottom triangle represents the values for the wild-type subset and the top the Tsc2$^{+/-}$ condition. Variables where Spearman was used are marked with an asterisk.*

	Ala	GPC + PCh	NAA+NAAG	Cr+PCr	Glu+Gln	GABA	GSH	Ins	Lac	Tau	nqa-gqi*	fa-gqi	md-gqi	ad-gqi	rd-gqi	gfa-gqi	iso-gqi*	fa-reg	md-reg	ad-reg	rd-reg	fa-dti	md-dti	ad-dti	rd-dti
Ala	1.000	0.311	-0.544	0.678	0.276	-0.685	-0.480	0.159	0.908	0.361	-0.357	0.069	0.321	0.499	0.220	0.211	-0.214	0.142	-0.026	0.037	-0.069	-0.050	0.094	0.014	0.063
GPC + PCh	**0.894**	1.000	0.058	0.255	0.493	0.431	0.411	**0.709**	-0.711	0.224	-0.139	0.341	-0.543	0.138	-0.577	0.281	-0.109	0.130	-0.556	-0.483	-0.545	0.267	-0.540	0.055	-0.506
NAA+NAAG	-0.498	0.098	1.000	-0.374	**0.669**	**0.720**	0.124	0.268	-0.172	0.339	-0.301	-0.384	0.119	-0.551	0.016	-0.462	0.220	-0.384	-0.195	-0.393	-0.058	-0.372	-0.321	**-0.681**	-0.066
Cr+PCr	0.517	0.163	0.194	1.000	-0.029	0.323	**0.613**	0.154	0.440	0.053	-0.355	0.017	0.325	0.584	0.415	0.096	-0.545	-0.099	0.325	0.269	0.331	-0.103	0.339	**0.097**	0.270
Glu+Gln	0.613	0.341	-0.261	**-0.836**	1.000	0.051	0.167	0.416	0.016	0.327	-0.255	-0.081	-0.123	-0.414	-0.224	-0.171	0.217	-0.237	**-0.617**	**-0.719**	-0.494	-0.220	-0.427	**-0.607**	-0.203
GABA		0.352	0.614	-0.062	-0.067	1.000	0.598	0.597	-0.830	0.515	-0.464	-0.053	0.080	0.135	0.020	-0.042	-0.119	-0.314	0.300	0.228	0.324	0.086	-0.184	-0.119	-0.198
GSH	-0.015	-0.544	0.102	0.468	-0.557	-0.552	1.000	0.058	-0.073	0.101	-0.309	-0.046	-0.072	0.496	0.216	0.028	-0.491	-0.091	0.125	0.095	0.135	0.113	-0.274	-0.184	-0.272
Ins	0.618	0.121	-0.167	0.425	0.149	0.729	0.124	1.000	-0.469	0.350	0.118	0.401	-0.233	-0.406	-0.527	0.329	0.063	0.211	-0.403	-0.313	-0.424	0.109	-0.078	-0.148	-0.075
Lac		-0.883	-0.536	0.079	-0.989	-0.198	0.753	0.255	1.000	0.443	0.100	-0.330	0.843	0.552	0.771	-0.154	-0.900	0.282	0.726	0.837	0.588	0.003	-0.070	-0.553	-0.098
Tau	**0.790**	0.360	-0.219	**0.809**	-0.231	0.252	0.270	**0.821**	0.038	1.000	-0.083	0.176	**0.771**	0.092	0.000	0.170	0.176	0.260	-0.093	-0.011	-0.142	0.234	-0.537	**-0.726**	-0.474
nqa-gqi	-0.050	0.125	0.446	-0.395	0.258	0.633	-0.296	0.120	-0.814	-0.060	1.000	**0.689**	-0.455	-0.263	**-0.698**	**0.623**	-0.084	**0.740**	-0.369	-0.014	-0.538	**0.608**	-0.052	0.331	-0.267
fa-gqi	-0.057	0.277	0.714	0.312	-0.558	0.491	-0.077	-0.147	-0.818	0.067	**0.780**	1.000	-0.464	0.184	**-0.814**	**0.950**	-0.093	**0.881**	-0.531	-0.131	**-0.710**	**0.827**	-0.237	0.272	-0.499
md-gqi	-0.444	-0.130	0.219	-0.343	0.136	-0.344	-0.094	**-0.734**	-0.994	**-0.646**	0.060	0.321	1.000	0.173	**0.873**	-0.313	-0.196	-0.240	**0.828**	**0.650**	**0.820**	-0.266	0.273	-0.447	0.281
ad-gqi	-0.571	0.108	0.656	-0.507	0.113	0.524	-0.239	-0.200	-0.993	-0.397	0.513	0.514	**0.757**	1.000	0.155	0.363	-0.427	0.294	0.287	0.510	0.151	0.416	-0.220	0.377	-0.384
rd-gqi	-0.264	0.133	0.317	-0.173	0.095	0.591	-0.169	-0.007	-0.965	-0.208	-0.012	0.158	**0.911**	**0.748**	1.000	**-0.699**	-0.181	**-0.666**	**0.810**	0.509	**0.901**	**-0.626**	0.422	-0.221	0.541
gfa-gqi	0.445	0.613	0.474	-0.400	0.130	0.317	-0.441	-0.196	-0.984	0.016	0.588	**0.784**	0.428	**0.834**	**0.654**	1.000	-0.181	**0.926**	-0.344	0.094	**-0.564**	**0.893**	-0.246	0.342	**-0.562**
iso-gqi	-0.053	-0.163	-0.551	-0.536	0.627	0.141	-0.391	0.196	**0.999**	-0.202	-0.140	**-0.710**	-0.377	-0.452	-0.368	-0.525	1.000	-0.299	**-0.593**	**-0.781**	-0.419	-0.229	-0.027	-0.071	0.140
fa-reg	-0.863	-0.068	0.849	-0.147	-0.350	0.544	-0.326	-0.270	0.985	-0.347	0.522	0.514	-0.229	-0.013	-0.381	-0.037	0.253	1.000	-0.321	0.157	**-0.567**	**0.892**	-0.340	0.198	**-0.625**
md-reg	-0.807	-0.195	0.416	0.548	-0.249	-0.677	0.121	-0.348		-0.257	-0.541	-0.016	0.508	0.178	0.386	0.015	-0.150	-0.160	1.000	**0.883**	**0.961**	-0.246	0.469	0.090	0.388
ad-reg	0.010	0.273	0.298	0.362	-0.113	-0.001	-0.161	-0.180	**-0.994**	0.085	0.089	0.489	0.575	0.571	0.529	0.615	**-0.655**	-0.541	**0.802**	1.000	**0.720**	0.185	0.308	0.248	0.083
rd-reg	-0.841	-0.246	0.063	0.243	0.187	-0.026	-0.011	-0.164		-0.301	-0.018	-0.041	0.440	0.336	0.294	0.151	0.086	-0.332	**0.769**	0.623	1.000	-0.474	0.514	0.004	0.526
fa-dti	0.031	-0.061	0.109	-0.067	-0.255	0.430	0.097	-0.129	-0.588	0.070	**0.609**	**0.641**	-0.277	-0.058	**-0.587**	0.011	-0.203	0.357	-0.530	-0.037	0.035	1.000	-0.502	0.262	**-0.783**
md-dti	-0.459	-0.102	0.459	-0.321	0.097	-0.524	-0.081	**-0.770**	-0.995	**-0.643**	0.050	0.365	**0.984**	**0.751**	**0.884**	0.537	-0.462	-0.145	0.566	**0.616**	0.343	-0.379	1.000	0.406	**0.919**
ad-dti	-0.866	**-0.774**	-0.133	-0.530	0.489		-0.008	0.282		-0.422	0.562	-0.476	0.350	0.201	-0.048	-0.458	0.682	-0.120	-0.193	0.020	0.382	0.124	0.287	1.000	0.105
rd-dti	-0.307	0.091	0.332	-0.269	0.115	0.489	-0.204	-0.102	-0.956	-0.290	0.058	0.216	**0.936**	**0.745**	**0.985**	**0.648**	-0.379	-0.245	0.347	0.525	0.230	-0.557	**0.939**	0.089	1.000

Supplementary Table 2. *R values for females, in the prefrontal cortex. Orange boxes represent strong positive correlation, and blue strong negative. Bolded values mean a significant P-value (P<0.05). In relation to the table diagonal, the bottom triangle represents the values for the wild-type subset and the top the Tsc2$^{+/-}$ condition. Variables where Spearman was used are marked with an asterisk.*

	Ala	GPC + PCh	NAA+NAAG	Cr+PCr	Glu+Gln	GABA*	GSH	Ins	Lac	Tau	nqa-gqi	fa-gqi	md-gqi	ad-gqi	rd-gqi	gfa-gqi	iso-gqi	fa-reg	md-reg	ad-reg	rd-reg	fa-dti	md-dti	ad-dti	rd-dti
Ala	1.000	-0.476	-0.088	0.608	-0.214	-1.000	-0.132	0.641	0.845	**0.715**	-0.040	0.268	0.453	0.419	0.241	0.398	-0.226	0.010	0.600	0.866	0.593	0.308	0.289	0.230	0.144
GPC + PCh	-0.519	1.000	0.474	-0.383	0.071	-0.800	-0.345	-0.702	-0.503	-0.661	0.168	0.216	-0.075	0.070	-0.036	0.083	0.013	-0.110	-0.124	0.185	-0.009	0.122	-0.081	-0.172	-0.026
NAA+NAAG		0.174	1.000	-0.422	0.262	0.700	-0.120	-0.309	-0.676	-0.115	0.073	0.426	-0.189	0.465	-0.362	0.107	-0.320	0.450	-0.484	-0.086	-0.489	0.365	-0.169	0.434	-0.274
Cr+PCr	0.857	-0.152	0.124	1.000	**-0.647**	-0.800	0.606	**0.609**	0.587	**0.797**	-0.019	0.010	0.333	-0.127	0.180	0.172	0.151	-0.160	0.437	0.576	0.418	0.102	0.261	0.014	0.163
Glu+Gln	0.449	0.410	0.673	0.271	1.000	0.600	-0.315	-0.273	0.277	-0.507	-0.091	-0.097	-0.126	0.521	-0.088	-0.226	0.175	0.014	-0.444	-0.575	-0.337	-0.151	0.020	0.334	0.061
GABA		0.279	-0.360	-0.789	-0.747	1.000	0.278	-0.806	-0.466	-0.684	0.574	-0.501	-0.008	-0.657	-0.023	-0.388	-0.360	-0.033	-0.526	-0.813	-0.504	-0.432	0.035	0.032	0.060
GSH	0.879	0.140	-0.409	**0.882**	0.252	-0.734	1.000	0.515	0.151	0.249	0.353	0.441	-0.125	0.100	-0.411	0.232	0.367	0.569	-0.154	-0.336	-0.329	0.575	-0.046	0.127	-0.296
Ins	**0.954**	-0.109	0.663	0.710	0.435	-0.507	0.579	1.000	0.677	**0.694**	-0.225	0.256	0.103	0.384	-0.173	0.200	-0.051	0.256	0.539	0.517	0.404	0.379	0.104	0.282	-0.077
Lac		0.227	0.164	-0.856	-0.030	**0.958**	-0.575	-0.311	1.000	0.436	0.135	-0.378	**0.893**	0.275	**0.737**	0.249	-0.028	-0.627	0.749	0.394	0.750	-0.364	**0.877**	0.129	**0.972**
Tau	-0.235	**0.861**	0.149	-0.310	0.574	0.469	0.126	0.127	-0.151	1.000	-0.196	0.077	0.268	0.219	0.171	0.261	0.024	-0.157	0.482	0.622	0.442	0.073	0.237	0.240	0.141
nqa-gqi	**-0.965**	0.013	0.109	-0.615	-0.542	0.877	**-0.853**	-0.488	-0.094	-0.034	1.000	-0.158	-0.064	**-0.722**	-0.043	-0.122	0.197	0.125	-0.234	-0.542	-0.221	-0.086	-0.075	**-0.643**	-0.027
fa-gqi	-0.427	-0.326	0.564	-0.155	0.060	-0.284	-0.575	-0.260	0.318	-0.595	0.221	1.000	-0.458	0.460	**-0.542**	**0.822**	-0.018	**0.580**	-0.320	0.015	-0.405	**0.966**	-0.489	0.245	**-0.722**
md-gqi	-0.455	0.119	-0.061	0.069	0.152	-0.672	0.241	0.289	**-0.919**	**0.743**	0.068	-0.186	1.000	**0.628**	**0.961**	-0.131	-0.175	**-0.625**	**0.627**	0.381	**0.658**	-0.458	**0.970**	**0.577**	**0.916**
ad-gqi	**-0.996**	-0.082	0.268	-0.093	0.138	-0.919	-0.125	0.186	**-0.915**	0.340	0.194	0.338	**0.856**	1.000	0.286	**0.625**	-0.332	-0.078	0.333	0.249	0.294	0.379	0.571	**0.943**	0.261
rd-gqi	-0.109	0.179	-0.239	-0.011	-0.036	0.161	0.505	0.321	-0.604	**0.816**	-0.008	-0.485	**0.844**	0.649	1.000	-0.058	0.078	**-0.731**	**0.613**	0.353	**0.664**	**-0.624**	**0.948**	0.350	0.977
gfa-gqi	-0.551	-0.302	0.590	-0.129	0.047	-0.425	-0.501	-0.218	-0.096	-0.445	0.267	**0.966**	0.050	0.541	-0.263	1.000	-0.021	0.106	0.039	0.081	-0.033	**0.715**	-0.198	0.360	-0.468
iso-gqi	-0.836	-0.996	0.327	-0.346	-0.182	0.020	-0.271	-0.237	0.122	-0.178	0.038	0.615	0.063	0.495	0.073	**0.708**	1.000	0.189	-0.260	0.102	-0.261	-0.018	-0.053	-0.311	0.011
fa-reg	0.082	-0.410	0.252	-0.187	-0.066	0.382	-0.689	-0.292	0.830	**-0.793**	0.246	**0.698**	**-0.742**	-0.329	**-0.885**	0.514	0.035	1.000	**-0.626**	-0.012	**-0.760**	**0.686**	**-0.599**	-0.090	**-0.696**
md-reg	0.365	0.030	-0.271	0.735	0.252	-0.717	0.751	0.493	**-0.918**	0.461	-0.178	-0.211	**0.808**	0.633	**0.733**	-0.027	-0.185	-0.618	1.000	0.754	**0.979**	-0.298	**0.598**	0.283	**0.566**
ad-reg	0.541	-0.090	-0.172	0.679	0.350	**-0.964**	0.510	0.428	**-0.954**	0.290	-0.141	-0.111	**0.747**	0.638	0.473	0.054	-0.368	-0.461	**0.897**	1.000	0.601	0.045	0.294	0.224	0.256
rd-reg	0.276	0.097	-0.286	0.642	0.168	-0.299	**0.803**	0.461	-0.787	0.495	-0.193	-0.255	**0.769**	0.618	**0.813**	-0.065	-0.065	**-0.682**	**0.968**	**0.757**	1.000	-0.399	**0.623**	0.232	**0.625**
fa-dti	-0.282	-0.392	0.431	-0.112	0.075	-0.123	-0.569	-0.282	0.433	-0.667	0.141	**0.958**	-0.384	0.123	-0.648	**0.886**	0.528	**0.806**	-0.339	-0.215	-0.391	1.000	-0.493	0.189	**-0.729**
md-dti	-0.114	0.123	0.033	0.015	0.286	-0.679	0.210	0.447	**-0.920**	**0.796**	0.013	-0.246	**0.968**	**0.816**	**0.848**	-0.031	-0.028	**-0.713**	**0.780**	**0.727**	**0.740**	-0.429	1.000	0.611	**0.949**
ad-dti	-0.457	-0.049	0.260	-0.145	0.302	-0.886	-0.052	0.400	**-0.939**	0.559	0.081	0.094	**0.892**	**0.931**	**0.749**	0.293	0.285	-0.449	0.654	**0.676**	0.631	-0.089	**0.931**	1.000	0.350
rd-dti	0.021	0.180	-0.095	-0.084	0.105	0.219	0.359	0.442	-0.568	**0.819**	-0.024	-0.443	**0.818**	**0.685**	**0.971**	-0.237	0.044	**-0.817**	**0.698**	0.454	**0.772**	-0.612	**0.876**	**0.834**	1.000

Supplementary Table 3. *R values for males, in the hippocampus. Orange boxes represent strong positive correlation, and blue strong negative. Bolded values mean a significant P-value (P<0.05). In relation to the table diagonal, the bottom triangle represents the values for the wild-type subset and the top the Tsc2$^{+/-}$ condition. Variables where Spearman was used are marked with an asterisk.*

	Ala	GPC + PCh	NAA+NAAG	Cr+PCr	Glu+Gln	GABA*	GSH	Ins	Lac	Tau	nqa-gqi	fa-gqi	md-gqi	ad-gqi	rd-gqi	gfa-gqi	iso-gqi*	fa-reg	md-reg	ad-reg	rd-reg	fa-dti	md-dti	ad-dti	rd-dti
Ala	1	-0.1665113	-0.0475374	-0.43878	0.264428		-0.97299	0.88588	0.412597	-0.9334	-0.26168	-0.96733	0.973365	0.730791	0.996216	-0.59992	0	0.255229	0.888615	0.921369	0.867605	-0.34592	0.889297	0.080985	**0.994858**
GPC + PCh		1	0.60563526	-0.1636	-0.121	-0.10714	-0.23021	0.374953	0.272004	-0.30391	0.406559	-0.07388	0.098031	0.236207	0.172669	0.333227	0.076923	-0.38335	-0.29659	-0.40591	-0.21269	0.03476	0.215305	0.10774	0.277891
NAA+NAAG	0.817651	-0.4572031	1	-0.33831	-0.34672	-0.35714	-0.30462	0.413135	0.068752	-0.13512	**0.652667**	-0.03369	0.380299	0.121776	0.423168	-0.26671	0.454545	-0.38932	0.119412	-0.01185	0.207461	-0.01324	0.285009	-0.17192	0.362033
Cr+PCr	0.868686	0.03447936	0.22868347	1	0.076066	0.428571	-0.40372	0.015759	-0.23772	0.324179	0.246368	0.286352	-0.19129	0.027931	-0.30301	0.025197	-0.23626	-0.14644	0.01795	0.04731	-0.00327	0.336175	0.125058	0.057326	-0.02307
Glu+Gln	0.553444	-0.1263582	**0.71911371**	0.555752	1	0.25	-0.42118	0.495119	-0.46047	0.328624	-0.37948	**-0.65873**	-0.31748	-0.57669	-0.11886	-0.60461	0.216783	-0.41842	-0.20559	-0.27098	-0.15309	-0.03039	-0.51349	-0.47382	-0.31454
GABA	0.960679	0.16736573	0.43741525	**0.711003**	0.09243	1	-0.07869	0.655963	0.386536	-0.10947	-0.24522	-0.58213	-0.3045	0.15106	-0.27372	-0.0392	-0.67857	0.236195	0.359482	0.492685	0.259009	0.100906	-0.14328	0.032732	-0.16046
GSH	**-0.9724**	0.5216827	-0.4655266	-0.40578	**-0.72056**	-0.2701	1	0.32662	0.559688	**-0.60951**	-0.01941	-0.07177	-0.08644	-0.03602	-0.10206	0.049648	-0.46154	**0.860401**	-0.03636	0.059622	-0.10386	-0.32692	-0.11728	0.427081	-0.0901
Ins	-0.76373	0.04324595	-0.2869764	0.05208	0.231868	-0.73689	0.001874	1	0.436374	0.561134	0.390265	-0.6214	0.544354	0.386664	0.560066	-0.54093	-0.06667	-0.12986	0.075279	0.016323	0.115833	0.57604	0.042141	-0.19639	0.169044
Lac	0.975865	-0.7485346	0.58702605	0.003046	0.048527	-0.07074	0.075219	-0.14418	1	-0.22329	0.219093	0.048316	0.622328	0.658028	0.549666	0.353836	-0.38333	**0.727328**	0.226895	0.311685	0.167428	0.292706	**0.799896**	**0.79942**	**0.738035**
Tau	-0.20253	-0.1967465	0.4864297	**0.62807**	0.650688	0.371667	**-0.67501**	-0.16627	0.064358	1	-0.02243	0.555344	0.234084	-0.14971	0.170404	-0.3782	-0.07692	-0.20917	0.280938	0.291644	0.268456	0.396157	-0.06063	-0.57859	-0.17889
nqa-gqi	0.096743	0.49167904	0.1615463	0.224066	0.212983	0.249837	-0.31109	-0.01672	0.526008	0.271786	1	0.452137	0.364945	0.373241	0.229884	-0.13436	-0.13187	0.051492	0.040583	0.004622	0.06531	0.522283	0.384443	0.11553	0.31709
fa-gqi	-0.07985	0.18590397	-0.3776926	-0.11119	-0.35744	-0.21292	-0.05441	0.032894	0.409019	-0.37572	0.490254	1	0.10283	0.203355	-0.12019	0.589455	0.009091	0.135385	0.023579	0.076993	-0.01293	**0.785991**	0.287562	0.126069	0.03986
md-gqi	0.071573	0.10407066	0.04006729	-0.30302	-0.30041	0.184348	-0.17974	-0.5454	0.086325	-0.08965	0.524209	0.368492	1	**0.922595**	**0.958496**	-0.31617	-0.23636	0.14466	**0.736997**	**0.709612**	**0.741426**	0.465757	**0.842855**	0.365137	**0.873174**
ad-gqi		0.15442708	0.11193065	-0.3017	-0.33957	0.191971	0.286983	0.066998	0.328196	-0.28561	0.615553	0.2607	**0.904027**	1	**0.774959**	0.390795	-0.32168	0.257227	**0.620676**	**0.644415**	0.592452	0.471296	**0.800658**	0.593396	**0.75043**
rd-gqi	0.112691	0.06770993	0.05206467	-0.1215	-0.19965	-0.28544	-0.21512	-0.404	0.17168	0.216862	0.483938	0.269413	**0.959214**	**0.690305**	1	-0.432	0.009091	0.040679	**0.746151**	**0.685497**	**0.773115**	0.26338	**0.767309**	0.221872	**0.867392**
gfa-gqi	-0.06209	0.22727727	-0.3235668	-0.31308	-0.41016	-0.18302	0.020784	-0.16196	0.33049	-0.50928	0.554485	**0.94367**	**0.636123**	0.575391	0.506087	1	-0.1	0.0552	**-0.8752**	**-0.81636**	**-0.8939**	0.405467	0.239172	0.587881	0.008025
iso-gqi	0.668063	-0.3678059	**0.77969567**	-0.06839	0.583232	0.413134	-0.5019	-0.19872	0.113544	0.108224	0.062481	-0.37529	0.170399	0.184787	-0.08324	-0.29526	1	-0.44594	0.016808	-0.11743	0.111892	0.048914	-0.11336	-0.36649	0.004056
fa-reg	0.160331	0.25485706	-0.3768547	-0.12314	-0.30919	-0.45109	0.499351	0.305904	-0.10376	-0.53884	-0.24124	0.417365	0.122108	0.073791	0.312149	**0.597851**	-0.4861	1	0.181556	0.319402	0.079756	0.030786	0.133468	0.50253	0.075163
md-reg	-0.6987	0.01882355	0.05140876	-0.40899	-0.15605	-0.29394	-0.06447	-0.00818	-0.23064	0.330395	0.36723	-0.31569	0.508039	0.601732	0.486835	-0.04235	0.247072	-0.48452	1	0.982914	0.991398	-0.07281	0.613792	-0.20762	**0.64494**
ad-reg	-0.62901	0.08232785	-0.0723425	-0.41626	-0.2301	-0.39436	-0.03519	0.098927	-0.22231	0.291364	0.427255	-0.15907	0.565152	**0.688538**	0.575624	0.113722	0.097877	-0.28626	**0.974559**	1	0.950369	-0.05796	0.590132	-0.13926	0.590716
rd-reg	-0.75115	-0.0226119	0.12458579	-0.39463	-0.10599	-0.23119	-0.08303	-0.06999	-0.22954	0.344652	0.322153	-0.40218	0.461277	0.539821	0.417106	-0.13518	0.330766	-0.59193	**0.990872**	**0.93545**	1	-0.08281	0.618079	-0.24652	**0.669484**
fa-dti	-0.13933	0.54293919	-0.4642036	-0.27197	-0.17714	-0.32135	0.089633	0.319733	0.193047	-0.40923	0.345342	**0.846438**	0.089135	0.14354	0.12398	**0.68165**	-0.3219	0.400149	-0.29774	-0.12633	-0.40048	1	0.339082	0.223788	0.155762
md-dti		-0.2339154	0.38916289	-0.19209	-0.17095	0.150617	0.076129	-0.20642	0.628588	0.090711	0.581283	-0.08139	**0.837644**	**0.791224**	**0.713677**	0.232421	0.327824	-0.34193	**0.854003**	**0.840398**	**0.842374**	-0.34932	1	0.861878	**0.960309**
ad-dti		-0.0645301	0.02037241	-0.08456	-0.30245	-0.09177	0.316033	0.252841	0.694207	-0.31525	**0.704903**	0.565179	0.586874	**0.822033**	0.362719	**0.788071**	-0.06223	0.233075	0.399295	0.50439	0.331754	0.154609	**0.751555**	1	**0.672811**
rd-dti	0.012312	-0.2809884	0.15013983	-0.31357	-0.20921	0.061114	-0.30674	**-0.66869**	0.215462	0.168243	0.460961	0.242562	**0.90581**	0.590083	**0.872613**	0.516922	0.211291	-0.11829	0.588225	0.595993	0.569184	-0.12291	**0.917879**	0.428134	1

Supplementary Table 4. *R values for females, in the hippocampus. Orange boxes represent strong positive correlation, and blue strong negative. Bolded values mean a significant P-value (P<0.05). In relation to the table diagonal, the bottom triangle represents the values for the wild-type subset and the top the Tsc2$^{+/-}$ condition. Variables where Spearman was used are marked with an asterisk.*

	Ala	GPC + PCh	NAA+NAAG	Cr+PCr	Glu+Gln	GABA	GSH	Ins	Lac	Tau	nqa-gqi	fa-gqi	md-gqi	ad-gqi	rd-gqi	gfa-gqi	iso-gqi	fa-reg	md-reg	ad-reg	rd-reg	fa-dti	md-dti	ad-dti	rd-dti
Ala	1	-0.6478176	-0.6923589	-0.15944	0.937277	-0.3598		-0.93645	-0.73143	-0.37807	-0.46983	0.022422	-0.91831	-0.92129	-0.91229	-0.86727	-0.2999	0.996684	-0.86625	-0.8162	-0.88691	-0.6472	-0.90005	-0.87483	-0.87837
GPC + PCh		1	-0.1812039	-0.13312	-0.50213	-0.14716	0.321843	-0.13527	0.081148	-0.25072	-0.36642	-0.09382	0.419157	0.459866	-0.06611	0.166995	-0.25906	-0.23623	0.340196	0.342968	0.328276	-0.00355	0.428802	0.401484	-0.11838
NAA+NAAG	0.964842	-0.1303985	1	0.067652	0.043129	0.642244	0.153365	0.218391	0.453158	0.241721	-0.09397	-0.27166	0.108593	0.087892	0.092312	-0.28088	-0.05689	-0.50882	-0.09464	0.074324	0.013478	0.027588	0.275143	0.155577	0.268891
Cr+PCr		-0.3662551	0.37335832	1	0.407356	0.048373	0.406712	0.438713	0.672511	0.448669	-0.06583	0.672888	-0.50743	-0.31001	-0.34485	0.370279	-0.43309	0.612923	-0.19639	-0.45871	-0.32359	0.454652	-0.60135	-0.37858	-0.36484
Glu+Gln	0.993898	-0.3497905	0.79712642	0.127524	1	0.067317	-0.48764	0.56578	-0.21005	0.262496	-0.15834	0.033225	-0.7829	-0.81327	0.30194	-0.22764	-0.2343	0.289562	-0.45702	-0.65551	-0.49725	-0.24272	-0.55777	-0.66979	-0.02487
GABA		-0.538261	0.21396755	-0.20857	0.298065	1	-0.22393	0.607457	0.454078	0.063037	-0.03606	0.323516	0.129762	0.197361	0.060682	-0.27488	0.116597	-0.40846	-0.41562	-0.29344	-0.33249	0.341091	0.086426	0.15792	-0.00148
GSH	-0.05494	0.41141037	0.03440416	-0.04397	-0.15319	-0.1024	1	-0.35617	0.638185	0.045916	0.481449	0.387315	0.214756	0.456574	0.067397	0.300287	-0.36625	0.242152	0.474409	0.411341	0.413932	0.572928	0.216978	0.443278	0.065324
Ins	0.338193	0.3598871	0.04210875	0.380352	0.00023	0.275064	0.526018	1	0.078499	0.439066	0.070509	0.193038	-0.17709	-0.06179	-0.12086	0.328467	-0.04675	-0.23514	-0.00199	-0.17616	0.017742	0.311481	-0.03946	-0.00234	0.049327
Lac	-0.47116	-0.5618612	0.20201887	0.98368	0.370023	0.006406	-0.41661	-0.71147	1	-0.26612	0.101323	0.225874	0.709315	0.698138	0.740122	0.074736	0.011655	-0.07286	0.099372	0.243542	0.110626	0.644979	0.58027	0.660118	0.452631
Tau		-0.656458	-0.5938127	0.542028	-0.44943	-0.21105	-0.16441	-0.23004	0.288322	1	0.328755	0.055205	-0.25429	-0.1968	-0.32562	0.265635	-0.3204	-0.21638	0.313354	0.179272	0.3088	0.13408	-0.1896	-0.24459	-0.17394
nqa-gqi	-0.6204	0.66354143	-0.07068677	0.21005	-0.43604	-0.46521	0.044008	0.198073	-0.29591	-0.01175	1	0.166388	0.52389	0.58531	0.578676	0.344943	0.28603	0.07652	0.542632	0.503604	0.517166	0.477874	0.388969	0.456249	0.474743
fa-gqi	-0.87838	0.10498055	0.14484247	-0.00545	0.097034	-0.17608	0.244941	0.081796	-0.13895	-0.46059	0.547395	1	-0.20739	0.047672	-0.35936	0.643569	-0.10013	0.566914	-0.24086	-0.36949	-0.31882	0.796874	-0.37992	-0.11233	-0.5394
md-gqi	-0.97671	0.31069744	0.09176385	0.121184	-0.1942	-0.59585	0.272937	-0.18468	0.656512	-0.44132	0.497358	0.885161	1	0.957299	0.982528	0.202577	0.439752	-0.28166	0.719413	0.906434	0.755031	0.356587	0.916189	0.887171	0.867322
ad-gqi	-0.9604	0.5139984	0.08678399	-0.28319	-0.31523	-0.5009	0.043664	-0.04885	-0.2138	-0.63725	0.562356	0.869448	0.988707	1	0.886949	0.458152	0.399917	-0.2133	0.71554	0.85321	0.736936	0.571075	0.86406	0.926436	0.754123
rd-gqi	-0.99838	0.15012682	0.07866802	0.177521	-0.09753	-0.75507	-0.01041	-0.33204	0.7561	-0.35376	0.358446	0.65811	0.930954	0.866642	1	0.045055	0.394994	-0.11505	0.538729	0.697845	0.56038	0.193783	0.90925	0.821932	0.92556
gfa-gqi	-0.91453	0.05618736	0.11824729	-0.0062	0.142316	-0.35649	0.061018	0.041441	-0.11785	-0.42856	0.619157	0.972431	0.953184	0.954663	0.778729	1	0.178232	-0.02089	0.351783	0.31003	0.338835	0.63757	0.13874	0.404316	-0.06535
iso-gqi	0.864399	-0.2666327	0.27550003	0.328241	0.272252	0.022257	-0.24957	0.251708	-0.24623	0.534042	-0.2851	-0.63386	-0.77243	-0.69987	-0.61019	-0.52468	1	-0.06441	0.200377	0.392662	0.246802	0.108981	0.363397	0.382856	0.271877
fa-reg	0.671665	0.09455264	-0.3551924	0.316782	-0.3468	0.63464	0.539341	0.344387	0.132427	0.111045	0.136071	0.071733	0.072069	-0.13422	-0.1708	-0.08979	-0.41955	1	-0.3062	-0.48074	-0.44671	0.108422	-0.47532	-0.41811	-0.22157
md-reg	-0.90486	-0.2220595	0.47184305	0.294182	0.28109	-0.75105	0.160789	0.011919	0.696818	-0.36946	-0.29468	0.398733	0.506833	0.473118	0.584754	0.423821	-0.03517	-0.58439	1	0.987324	0.985748	0.504891	0.790489	0.805349	0.53812
ad-reg	-0.95506	-0.088278	0.31304426	0.203684	0.101698	-0.75671	0.31007	0.094714	0.729159	-0.47935	-0.37034	0.354233	0.521456	0.498376	0.566893	0.322387	-0.22265	-0.30067	0.941749	1	0.971025	0.435371	0.933811	0.910649	0.648379
rd-reg	-0.87202	-0.278473	0.52791884	0.326431	0.365458	-0.73089	0.073951	-0.02857	0.679081	-0.30074	-0.24854	0.403665	0.485664	0.447492	0.577883	0.455214	0.056872	-0.69723	0.986719	0.874612	1	0.449835	0.843865	0.84949	0.567458
fa-dti	-0.93702	0.16413604	0.19499194	-0.40965	0.119619	-0.48814	0.175551	-0.07067	-0.34305	-0.69134	0.242281	0.873098	0.804506	0.891229	0.647137	0.871656	-0.59096	-0.24694	0.543656	0.520248	0.532411	1	0.349524	0.562504	0.130728
md-dti	-0.99542	0.05451577	-0.2709993	-0.20433	0.071015	-0.70201	0.025177	-0.19557	0.805506	-0.47213	-0.17152	0.304666	0.580982	0.493435	0.732592	0.391537	-0.47738	-0.11685	0.617722	0.733203	0.542651	0.47572	1	0.931078	0.960863
ad-dti	-0.99819	0.19035766	-0.0116797	-0.32863	0.024779	-0.79282	0.304921	-0.26161	0.745471	-0.68414	-0.0153	0.668962	0.826307	0.7927	0.841044	0.715406	-0.70455	-0.11265	0.662291	0.73721	0.606484	0.854265	0.856484	1	0.793696
rd-dti	-0.9055	0.16375328	-0.3656195	-0.29954	-0.12822	-0.37459	-0.55158	0.032234	-0.24812	-0.32577	-0.02955	-0.06641	-0.05127	0.345275	0.218818	0.11562	-0.03654	-0.31327	0.221904	0.335358	0.158614	0.186952	0.700765	0.232599	1

Supplementary Table 5. *R values for males, in the striatum. Orange boxes represent strong positive correlation, and blue strong negative. Bolded values mean a significant P-value (P<0.05). In relation to the table diagonal, the bottom triangle represents the values for the wild-type subset and the top the Tsc2$^{+/-}$ condition. Variables where Spearman was used are marked with an asterisk.*

	Ala	GPC + PCh	NAA+NAAG	Cr+PCr	Glu+Gln	GABA	GSH	Ins	Lac	Tau	nqa-gqi	fa-gqi	md-gqi	ad-gqi	rd-gqi	gfa-gqi	iso-gqi*	fa-reg	md-reg	ad-reg	rd-reg	fa-dti	md-dti	ad-dti	rd-dti
Ala	1	0.2984365	-0.6928109	0.390199	-0.75301	0.206318	-0.04906	0.280486	0.623479	-0.05927	-0.07548	0.024991	-0.56806	-0.83033	0.160411	0.441803	-0.46667	0.165798	0.719906	0.584236	0.739399	-0.01765	-0.62167	0.51331	-0.37839
GPC + PCh	0.699012	1	0.1973907	0.28214	0.381443	0.463586	-0.09189	0.676132	0.590179	-0.08159	0.393885	0.13607	-0.07504	-0.12816	0.015404	0.160493	-0.02198	0.009602	0.252671	0.137644	0.321986	0.19787	-0.23961	-0.16151	-0.11654
NAA+NAAG	0.642756	0.1146311	1	-0.03029	0.397718	-0.03556	-0.13623	0.537678	-0.13132	-0.02426	0.19289	0.204972	-0.34341	0.049884	-0.49874	-0.15047	0.781818	-0.24825	-0.30768	-0.32957	-0.27946	0.425734	-0.10611	-0.4181	-0.29559
Cr+PCr	0.081341	-0.197278	-0.089595	1	-0.15511	0.285113	0.011806	0.61585	0.41057	0.247193	-0.06527	0.70427	0.060019	0.11092	-0.01573	0.755793	-0.22378	0.445464	0.240291	0.141125	0.298075	0.682006	-0.21273	0.065591	-0.15816
Glu+Gln	0.215328	0.5814047	-0.2561082	0.213565	1	0.222992	0.014387	0.041497	0.103755	-0.46599	0.741534	0.219531	0.334049	0.433191	0.175761	-0.06992	0.127273	0.070997	0.102655	0.11391	0.090461	0.244195	-0.03826	-0.66892	0.05606
GABA	0.412499	0.5539412	0.2829157	0.040024	0.340582	1	0.561832	0.337991	0.618627	0.071024	0.284909	0.12404	-0.28549	-0.12426	-0.28283	0.171671	-0.12587	0.451629	-0.02251	0.132855	-0.13468	0.171805	-0.34686	0.012242	-0.33978
GSH	-0.1537	0.3303188	0.46655	0.050313	-0.2677	-0.24776	1	-0.08432	-0.02817	0.464886	-0.33252	-0.27156	-0.34711	-0.51234	-0.07408	-0.20833	-0.24209	0.179935	-0.30704	-0.23256	-0.33822	-0.18729	-0.33372	-0.18672	-0.17697
Ins	0.188044	-0.257938	0.0369235	0.195661	0.052811	0.056385	-0.22986	1	0.493375	0.092655	0.158652	0.375378	-0.29854	-0.08192	-0.32795	0.214071	0.28022	-0.12325	0.063085	-0.02586	0.129339	0.535017	-0.37735	-0.28609	-0.40619
Lac	0.568281	0.7400078	0.1892644	-0.14895	0.14276	0.63303	-0.05766	0.000731	1	-0.25729	0.590135	0.716407	-0.25715	0.3151158	-0.59625	0.73114	-0.18182	0.660644	0.653482	0.695941	0.555371	0.763459	-0.44462	0.517886	-0.71185
Tau	-0.04252	-0.1181107	-0.0391665	0.469601	-0.20146	0.04497	0.011751	0.206698	0.354913	1	-0.63041	-0.09341	-0.20978	-0.47015	0.091266	-0.02068	-0.0979	-0.18871	-0.42961	-0.55961	-0.28163	-0.09313	0.114289	-0.2197	0.312716
nqa-gqi	0.124413	-0.307415	0.3671307	-0.16903	-0.62518	0.057935	-0.13885	0.311695	0.055262	0.452092	1	0.595417	0.082456	0.542593	-0.30464	0.507282	0.06044	0.373561	0.465913	0.582249	0.326804	0.551363	0.204964	0.37058	-0.08428
fa-gqi	0.634496	-0.12899	0.4466782	-0.12484	-0.45159	-0.10299	-0.18521	0.123953	0.20301	0.057696	0.562533	1	-0.0764	0.586145	-0.54797	0.828552	0.048951	0.585944	0.248627	0.372298	0.15009	0.953335	-0.06883	0.263456	-0.3475
md-gqi	0.632614	0.0308233	0.1066668	-0.01949	-0.26806	0.066799	-0.16039	0.04213	-0.13852	-0.5571	0.16643	0.580312	1	0.67359	0.814585	0.108717	-0.44545	-0.21933	0.631386	0.497245	0.633294	-0.24005	0.799806	0.493378	0.820174
ad-gqi	0.106609	0.0772472	0.1224061	-0.40455	-0.48746	-0.37893	0.245215	-0.18176	0.199344	-0.16987	0.366287	0.712083	0.874283	1	0.120366	0.697936	-0.15455	0.189926	0.680088	0.826571	0.478337	0.439792	0.648619	0.901206	0.301547
rd-gqi	0.229513	0.0207745	-0.1517724	-0.03475	-0.07641	0.137162	-0.14157	-0.04207	-0.25097	-0.66144	-0.14746	0.075149	0.846288	0.460431	1	-0.36394	-0.63636	-0.46038	0.320789	0.024358	0.481652	-0.67555	0.528585	-0.02442	0.786604
gfa-gqi	0.545733	-0.077668	0.4121158	-0.17509	-0.56314	-0.03859	-0.17972	0.064956	0.280404	0.107322	0.667714	0.972841	0.64645	0.831633	0.154703	1	-0.44056	0.61989	0.596797	0.713139	0.489618	0.705942	0.245318	0.764525	-0.0273
iso-gqi	-0.35591	-0.063061	-0.166596	0.016742	0.325325	0.091176	0.031229	-0.00932	0.024019	0.207177	-0.15841	-0.71341	-0.70154	-0.47206	-0.42028	-0.67921	1	-0.33981	-0.44955	-0.35387	-0.48431	0.284903	-0.36764	-0.47831	-0.67172
fa-reg	-0.01658	-0.235439	0.3221248	0.042722	-0.2285	-0.32627	0.410043	0.003073	0.235548	0.077957	-0.18127	0.194134	-0.21826	0.320169	-0.3249	0.077531	0.195887	1	0.070533	0.314345	-0.10697	0.474625	-0.37938	0.293136	-0.464
md-reg	-0.16899	0.0746482	-0.0077038	-0.64307	-0.29901	-0.28506	0.081196	-0.74073	-0.12813	-0.56024	0.026465	0.157424	0.674636	0.715581	0.618074	0.305796	-0.19835	-0.03105	1	0.93475	0.957397	0.15647	0.660528	0.863193	0.480649
ad-reg	0.720573	-0.024306	0.3800385	-0.25008	-0.1828	-0.34812	0.316863	-0.52147	-0.1253	-0.60493	-0.38976	0.517685	0.682035	0.746592	0.412124	0.487313	-0.36979	0.561107	0.756892	1	0.792324	0.268954	0.517666	0.934053	0.164344
rd-reg	-0.36932	0.0938438	-0.1758129	-0.60652	-0.20633	-0.22957	0.022212	-0.64644	-0.26155	-0.60605	-0.02384	-0.10193	0.508844	0.491997	0.599023	0.048631	-0.21419	-0.37808	0.929277	0.424241	1	0.069627	0.621314	0.698284	0.592412
fa-dti	0.42252	-0.164996	0.3491712	-0.18117	-0.43479	-0.23816	-0.15027	0.212317	0.233188	0.100242	0.496426	0.918619	0.412698	0.661194	-0.05605	0.88126	-0.73126	0.338189	0.149792	0.419162	-0.06934	1	-0.21806	0.106128	-0.4985
md-dti	0.222516	0.0379191	0.0658182	-0.19075	-0.23949	-0.07245	0.307747	0.084637	-0.19062	-0.63232	-0.15835	0.122542	0.906241	0.650987	0.916614	0.203302	-0.48881	-0.01322	0.717598	0.581749	0.631006	0.125565	1	0.795123	0.898
ad-dti	0.416709	-0.084095	0.0540478	-0.22992	-0.41507	-0.19376	0.112081	-0.33213	-0.03172	-0.50463	-0.38353	0.400645	0.87507	0.818835	0.654947	0.455956	-0.77089	0.276457	0.688114	0.71751	0.50539	0.454193	0.826674	1	0.447423
rd-dti	-0.2729	0.0768719	-0.0748204	-0.34733	-0.26442	0.047817	0.162003	-0.26122	-0.06897	-0.4886	0.039284	-0.12454	0.720534	0.541612	0.952355	0.053856	0.051602	-0.11447	0.742288	0.395701	0.712648	-0.13059	0.907786	0.565706	1

Supplementary Table 6. *R values for females, in the prefrontal cortex. Orange boxes represent strong positive correlation, and blue strong negative. Bolded values mean a significant P-value (P<0.05). In relation to the table diagonal, the bottom triangle represents the values for the wild-type subset and the top the Tsc2$^{+/-}$ condition. Variables where Spearman was used are marked with an asterisk.*

	Ala	GPC + PCh	NAA+NAAG	Cr+PCr	Glu+Gln	GABA	GSH	Ins	Lac	Tau	nqa-gqi	fa-gqi	md-gqi	ad-gqi	rd-gqi	gfa-gqi	iso-gqi	fa-reg	md-reg	ad-reg	rd-reg	fa-dti	md-dti	ad-dti	rd-dti
Ala	1	-0.249972	0.1329065	0.062591	0.05275	-0.30378	0.126812	-0.17096	0.210284	0.104631	-0.00249	0.01935	0.116562	-0.34066	0.334536	0.245722	-0.05319	0.135843	-0.12527	-0.08404	-0.14182	0.186358	-0.0857	0.063874	0.098551
GPC + PCh	0.847124	1	0.1211452	0.023084	-0.05686	0.04815	-0.26862	-0.32267	0.127425	-0.28834	-0.60197	-0.1818	-0.51215	-0.31413	-0.3646	-0.13553	-0.45103	-0.04767	-0.41679	-0.44839	-0.37254	-0.03574	-0.51272	-0.27988	-0.34717
NAA+NAAG	0.061269	0.5663646	1	0.26575	-0.30776	-0.1462	0.653038	0.597208	0.285351	0.722355	0.124505	0.210055	-0.08996	0.326541	0.083427	0.366075	0.196246	0.248282	-0.31101	-0.23071	-0.33894	0.359288	-0.22755	0.100553	-0.04612
Cr+PCr	-0.1217	0.68348	0.373154	1	0.590025	0.459411	-0.08763	0.71978	-0.08705	0.469388	-0.19788	0.332078	-0.33109	0.200106	-0.33309	0.326263	-0.16809	-0.04978	-0.52801	-0.57769	-0.47033	0.383523	-0.46642	0.036796	-0.4986
Glu+Gln	0.235386	0.2940904	0.1377202	0.504758	1	0.664506	-0.56873	0.171227	-0.11126	0.009872	-0.49429	0.074592	-0.27709	-0.08801	-0.22895	0.067579	-0.44035	-0.06028	-0.22129	-0.2433	-0.19393	0.163102	-0.41525	-0.06273	-0.4205
GABA	0.705551	0.6933056	0.2501647	-0.07469	0.263907	1	-0.48878	0.545452	0.223433	0.372839	0.114855	0.259195	-0.07922	0.115409	-0.27662	0.120306	-0.28769	0.019275	-0.27217	-0.30404	-0.24084	0.168811	-0.04364	0.035759	-0.24678
GSH	0.669204	0.7037929	0.4730042	0.241214	0.077013	-0.29717	1	0.366529	0.01595	0.59164	0.379036	0.4912	0.219728	0.352781	0.145232	0.632691	0.455093	0.457459	0.112448	0.320121	-0.01157	0.483656	0.138123	0.381389	0.04511
Ins	0.579994	0.4140295	0.1856696	0.118276	0.046199	-0.59284	0.843504	1	-0.04968	0.764913	0.394327	0.418322	0.168158	0.569218	0.014923	0.373676	0.293258	0.027344	-0.03517	-0.00716	-0.04853	0.316191	0.063943	0.408728	-0.1414
Lac	0.468046	0.6175644	0.6519328	0.786309	0.51327	0.267142	0.381557	0.06085	1	0.114857	0.170954	-0.16618	-0.0812	-0.16662	0.032444	-0.18023	-0.13763	0.018803	-0.22165	-0.25363	-0.1907	-0.06768	-0.23672	-0.11845	-0.1375
Tau	-0.52232	-0.41833	0.4805912	0.135659	-0.02641	-0.17307	-0.15403	-0.3607	0.43396	1	0.373377	0.428167	0.313403	0.62149	0.246906	0.522564	0.303127	0.37816	-0.23773	-0.07684	-0.31472	0.399085	0.123197	0.33706	0.033346
nqa-gqi	-0.28801	0.0476473	-0.0861996	0.141285	0.266478	0.765685	-0.3957	-0.28944	-0.38046	-0.46941	1	0.210035	0.615546	0.364562	0.347815	0.030014	0.465963	0.074891	0.268993	0.301044	0.234255	-0.08558	0.84135	0.399489	0.585333
fa-gqi	0.057922	-0.11327	-0.4899131	-0.30659	0.316774	0.060596	-0.0119	0.239761	-0.58284	-0.69459	0.662161	1	-0.19865	-0.1113	-0.49298	0.898107	0.431735	0.695641	-0.34661	-0.0586	-0.49662	0.985372	-0.26463	0.052799	-0.59586
md-gqi	-0.49071	-0.1025564	0.175945	-0.3145	0.178506	-0.12448	0.456729	-0.22413	0.134806	-0.1291	0.056182	1	0.801412	0.942331	-0.02706	0.258544	-0.22534	0.70995	-0.27217	-0.30404	-0.24084	0.168811	-0.04364	0.035759	-0.24678
ad-gqi	0.392892	0.3453086	0.401328	-0.52813	0.374995	-0.05279	0.626561	0.630072	0.138935	-0.08243	-0.30106	0.117572	0.92386	1	0.732705	0.104578	0.087483	-0.1178	0.446678	0.453064	0.420723	-0.16876	0.627592	0.82077	0.532173
rd-gqi	-0.67959	-0.127623	0.6591016	-0.09568	0.082084	-0.18322	0.443498	0.366166	-0.0275	0.383423	-0.29357	-0.21549	0.956772	0.772806	1	-0.16099	-0.1002	-0.24331	0.663936	0.577286	0.668526	-0.48974	0.893754	0.639794	0.904597
gfa-gqi	0.429156	0.3696533	-0.1111737	-0.42193	0.42373	0.20025	0.335569	0.444683	-0.26347	-0.61098	0.446029	0.814954	0.368948	0.62352	0.090746	1	0.108885	0.560073	-0.20523	0.051298	-0.33891	0.860352	-0.094	0.248641	-0.26631
iso-gqi	0.535485	0.2887616	-0.0941911	-0.60234	0.693982	0.256127	0.230075	0.305886	0.260661	-0.17721	-0.39827	0.225831	0.261702	0.664692	0.088629	0.571182	1	0.149293	0.07986	0.112538	0.057615	0.043568	0.212055	-0.09728	-0.16439
fa-reg	0.26171	-0.109018	-0.8993564	-0.14556	0.092985	-0.00072	-0.46732	-0.19728	-0.3671	-0.64089	-0.03453	0.170334	-0.5734	-0.37363	-0.62009	-0.02972	0.312805	1	-0.35982	-0.0096	-0.53732	0.781836	-0.26122	-0.022	-0.30596
md-reg	0.511602	0.6152191	0.3832983	0.431794	0.146658	-0.49774	0.742036	0.871705	0.382466	-0.22776	-0.32146	-0.08985	0.124751	0.430427	0.105168	0.146096	0.207399	-0.03778	1	0.929438	0.977926	-0.47163	0.775364	0.636557	0.656177
ad-reg	0.559485	0.4448218	0.0759142	0.253397	0.079345	-0.15406	-0.58879	0.688372	0.456729	0.224213	0.134806	-0.1291	0.056182	1	0.042331	-0.02706	0.258544	0.242507	0.207754	0.22534	0.70995	0.677471	0.885074	-0.10424	0.692141	0.771218	0.509558
rd-reg	-0.23252	0.431069	0.4211005	0.54332	-0.02239	-0.36183	0.475478	0.68036	0.100319	-0.15183	0.191786	-0.04443	0.262202	0.174485	0.291301	-0.03092	-0.43047	-0.21735	0.919093	0.681604	1	-0.60621	0.766401	0.556156	0.697568
fa-dti	0.085712	0.1832237	-0.181671	-0.13549	0.429495	0.231995	0.078398	0.290326	-0.40102	-0.66609	0.707505	0.9249	0.093417	0.165233	-0.13816	0.788136	0.243231	0.105007	0.074789	0.281585	0.122101	1	-0.4769	-0.04149	-0.59747
md-dti	0.38928	0.2710584	0.4292855	-0.4783	0.130784	-0.25242	0.751057	0.673243	0.13225	0.058542	-0.55107	-0.0523	0.9064	0.91829	0.836327	0.422562	0.590903	-0.44558	0.436928	0.333207	0.10021	-0.00328	1	0.677468	0.926263
ad-dti	0.379009	0.2746808	0.3194783	-0.52026	0.2502	-0.12516	0.659338	0.667755	-0.00227	-0.13677	-0.307	0.242723	0.849202	0.950415	0.696914	0.669578	0.6836	-0.35689	0.426811	0.382788	0.12566	0.303504	0.947268	1	0.394388
rd-dti	0.377913	0.2673215	0.4899339	-0.40421	0.037738	-0.34587	0.778962	0.637183	0.238315	0.207075	-0.67582	-0.26314	0.872722	0.837776	0.875473	0.218512	0.487955	-0.46995	0.418696	0.277926	0.06787	-0.22478	0.973129	0.848153	1

Supplementary Table 7. *R values for males, in the cerebellum. Orange boxes represent strong positive correlation, and blue strong negative. Bolded values mean a significant P-value (P<0.05). In relation to the table diagonal, the bottom triangle represents the values for the wild-type subset and the top the Tsc2$^{+/-}$ condition. Variables where Spearman was used are marked with an asterisk.*

	Ala	GPC + PCh	NAA+NAAG	Cr+PCr	Glu+Gln	GABA	GSH	Ins	Lac	Tau	nqa-gqi	fa-gqi*	md-gqi	ad-gqi	rd-gqi	gfa-gqi*	iso-gqi*	fa-reg*	md-reg	ad-reg	rd-reg	fa-dti	md-dti	ad-dti	rd-dti
Ala	1																								
GPC + PCh		1	-0.1295067	0.390907	0.290574	0.374325	0.556879	0.357577	0.330434	0.102629	-0.30584	-0.36667	-0.1726	-0.33427	-0.23103	0	-0.05	0.283333	0.302562	0.495717	0.188574	0.092667	-0.49956	-0.51457	-0.47918
NAA+NAAG		0.3448637	1	0.259155	0.647168	-0.11815	-0.32185	0.430224	-0.66629	0.596626	0.20021	-0.61905	-0.56996	0.16415	0.312673	-0.69048	0.47619	-0.2619	0.66187	0.449609	0.741846	-0.03213	0.068444	0.094172	0.052081
Cr+PCr		0.5855841	0.53743079	1	0.234581	-0.44114	0.422945	**0.693934**	-0.86243	**0.70207**	**-0.76674**	-0.7	0.149397	0.251021	0.234482	-0.43333	0.066667	-0.51667	0.63098	0.648729	0.58944	0.159272	-0.02136	0.056268	-0.06951
Glu+Gln		0.4811201	**0.66938473**	**0.763906**	1	0.732279	-0.04963	0.189915	0.248993	0.257893	0.063647	-0.40476	-0.56552	0.084749	0.262522	-0.5	**0.571429**	-0.19048	0.145733	0.065897	0.19157	-0.33742	0.023671	-0.0288	0.058112
GABA		0.0939212	0.497425	0.338646	-0.09969	1	0.811699	-0.14744	0.802621	**-0.93133**	0.648464	0.2	-0.47977	0.309981	0.541062	-0.2	-0.6	-0.4	-0.01032	-0.07955	0.040757	**-0.88611**	0.48842	0.337459	0.5877
GSH		0.2875951	-0.1778019	-0.19191	-0.05003	-0.08838	1	0.214364	-0.52825	-0.21094	-0.2879	0.25	0.245372	0.497268	0.519552	0.071429	-0.28571	-0.39286	0.744406	0.569709	0.767833	-0.0834	0.300254	0.332909	0.272044
Ins		0.5107252	0.69685848	0.488495	0.569311	-0.323	-0.2259	1	-0.77101	0.583789	-0.32726	**-0.78333**	-0.2397	0.006265	0.056417	-0.16667	-0.01667	-0.16667	**0.790138**	**0.900295**	0.693319	0.209548	-0.08651	-0.04602	-0.11064
Lac									1	**-0.97915**	0.339787	0.1	-0.76187	-0.31304	-0.51067	0.5	0.1	0.9	-0.92237	-0.73263	**-0.959**	-0.07573	-0.13624	-0.17763	-0.10718
Tau		0.233275	0.59472697	**0.690323**	**0.718586**	0.566221	-0.43616	0.207635		1	-0.64953	**-0.81667**	0.201163	-0.04321	0.070519	-0.46667	0.15	-0.46667	**0.703929**	0.647545	0.696398	0.212626	-0.2514	-0.2056	-0.27211
nqa-gqi		0.6438911	0.30926798	-0.00229	0.300161	-0.12035	0.572099	0.40299		-0.1154	1	0.335165	-0.19298	-0.06776	-0.06292	0.461538	0.21978	**0.697802**	-0.26394	-0.19016	-0.31417	0.072737	0.012772	-0.01243	0.028317
fa-gqi		-0.5483764	-0.4535466	**-0.82376**	-0.64334	-0.26375	0.393422	-0.26491		-0.68517	0.359628	1	-0.23146	0.054852	0.144679	0.208791	0.06044	0.10989	**-0.81872**	**-0.81704**	**-0.79421**	-0.41382	0.04414	-0.03882	0.102345
md-gqi*		-0.2	-0.5757576	-0.32121	-0.32121	0.5	0.078788	-0.63333		-0.11515	0.302198	-0.24725	1	0.338947	0.025465	0.263736	-0.34615	-0.1978	0.582722	0.630166	0.521392	**0.704672**	0.221979	0.398127	0.089823
ad-gqi*		0.1636364	-0.5151515	-0.47879	-0.15152	-0.64286	0.321212	-0.55		-0.18788	**0.659341**	0.181319	**0.637363**	1	**0.892386**	0.104396	-0.28022	-0.54396	0.469916	0.332555	0.534128	-0.06343	**0.904113**	**0.928365**	**0.854605**
rd-gqi*		0.4424242	0.21212121	0.478788	0.418182	0.142857	0.018182	0.15		0.030303	0.225275	-0.3956	0.247253	0.274725	1	-0.25824	-0.18132	**-0.65934**	0.451344	0.218067	**0.579738**	-0.42048	**0.833952**	**0.76764**	**0.85189**
gfa-gqi*		0.011432	-0.0573489	-0.52793	0.084287	-0.62294	0.157485	-0.10714		-0.12662	**0.576807**	0.221765	0.417582	**0.89011**	0.322815	1	-0.41758	0.43956	0.408987	0.476205	0.35982	**0.707449**	0.52589	**0.671184**	0.38251
iso-gqi		0.3381631	0.49789577	0.280798	0.072486	0.186302	-0.27961	0.288481		0.019971	-0.00952	-0.10808	**-0.60356**	-0.4183	-0.16356	-0.36572	1	0.373626	-0.51217	-0.50659	-0.48181	-0.35466	-0.05486	-0.09158	-0.03144
fa-reg*		0.4181818	-0.1272727	0.078788	0.10303	0.035714	0.551515	-0.48333		0.054545	0.258242	0.417582	0.148352	0.340659	-0.26923	**0.587912**	-0.28571	1	-0.08288	0.104501	-0.22899	0.486335	**-0.61748**	-0.55481	**-0.64157**
md-reg		-0.3126396	**-0.689441**	-0.61285	-0.42159	-0.20815	0.258454	-0.60221		-0.21296	0.152786	0.096379	**0.754018**	**0.733454**	0.333582	**0.656134**	**-0.85269**	0.163925	1	**0.948585**	**0.978048**	0.312746	0.409902	0.472887	0.345143
ad-reg*		-0.2	**-0.7090909**	-0.50303	-0.10303	-0.32143	0.175758	**-0.76667**		-0.00606	0.494505	0.093407	**0.796703**	**0.912088**	0.186813	**0.769231**	**-0.61538**	0.274725	**0.945055**	1	**0.861806**	0.501591	0.296196	0.396282	0.208093
rd-reg		-0.5046201	0.00784811	-0.1658	0.085678	-0.13626	-0.46759	-0.00665		0.189713	0.137644	0.219762	0.28001	**0.610023**	0.267584	0.544042	-0.44072	-0.08139	0.452554	**0.844981**	1	0.170972	0.461888	0.496933	0.41611
fa-dti*		0.2727273	-0.1757576	-0.27273	-0.13939	0.035714	0.50303	-0.63333		-0.04242	0.313187	**0.565934**	0.021978	0.368132	-0.35714	**0.631868**	-0.13736	**0.901099**	0.093407	0.225275	-0.48901	1	-0.19953	0.030759	-0.35681
md-dti		0.0076931	-0.2336885	-0.20043	0.202256	-0.60719	-0.02346	-0.01214		-0.05123	0.599571	0.371988	0.159696	**0.906562**	**0.613642**	**0.834376**	-0.33854	0.386237	0.496574	**0.751329**	**0.64582**	0.344164	1	**0.969782**	**0.984867**
ad-dti		0.1675718	-0.2376128	-0.33987	0.163102	-0.50679	0.279525	-0.20936		-0.07193	**0.690315**	0.349929	0.200238	**0.931184**	0.561395	**0.904665**	-0.29233	0.563932	**0.609928**	**0.692108**	0.492895	0.544479	**0.945141**	1	**0.912841**
rd-dti*		-0.0666667	-0.2121212	0.006061	0.357576	**-0.78571**	-0.24848	-0.06667		-0.0303	0.269231	-0.0989	0.181319	0.406593	**0.648352**	0.247253	-0.10989	-0.3022	0.401099	0.417582	**0.758242**	-0.34615	**0.901099**	0.428571	1

Supplementary Table 8. *R values for females, in the cerebellum. Orange boxes represent strong positive correlation, and blue strong negative. Bolded values mean a significant P-value (P<0.05). In relation to the table diagonal, the bottom triangle represents the values for the wild-type subset and the top the Tsc2$^{+/-}$ condition. Variables where Spearman was used are marked with an asterisk.*

	Ala	GPC + PCh	NAA+NAAG	Cr+PCr	Glu+Gln	GABA	GSH	Ins	Lac	Tau	nqa-gqi	fa-gqi	md-gqi	ad-gqi	rd-gqi	gfa-gqi	iso-gqi	fa-reg	md-reg*	ad-reg*	rd-reg*	fa-dti*	md-dti	ad-dti*	rd-dti
Ala	1																								
GPC + PCh*	-0.5	1	-0.0596787	-0.10335	-0.22953	0.23301	0.147705	0.491871	0.369859	-0.46916	0.015418	0.304191	-0.05212	-0.46221	-0.30177	-0.50043	0.105014	0.118591	-0.40606	-0.28485	-0.33333	0.090909	-0.37352	-0.21212	-0.32745
NAA+NAAG	0.506295	0.8610511	1	-0.0297	0.327542	**0.776473**	**-0.54001**	0.211932	0.391685	0.422763	0.142612	0.017457	-0.10502	**-0.69276**	**-0.64967**	-0.1126	0.145493	0.07673	-0.23077	-0.43357	-0.18182	0.328671	**-0.69066**	**-0.44755**	**-0.65584**
Cr+PCr	0.939698	0.6382312	0.70266013	1	0.038055	-0.57836	0.034188	**-0.82965**	0.358224	0.459571	0.079925	**-0.71347**	**0.912395**	0.29672	0.578668	-0.41183	0.027398	-0.49455	0.416667	0.266667	0.433333	-0.58333	**0.562588**	0.466667	**0.612337**
Glu+Gln	-0.30108	0.7266988	0.37746522	0.328038	1	0.207778	-0.34948	-0.02051	**-0.70751**	0.016532	0.028057	-0.31674	0.092717	-0.50426	-0.38581	-0.22239	-0.30574	-0.14204	-0.32121	-0.62424	-0.30909	0.030303	-0.30151	-0.52727	-0.26787
GABA		0.8840365	0.64617025	-0.22664	0.191017	1	-0.43502	0.517538	-0.64877	0.061161	**-0.61383**	0.146474	-0.41137	**-0.79277**	**-0.8187**	-0.34257	0.075566	0.090858	-0.48651	**-0.84688**	-0.45047	0.126131	**-0.85225**	**-0.75679**	**-0.84289**
GSH	-0.91495	0.0624508	0.31182306	0.392992	0.194133	0.562167	1	-0.20292	**0.662721**	-0.219	-0.28575	0.06992	0.049738	0.347104	0.349159	0.057348	-0.34329	-0.26903	**0.636364**	0.472727	**0.627273**	-0.33636	0.293902	0.163636	0.296546
Ins	-0.03101	0.746244	0.87015834	0.336001	0.464223	**0.975895**	0.410262	1	-0.43635	0.121805	-0.36664	0.248005	-0.4549	**-0.76404**	**-0.56974**	-0.40606	-0.25343	-0.40019	-0.49091	**-0.7**	-0.29091	0.072727	**-0.64566**	**-0.63636**	**-0.56848**
Lac		0.2350005	0.20756444	0.487292	0.623982	**0.826744**	**0.941003**	0.596626	1	0.123318	0.477916	0.253794	-0.15689	0.267584	0.137006	0.284475	0.545054	0.04662	**0.785714**	**0.714286**	0.690476	0.095238	0.052613	**0.809524**	0.412441
Tau	0.943901	0.3637561	0.74507572	0.735443	-0.06937	0.39844	0.679102	0.56327	0.429681	1	-0.14922	-0.05168	-0.11806	-0.18783	0.088483	-0.27963	0.117281	-0.33246	0.2662	-0.01401	0.343258	-0.12259	-0.03853	-0.08056	0.099515
nqa-gqi*	1	0.1	0.3	0.5	-0.37143	0.4	0.7	0.2	1	0.8	1	0.397052	0.043023	0.33515	0.030495	**0.511532**	0.365403	0.252417	0.135714	0.282143	-0.025	**0.657143**	0.09681	**0.521429**	0.121527
fa-gqi	-0.96416	0.156198	-0.3116168	0.121794	-0.44363	-0.60375	-0.15334	-0.37015	0.147446	-0.51478	0.28218	1	-0.425	0.163341	-0.26651	**0.482284**	**0.534366**	**0.472661**	-0.06786	0.1	-0.17143	**0.628571**	-0.3154	0.1	-0.34135
md-gqi*	-1	-0.1	-0.3	-0.5	-0.48571	-0.4	-0.7	-0.2	-1	-0.8	-0.18333	-0.23333	1	0.342545	0.391855	0.056967	-0.17395	0.004997	0.067857	0.242857	0.085714	-0.09286	0.360782	0.007143	0.302166
ad-gqi*	-0.5	-0.6	-0.7	-0.2	-0.08571	-0.4	0	-0.3	-0.5	-0.7	-0.06667	-0.1	**0.877872**	1	**0.786071**	**0.487067**	0.293579	0.158697	0.507143	**0.760714**	0.378571	0.1	**0.798213**	**0.757143**	**0.691654**
rd-gqi*	-1	-0.2	-0.4	-0.1	0.028571	-0.4	-0.1	0.1	-0.5	-0.6	0.033333	-0.18333	**0.905059**	**0.87965**	1	-0.09095	0.095153	-0.3783	**0.778571**	**0.7**	**0.746429**	**-0.52143**	**0.971386**	**0.642857**	**0.975964**
gfa-gqi	-0.79357	-0.5677941	-0.8709902	-0.78762	-0.1395	-0.48088	-0.64614	-0.70707	-0.46373	**-0.97163**	-0.93448	-0.09543	0.572393	**0.720068**	0.41987	1	0.276167	**0.770654**	-0.13571	0.275	-0.34286	**0.835714**	-0.02939	0.271429	-0.13899
iso-gqi	-0.01813	**0.8800588**	0.80697093	0.263451	**0.843513**	0.843233	0.015315	**0.895063**	-0.09887	0.248896	-0.37749	**-0.82403**	**0.734961**	0.471664	**0.763686**	-0.08629	1	0.391555	0.160714	0.242857	-0.00357	0.432143	0.022646	0.371429	0.090561
fa-reg	0.755894	-0.349169	-0.3548169	-0.11773	**-0.8503**	-0.77491	-0.76014	-0.65976	-0.9954	-0.29189	0.539283	0.600044	-0.49455	-0.48304	-0.6386	0.073083	**-0.74519**	1	-0.48571	-0.08929	**-0.675**	**0.807143**	-0.34401	0.078571	-0.45218
md-reg*	-1	0.2	-0.1	-0.1	0.028571	0.6	0.5	0.6	0.5	-0.1	0.183333	-0.16667	**0.75**	**0.816667**	**0.933333**	0.4	0.166667	-0.38333	1	**0.832143**	**0.957143**	-0.32143	**0.621467**	0.617857	**0.716897**
ad-reg*	-1	0.2	-0.1	-0.1	0.028571	0.6	0.5	0.6	0.5	-0.1	0.183333	-0.16667	**0.75**	**0.816667**	**0.933333**	0.4	0.166667	-0.38333	1	1	**0.714286**	-0.06429	**0.668826**	**0.767857**	**0.695366**
rd-reg*	-1	0.2	-0.1	-0.1	0.028571	0.6	0.5	0.6	0.5	-0.1	0.183333	-0.16667	**0.75**	**0.816667**	**0.933333**	0.4	0.166667	**-0.38333**	1	1	1	-0.50714	**0.566755**	0.428571	**0.688108**
fa-dti	0.222919	0.474414	0.00854216	0.069877	-0.3808	-0.70241	-0.68879	-0.12012	-0.64873	-0.55513	0.089767	**0.802196**	-0.2425	-0.09631	-0.27639	0.315821	-0.63397	0.526332	-0.37448	-0.24268	-0.43251	1	-0.39782	0.125	**-0.55786**
md-dti	-0.93027	0.2436656	-0.1734072	0.007944	0.836645	-0.09807	0.151529	-0.01679	0.486297	-0.4186	-0.24841	-0.65761	**0.876626**	**0.941713**	**0.9584**	0.46923	0.692065	-0.68947	**0.828212**	**0.92361**	0.748226	-0.27	1	0.717857	**0.982284**
ad-dti	-0.8713	0.3103337	-0.1037975	0.067402	0.871741	-0.08648	0.168628	0.03724	0.507157	-0.36979	-0.48335	-0.54447	**0.836705**	**0.95502**	**0.90699**	0.536962	0.599853	-0.63913	0.749475	**0.881972**	0.652236	-0.10183	**0.979736**	1	**0.836565**
rd-dti	-0.95711	0.2029614	-0.2133063	-0.02088	0.813209	-0.10721	0.146654	-0.05051	0.479455	-0.44101	-0.05971	**-0.7251**	**0.884378**	**0.908379**	**0.970872**	0.405252	**0.743266**	**-0.71016**	**0.851845**	**0.916237**	**0.787736**	-0.38265	**0.990119**	**0.942069**	1